Aus der

Medizinischen Universitätsklinik Tübingen

Innere Medizin IV

Diabetologie, Endokrinologie, Nephrologie

Identification of proteases relevant for ENaC activation in nephrotic urine

Thesis submitted as requirement to fulfill the degree "Doctor of Philosophy" in *Experimental Medicine* (PhD)

at the
Faculty of Medicine
Eberhard Karls Universität
Tübingen

presented by

Wörn, Matthias

2026

Dean:	Prof. Dr. S. Y. Brucker
1st reviewer:	Prof. Dr. F. Artunc
2nd reviewer:	Prof. Dr. D. Rapaport

Date of oral examination: 07.05.2026

Table of contents

List of figures

List of tables

List of abbreviations

AA - Afferent arteriole
ADH - Antidiuretic hormone
AEBSF - 4-(2-Aminoethyl)benzenesulfonyl fluoride hydrochloride
AMC - 7-amino-4-methylcoumarin
AMCA - 7-amino-4-methylcoumarin-3-acetic acid
APS - Ammonium persulfate
ASDN - Aldosterone-sensitive distal nephron
AUC - Area under the curve
BSA - Bovine serum albumin
BCM - Body composition monitor
BMI - Body mass index
CAP1 - Channel activating protease 1
CKD - Chronic Kidney Disease
Crea - Creatinine
Cy3 - Cyanine dye 3 (fluorescence dye)
Cy5 - Cyanine dye 5 (fluorescence dye)
Da - Dalton
DMSO - Dimethyl sulfoxide
DNP - Dinitrophenyl
DMF - Dimethylformamide
DTT - Dithiothreitol
dH2O - Distilled water
EC - Enzyme Commission (classification)
ECL - Enhanced chemiluminescence
EDTA - Ethylenediaminetetraacetic acid
ENaC - Epithelial sodium channel
FDR - False discovery rate
Fmoc - Fluorenylmethyloxycarbonyl
FRET - Förster/fluorescence resonance energy transfer
FSAP - Factor VII activating protease
FSGS - Focal segmental glomerulosclerosis
GBM - Glomerular basement membrane
GFR - Glomerular filtration rate
GO - Gene Ontology
GPI - Glycosylphosphatidylinositol
HABP2 - Hyaluronan-binding protein 2
HA - Hemagglutinin (epitope tag)
HCD - Higher-energy collisional dissociation
HPLC - High-performance liquid chromatography
HRP - Horseradish peroxidase
IAA - Iodoacetamide
IgG - Immunoglobulin G
K+ - Potassium ion

KEGG - Kyoto Encyclopedia of Genes and Genomes
KLK1 - Kallikrein-1
KLKB1 - Plasma kallikrein
KO - Knockout
LC–MS/MS - Liquid chromatography–tandem mass spectrometry
LFQ - Label-free quantification
MALDI-TOF - Matrix-assisted laser desorption/ionization time-of-flight (mass spectrometry)
MCA - 7-methoxycoumarin-4-acetamide
MCD - Minimal change disease
MDRD - Modification of Diet in Renal Disease (study/formula)
MDRD-GFR - GFR estimated by the MDRD formula
MN - Membranous nephropathy
MS - Mass spectrometry
MS/MS - Tandem mass spectrometry
m/z - Mass-to-charge ratio
Na+ - Sodium ion
NS - Nephrotic syndrome
OH - Overhydration
PBS - Phosphate-buffered saline
PLAU - Urokinase-type plasminogen activator
PLG - Plasminogen
Plg-/- - Plasminogen knockout (mouse)
PMF - Peptide mass fingerprinting
Po - Open probability (channel open-state probability)
PPM - Parts per million (ppm)
PRSS8 - Prostasin
RAAS - Renin-angiotensin-aldosterone system
RFU - Relative fluorescence units
RP-HPLC - Reversed-phase high-performance liquid chromatography
RT - Room temperature
SDS-PAGE - Sodium dodecyl sulfate–polyacrylamide gel electrophoresis
SEM - Standard error of the mean
SLE - Systemic lupus erythematosus
TAMRA - Tetramethylrhodamine
TBS - Tris-buffered saline
TBS-T/Tween - Tris-buffered saline with Tween 20
TEMED - Tetramethylethylenediamine
TFA - Trifluoroacetic acid
t-PA - Tissue-type plasminogen activator
uPA - Urokinase-type plasminogen activator
UV/Vis - Ultraviolet–visible (spectrophotometry)
WT - Wild-type
XIC - Extracted ion chromatogram

1 Introduction

1.1 Structures and functions of the kidney

The kidneys have a number of functions that have a vital importance for an organism. They remove toxic and water-soluble waste products from the body, primarily from protein catabolism, such as urea, creatinine, ammonia, uric acid, and excess electrolytes, by filtering the blood and excreting these substances as urine. The kidneys efficiently filter these substances, preventing their accumulation in the bloodstream, which could otherwise lead to serious health problems, such as uremia, electrolyte imbalances, or hypertension [1].

In addition to waste elimination, the kidneys play a central role in maintaining the body's water and electrolyte balance. They regulate the levels of essential ions, including sodium (Na^+), potassium (K^+) and others, ensuring that concentrations remain within optimal ranges. For instance, sodium is crucial for maintaining blood pressure and fluid balance, while potassium is essential for proper nerve and muscle function. The kidneys adjust the excretion or retention of these electrolytes to maintain the equilibrium [2, 3].

Furthermore, the kidneys regulate the body's acid-base balance. They help control the levels of hydrogen ions and bicarbonate ions in the blood, preventing shifts in pH that could otherwise disrupt cellular functions. This acid-base balance is vital for various physiological processes, such as enzyme activity and oxygen transport [4].

The kidneys also contribute to metabolic processes by producing glucose through gluconeogenesis. In situations where the body requires additional glucose, the kidneys can convert amino acids and other precursors into glucose, thereby playing a role in energy metabolism.

Moreover, the kidneys serve as endocrine organs, producing hormones that influence various physiological functions. One important example is the hormone erythropoietin. When the oxygen level is low, erythropoietin is released and promotes the formation of new red blood cells, ensuring that the oxygen-carrying capacity in the blood remains stable [5].

The human kidney is composed of approximately 1 to 1.5 million nephrons, each serving as a highly specialized and autonomous functional unit [6]. Structurally, a nephron is organized into two major compartments: a filtering unit located at its origin and a

subsequent tubular system that executes highly coordinated processes of reabsorption and secretion. This arrangement ensures that substances essential for the body, such as glucose, amino acids, and ions, are conserved, while metabolic waste products and excess electrolytes are efficiently excreted [7].

The filtering unit of a nephron is referred to as the renal corpuscle. It consists of the glomerulus, a cluster of capillary loops, and the surrounding Bowman's capsule, which encloses the filtrate which emerges from the blood. Within the glomerulus, blood delivered by the afferent arteriole is exposed to hydrostatic pressure, which presses plasma water and small solutes through the capillary walls and across the filtration barrier. The resultant ultrafiltrate, also termed primary urine, accumulates in Bowman's space before entering the tubular system for further processing.

The selectivity of glomerular filtration is determined largely by both the size and the electrical charge of molecules. Small solutes such as electrolytes, glucose, and urea, as well as water, can pass the barrier freely, whereas larger proteins and cellular components of the blood are normally retained. Importantly, the negatively charged components of the basement membrane and slit diaphragms further hinder the passage of negatively charged plasma proteins, such as albumin, thereby ensuring that valuable proteins remain in blood circulation [8, 9].

The following graphic shows the names of the nephron sections in general:

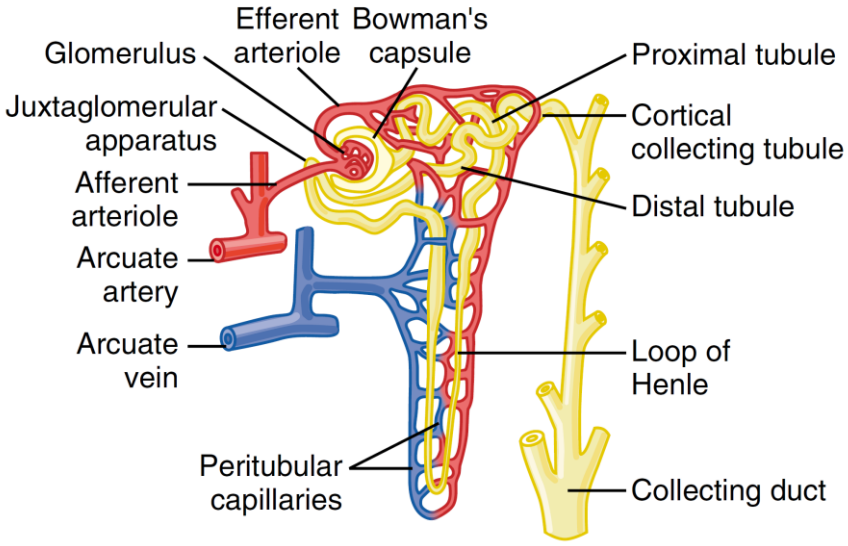

Figure 1: **General structure of a nephron [10]**

Section of an individual nephron and the major blood vessels that supply the blood flow to the kidney.

1.1.1 The glomerular filtration barrier

A property of the glomerular filter that is essential for the function of the kidney is its selective permeability (permselectivity) towards components of the plasma. On the basis of molecular size and charge, the glomerular filtration barrier retains plasma proteins in the blood. This barrier is uniquely structured and comprises three main layers [11].

Fenestrated endothelial cells form the inner surface of glomerular capillaries which prevent the passage of blood cells. The glomerular basement membrane (GBM), a thin film of specialized extracellular matrix with laminin, fibronectin and collagen type IV, is the second structure and a structural barrier for substances with a mass higher than 400 kDa [12, 13]. Specialized glomerular epithelial cells, called podocytes, stand directly on the basal membrane with their foot processes and form gaps between them called filtration slits. Together, these layers form a highly selective filtration system which is permeable to water and small dissolved solutes, but retains the majority of proteins, bigger molecules, and blood cells [14].

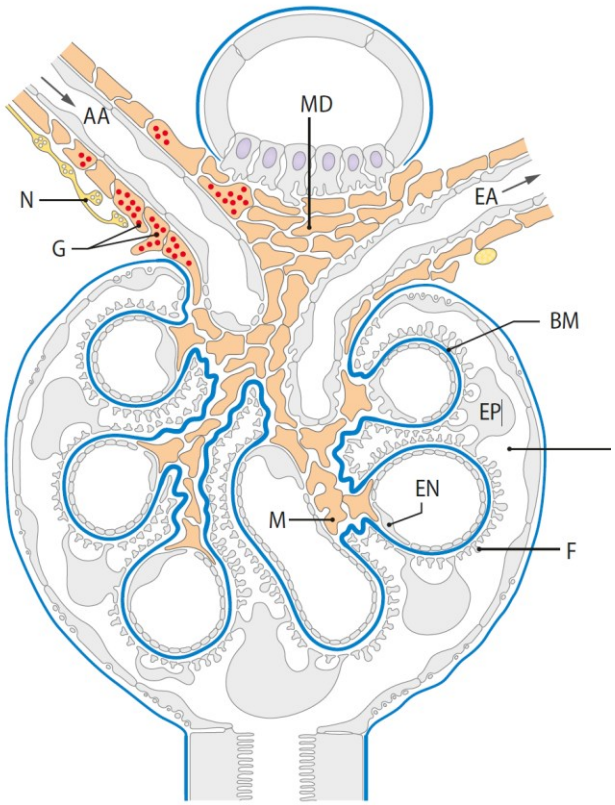

Figure 2: General structure of a glomerulus [15]

Pores of endothelial cells (EN), glomerular basement membrane (BM), epithelial cells (EZ) = podocytes with foot processes (F), AA = afferent arteriole, EA = efferent arteriole, N = nerve fibers, G = granules, M = mesangial cells, MD = Macula densa segment of the tubule

The structure of the podocyte slit diaphragm allows very small molecules to pass through with almost no restriction, and proteins below about 20 kDa usually cross the filtration barrier quite easily. The passage of larger molecules is increasingly limited, and proteins in the range of 60–70 kDa are held back so effectively that only very small amounts reach the Bowman's space [16]. Among the almost freely filtered molecules, there are metabolic waste products like urea, creatinine, etc. but also valuable substances like monosaccharides, amino acids, peptides, electrolytes and water itself. These valuable substances are reabsorbed by special transport systems and channels along the subsequent tubule sections [17].

Filtration also depends on ionic charge, and negatively charged proteins, such as albumin, are retained to a greater extent than would be predicted by size alone. The filtration slits contains negatively charged glycoprotein polymers (e.g. Heparan sulfate proteoglycans (HSPGs) with negatively charged heparan sulfate side chains) which impede the passage of negatively charged molecules [18]. This is important for protein filtration because the most plasma proteins have a negative excess charge and so their permeability is additionally impaired. For example, albumin as the most abundant protein in the blood plasma is negatively charged, but also immunoglobulins have a weak negative net charge, and many other plasma proteins like fibrinogen. Positively charged ions like sodium and potassium can easily passage through the filtration barrier, and also neutral small molecules like glucose, urea and creatinine [19, 20].

1.1.2 The kidney tubule system

After the formation of the primary urine in the glomerulus, the subsequent tubule system transport valuable substances and water back to the blood circulation, while actively secreting additional waste products and ions from the blood into the tubular fluid. In this way, the raw filtrate generated in Bowman's capsule is gradually transformed into the final urine [21].

The renal tubular system is divided into several segments, each with distinct structural and functional properties which are depicted in following image:

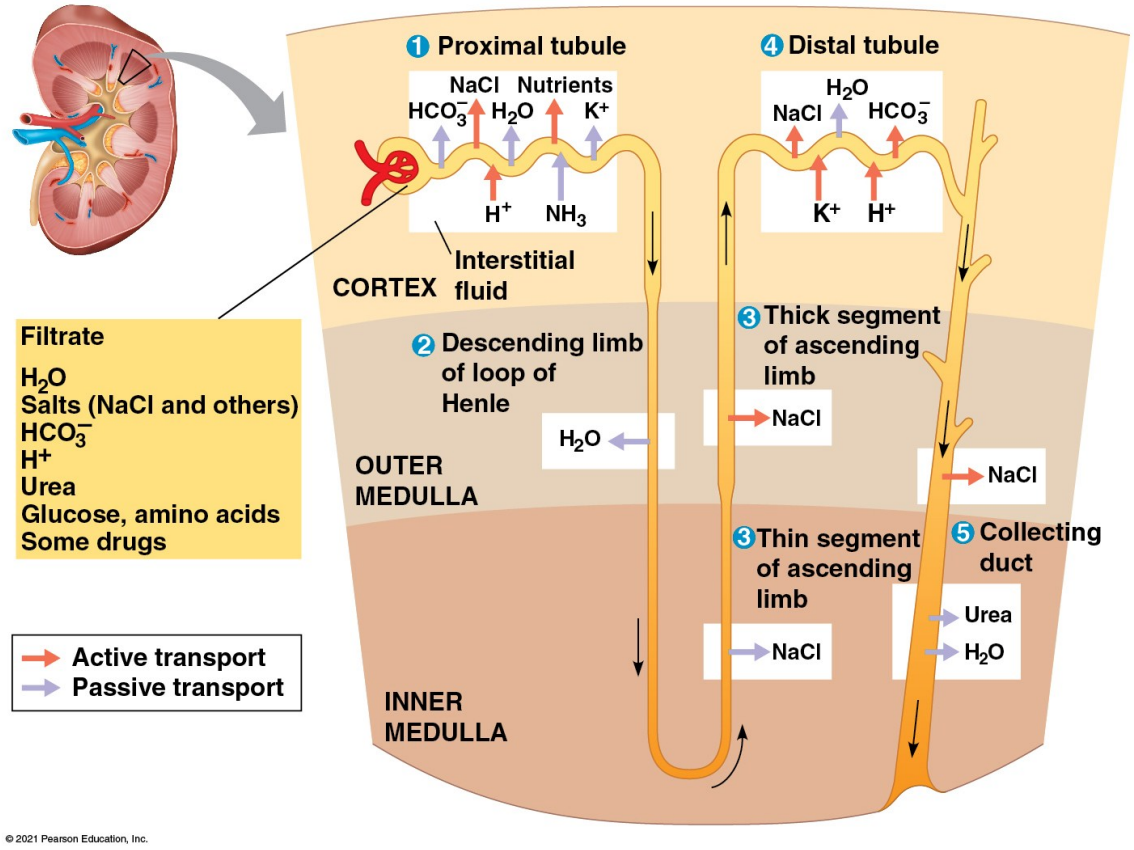

Figure 3: Sections and functions of the kidney tubule system [22]

- The first segment after the glomerulus is the proximal tubule, responsible for the reabsorption of a significant portion of the filtrate. The proximal tubule reabsorbs about 65-70% of water, sodium (NaCl), bicarbonate (HCO_3^-), and essential nutrients such as glucose and amino acids through active and passive transport mechanisms. Additionally, hydrogen ions (H^+) and ammonia (NH_3) are secreted into the filtrate, playing a role in acid-base balance [23].
- The descending limb of the loop of Henle is primarily responsible for water reabsorption. As the filtrate descends into the highly concentrated medulla, water is passively reabsorbed into the surrounding tissue due to the osmotic gradient, while solutes such as sodium are not permeable to this section.
- The ascending limb of the loop of Henle is impermeable to water but highly active in solute reabsorption, particularly NaCl. This is a crucial point for creating the osmotic gradient in the renal medulla, which is essential for water reabsorption later in the nephron. Here, NaCl is actively transported out of the filtrate into the interstitial fluid, but no water follows.

- In the distal convoluted tubule, further reabsorption of NaCl occurs, along with the active secretion of potassium (K^+) and hydrogen ions (H^+). The reabsorption of water here is regulated by hormones such as aldosterone and antidiuretic hormone (ADH), allowing for fine-tuning of urine concentration.
- The final segment of the tubular system, the collecting duct, is where the final concentration of urine is determined. Water is reabsorbed based on the body's needs, under the control of ADH. The duct also plays a role in urea reabsorption, which further contributes to the medullary osmotic gradient [24].

Each section of the kidney's tubule system works in a coordinated manner to ensure that waste products are effectively removed from the body while conserving essential substances such as water, sodium, and nutrients, contributing to the regulation of blood pressure, volume, electrolytes and acid-base balance.

1.2 Nephrotic syndrome

Nephrotic syndrome is a collection of symptoms that results from massive urinary protein losses due damage to the glomerular filter accompanied by hypalbuminemia and hyperlipidemia and which results in strong sodium and water retention and edema formation. This can be caused by inflammation or podocyte damage and involves also decreased negative charge of the basement membrane [17, 18]. As a result of the increased glomerular permeability, proteins greater than 69 kDa in size can pass the blood-urinary barrier in great quantity. Among urinary proteins, albumin can be found as the most abundant single protein, but also other plasma proteins such as antithrombin (58 kDa) and immunoglobulin G (150 kDa) are typically found.

NS can be divided into two categories: primary nephrotic syndrome, which is caused by a condition that affects just the kidneys, and secondary nephrotic syndrome, which is caused by systemic disorders such as diabetes and systemic lupus erythematosus (SLE) [25].

Primary nephrotic syndrome, also known as idiopathic nephrotic syndrome, arises from conditions that primarily affect the kidneys themselves, without systemic disease involvement. Here are the most common diseases of primary nephrotic syndrome:

- Minimal Change Disease (MCD) is most prevalent in children and is characterized by minimal changes seen under a light microscope, though electron microscopy reveals effacement of podocyte foot processes [26].
- Focal Segmental Glomerulosclerosis (FSGS) involves scarring in some segments of the glomeruli and can be challenging to treat, often leading to progressive kidney damage. It can present as primary (idiopathic) or secondary to other conditions such as obesity, reflux nephropathy, or infections [27].
- Membranous Nephropathy (MN) is more common in adults and involves thickening of the glomerular basement membrane due to immune complex deposition [28].

Secondary nephrotic syndrome occurs as a consequence of systemic diseases that impact multiple organ systems, including the kidneys. Examples therefore are:

- Diabetes mellitus, where chronic high blood sugar levels result in the thickening and eventual scarring of the glomerular basement membrane, reducing its ability to filter blood properly [29].
- Systemic lupus erythematosus, an autoimmune disorder, can cause lupus nephritis, wherein immune complexes deposit in the glomeruli, triggering inflammation and damage [30].

1.2.1 Proteinuria and Hypoalbuminemia

Proteinuria is the hallmark of nephrotic syndrome and is characterized by increased glomerular permeability for plasma proteins. Nephrotic-range proteinuria is defined as a urinary protein excretion that is greater than 3.5 g/24 hours or as a urinary protein/creatinine ratio that is greater than 2.0 g/g creatinine in spot urine samples. The main determining factor is albumin loss through into the urine [31].

It is often caused by a breakdown in the glomerular filtration barrier, which takes place in the area of the podocytes [32]. Glomerular proteinuria results from damage to the glomerular filter. These can be the endothelium, the basement membrane and the slit membrane between the foot processes of the podocytes. In either case, a reduction or loss of permselectivity results. If the negative fixed charges on the glomerular filter are neutralized in the case of inflammation of the glomerulus (glomerulonephritis), negatively charged plasma proteins are more easily be filtered. The albumins are

particularly affected, which are relatively small but are retained by the normal glomerular filter due to their strong negative charges.

The resulting damaged reduced barrier function causes an increased filtration of large molecular weight proteins across the membranes (especially albumin, but also other plasma proteins such as complement and coagulation factors, transferrin and immunoglobulins).

Nephrotic urine is characteristically foamy when shaken in a sample cup, due to the excess protein that lowers the surface tension and traps air bubbles. In contrast, healthy urine usually produces only a few bubbles that disappear quickly, while nephrotic urine forms persistent layers of foam. It is shown in following figure of representative samples:

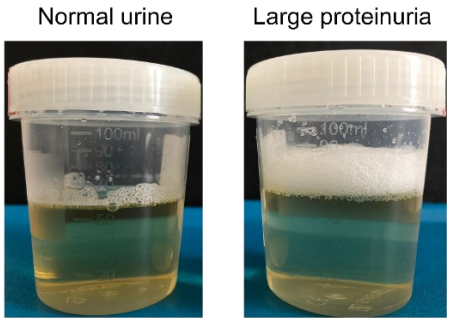

Figure 4: Urine appearance: Normal, healthy urine + nephrotic urine with large proteinuria

Foam is produced after shaking a sample cup of urine with large proteinuria.

1.2.2 Hyperlipoproteinemia

As a result of the significant loss of protein that occurs as a result of proteinuria, there is an increase in the rate of lipoprotein synthesis and α2-microglobulin in the liver as a form of compensatory response [33]. So, the reduced oncotic pressure caused by albumin loss can be stabilized. The lipoproteins contribute to this because they are too large due to their size to be filtered through the damaged filtration barrier. This leads to a typical appearance of the serum, which is no longer clear, but rather takes on a milky white-yellowish turbidity due to the lipoproteins.

Although the liver is able to increase the synthesis of albumin in a compensatory manner, this increase is not sufficient to maintain the plasma albumin at a sufficient level. As a result, the oncotic pressure, which is highly controlled by albumin, decreases.

1.2.3 Edema formation in NS

As a result of hypalbuminemia, the capillary colloid-osmotic pressure drops and the oncotic pressure to the extracellular space decreases. This promotes the formation of edema, a typical symptom of nephrotic syndrome.

There are two major competing views regarding the origin of sodium retention and edema formation in patients and rodents with nephrotic syndrome. The high plasma aldosterone levels in nephrotic mice favours the underfill theory, whereas the data from studies in mice using the serine protease inhibitor aprotinin support the overfill theory. The underfill theory which was proposed about 100 years ago [34], and claims that low plasma protein concentration, which is consequence of massive proteinuria, leads to intravascular volume depletion and activates renin-angiotensin-aldosterone system (RAAS) [35]. The decreased volume is sensed primarily by the juxtaglomerular apparatus in the kidney, where specialized granular cells respond by releasing renin. Renin then catalyzes the cleavage of angiotensinogen, produced by the liver, into angiotensin I, which is further converted by angiotensin-converting enzyme (ACE) in the pulmonary and renal endothelium into the active peptide angiotensin II. Angiotensin II exerts multiple effects, including direct vasoconstriction and stimulation of thirst, but most importantly it acts on the adrenal cortex to promote the secretion of aldosterone. Increased aldosterone levels bind to intracellular mineralocorticoid receptors in tubular cells, which translocate to the nucleus and act as transcription factors. This enhances the expression of genes encoding ion channels and transport proteins, most prominently the epithelial sodium channel (ENaC) in the luminal membrane and the Na^+/K^+-ATPase in the basolateral membrane. Increased ENaC insertion into the apical membrane facilitates sodium influx from the tubular lumen, while the Na^+/K^+-ATPase actively exports sodium into the interstitial space in exchange for potassium, thereby maintaining the electrochemical gradient. The augmented sodium reabsorption creates an osmotic driving force that promotes water flow into the interstitial space. This can, when excessively upregulated, result in the formation of edema.

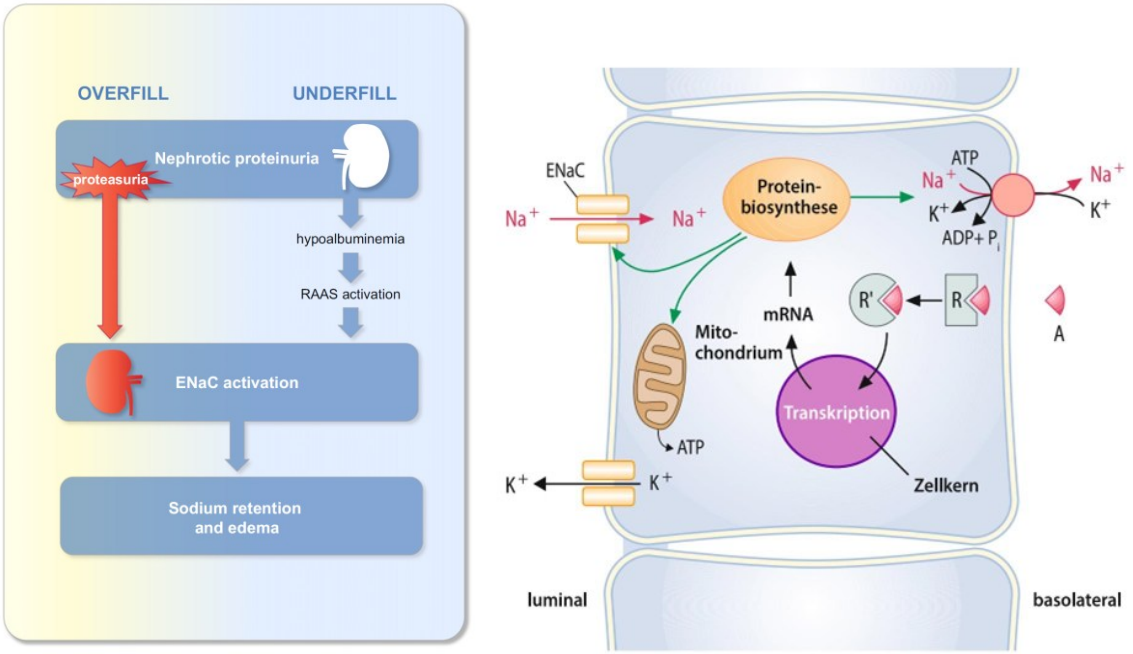

Figure 5: Scheme of the theories on the formation of edema [36] + cellular mechanisms of aldosterone effects [15]

The left scheme illustrates the two main theories discussed about edema formation in nephrotic syndrome and the possibility that they may be mutually supportive.

But there are also nephrotic cases where RAAS activation is absent, in patients as well as in animal models [36, 37]. For example, blocking the mineralocorticoid receptor by canrenoate did not prevent sodium retention and edema in nephrotic mice [38]. And the aldosterone-resistant mice with the serum-and-glucocorticoid-kinase 1 (SGK1) deficiency also developed sodium retention after induction of NS [39]. Besides, nephrotic patients do not display constantly increased level of plasma aldosterone [37]. All these findings point to some other activation of ENaC than aldosterone in NS.

Since the underfill theory cannot explain the mechanism of aldosterone independent ENaC activation, an overfill theory was formulated [40]. This theory states that edema formation could be a consequence of an intrarenal mechanism rather than systemic factors, so that regulation in tubular sodium handling may directly influence water retention. In this context, the epithelial sodium channel (ENaC), which is expressed at the collecting duct, has been identified as a key intrinsic factor, as its high activation in the distal nephron can clearly increase sodium reabsorption, water retention and volume expansion in NS, independently of circulating hormones such as aldosterone [41-43].

The elevated ENaC activity as the essential site of excessive sodium retention was first discovered by micropuncture-studies in experimental NS of mouse models [42, 43]. Another study performed by treatment with the blocker of ENaC, amiloride, also protected nephrotic mice from sodium retention and edema formation [38] which proved the essential role of ENaC activation there. This is supported by the finding that ENaC was activated by aberrantly filtered serine proteases [44], which could be prevented by treatment with the serine protease inhibitor aprotinin [45].

1.3 The epithelial sodium channel ENaC

The epithelial sodium channel (ENaC) is an ion channel, which is located on the luminal side of the main cells in the late distal tubule and is highly selective for sodium. As a constitutively active channel, it transports sodium ions through the apical cell membrane and thus it reabsorbs sodium from the urine. As a result, the ENaC in the kidney can be used to fine-tune the sodium absorption and excretion from or into the urine. ENaC can also be used to influence the sodium content of the extracellular fluid in the body, which helps to regulate blood pressure [46].

ENaC plays a relevant role in various tissues. For example, it is found in the lung and in the colon on the apical membrane of the epithelial cells. On the tongue, it is responsible for the perception of salt taste. In the kidney, ENaC is found in the late distal tubule and collecting tube, an area located in the so-called aldosterone-sensitive distal nephron ("aldosterone-sensitive distal nephron" (ASDN)).

ENaC is a transmembrane channel composed of three subunits, the α-subunit, the β-subunit and the γ-subunit (Figure 6), each encoded by the genes SCNN1A, SCNN1B and SCNN1G. Each subunit consists of two transmembrane domains and forms extracellularly large loops, so that in combination of all three subunits a heterotrimeric channel is formed. Both the N- and C-termini of the subunits are located within the cell membrane in the cytoplasm. However, this plays no role in the kidney. Each of the three subunits are essential for the function of ENaC. In some tissues, there is an additional δ-subunit that can replace the α-subunit.

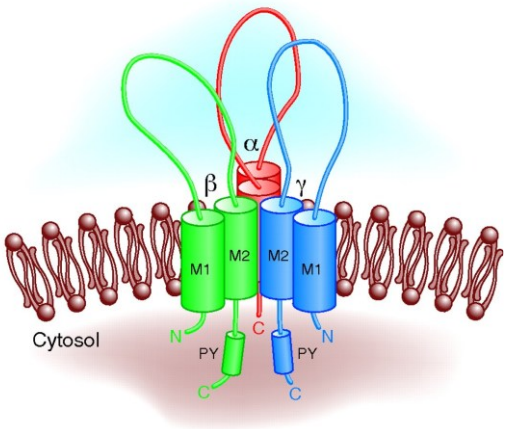

Figure 6: The three subunits of ENaC [47].

The epithelial sodium channel is built as a heterotrimer composed of one α, one β and one γ subunit. Each of these subunits contains two transmembrane domains (M1 and M2) and its N- and C-terminus are located inside the cell . The β and γ subunits also carry a characteristic PY motif in their C-terminal region.

1.3.1 Regulatory mechanisms of ENaC

As the final regulator of sodium reabsorption or excretion, the ENaC is controlled by various regulatory mechanisms that ensure that between 0% and 100% of the sodium in the lumen can be reabsorbed. The most important regulator is the mineralocorticoid hormone aldosterone, which is part of the renin-angiotensin-aldosterone system (RAAS) and is produced in the adrenal cortex. The synthesis of aldosterone is mainly stimulated by hypovolaemia and hyperkalaemia, whereas hypernatraemia has an opposite effect. In principle, several mechanisms can be distinguished from one another through which influence can be exerted on ENaC and its activity. Thus, it is already possible to intervene in protein biosynthesis, or in the further course in expression on the cell surface, in the degradation of the channels and in the open probability.

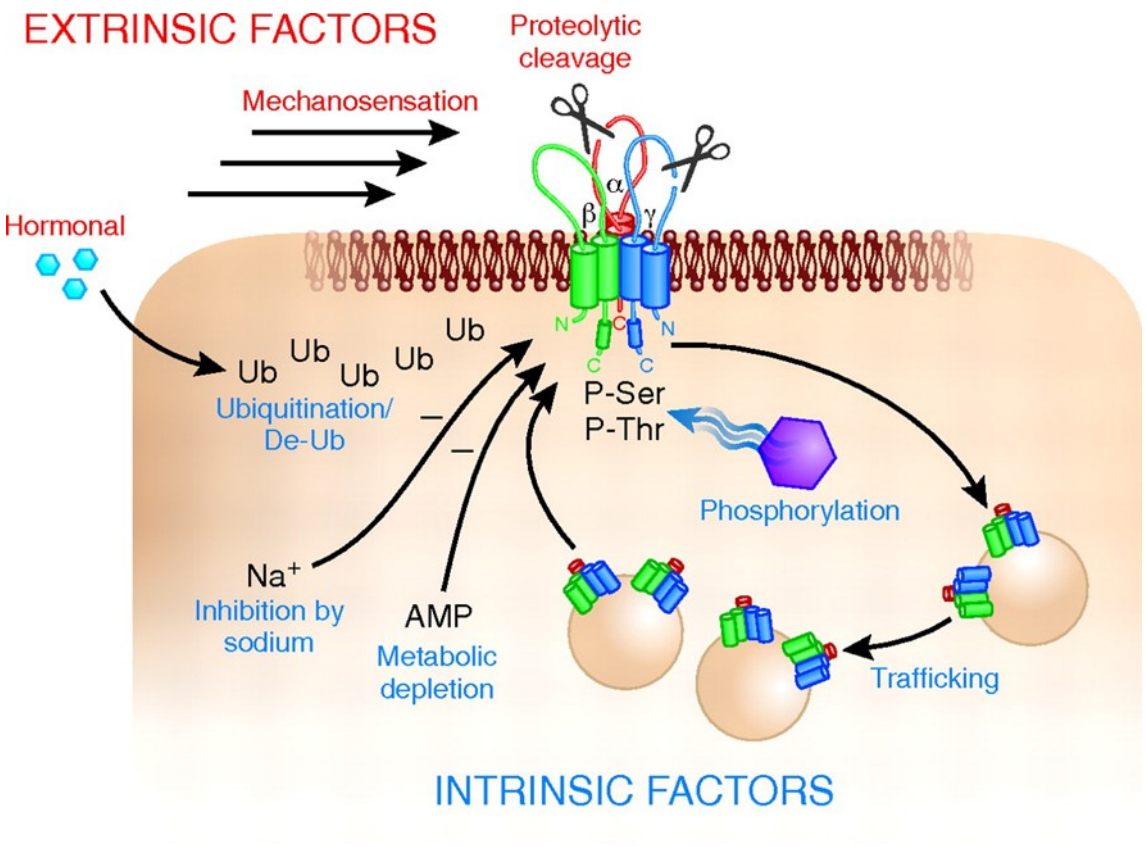

Figure 7: Modes of ENaC regulation [47]

This diagram illustrates some of the complex mechanisms and signalling pathways that exert a regulatory influence on ENaC. It shows several ways in which the channel biosynthesis, expression in the apical cell membrane, open probability and proteolytic activation can influence and regulate the channel and its activity

1.3.1.1 Regulation via intracellular proteolysis

ENaC has several regulatory mechanisms involving factors such as aldosterone as hormonal regulator, changes in intra- and extracellular Na^+ levels, phosphorylation, ubiquitination status, lipid composition and palmitoylation. Another special regulatory mechanism is its post-translational control by serine proteases. These proteases activate ENaC by cutting at defined sites in the extracellular domains of the α and γ subunits on the endoluminal side.

There are three sites which are cleaved by the protease furin during ENaC maturation before reaching the plasma membrane – two in the α subunit and one in the γ subunit . A second cleavage in γ-ENaC is catalyzed by extracellular serine proteases, such as the physiologically expressed prostasin. This step releases an inhibitory peptide that is at least

43 amino acids long. These proteolytic events increase ENaC activity by much higher open probability of the channel.

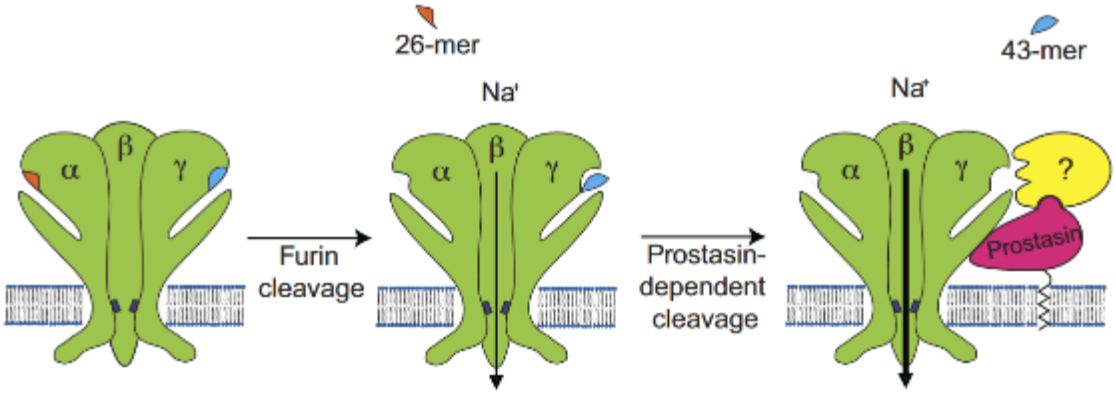

Figure 8: ENaC cleavage by furin + a protease, dependent by near prostasin binding [48]

During ENaC processing in the *trans*-Golgi network, furin cleaves the α subunit twice, which releases a 26 amino acid long inhibitory tract, and the γ-subunit at a single site upstream the γ inhibitory tract. Channels without these proteolytic cuts show a very low open probability (Po) for external Na^+. After furin cleavages and releasing the α-subunit inhibitory tract there is an intermediate *P*o of ~0.3–0.4. The serine protease prostasin, which is tethered to the plasma membrane by a glycosylphosphatidylinositol anchor, can interact with ENaC and not only to cleave the channel itself but also recruit additional serine proteases to the complex. These enzymes can then remove the inhibitory peptide from the γ-subunit, and the combined loss of it together with that one of the α subunit further elevates Po, with values about 1 as 100 percent Po.

It has been shown that an increase in the intracellular sodium concentration can lead to a change in N-glycosylation at the subunits so that they are no longer processed by proteases and thus activated. This prevents more sodium from being reabsorbed than the cell can tolerate. Furin is a serine protease that acts, among other things, in the trans-Golgi network and processes and activates proteins at the end of biosynthesis as a post-translational modification and thus also plays a role in the activation of ENaC.

Furin cleaves the α-subunit of ENaC at two sites, in the proximal region of the later extracellular domain (at amino acids Arg 205 and Arg 231). This cuts out the inhibitory part and partially activates the ENaC. If the α-subunit is only cleaved at one site by furin, it can be seen that the ENaC is only strongly reduced in activity. If the subunit is not cleaved at all, the channel activity fluctuates strongly. This suggests that the 26 amino acid long chain that is not completely removed by this destabilizes the active form of the ENaC. The γ-subunit is cleaved by furin at the amino acid Arg143.

For full channel activation, an additional cleavage at a distal site of the amino acid chain is necessary. The possibility of a second proteolytic cleavage is relevant because it has been shown that the γ-subunit or its inhibitory part is of great importance for channel activation [49, 50]. In particular, the γ-subunit must be cut twice to allow maximum channel activation and a maximal open probability. This is achieved by one or more extracellular proteases and therefore results in amino acid chains of different lengths, which are all at least 43 amino acids long [51].

1.3.1.2 Regulation via extracellular proteolysis

Experiments with the serine protease inhibitor aprotinin has shown that extracellular proteolysis is mediated by various trypsin-like serine proteases of the S1 clan [38].

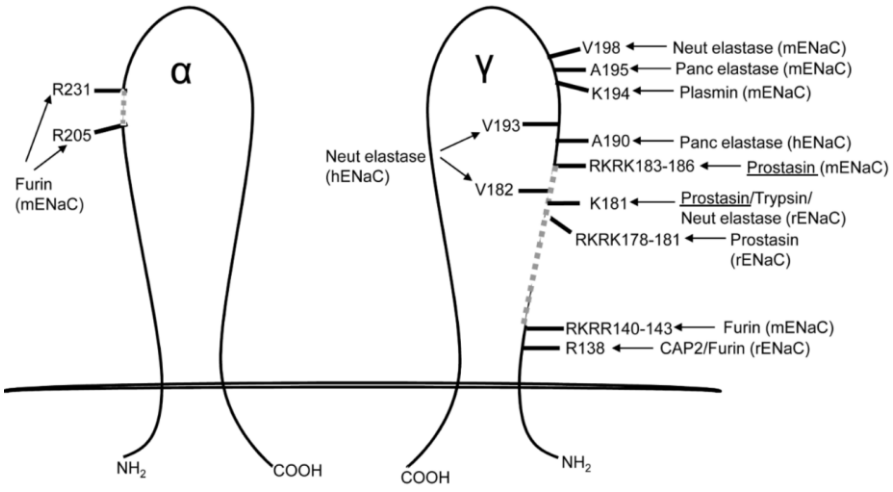

Figure 9: Possible cleavage sites of the α- and γ-subunit for different proteases (modified from [52] and [53])

The diagram shows the different sites of the α- and γ-subunit that can be cut by proteases. On the left of the picture, the two interfaces (position 205 and 231) of the α-subunit can be seen. Here, furin cuts the amino acid chain.
The γ-subunit is shown on the right. The protease interfaces that were detected in humans (hENaC), mice (mENaC) and rats (rENaC) can be seen. On the one hand, the furin interface (in the region of amino acid 140-143 in humans) and, on the other hand, possible interfaces of proteases, including prostasin. The letter code and the position of the cut amino acid are indicated. Prostasin is underlined in each case.

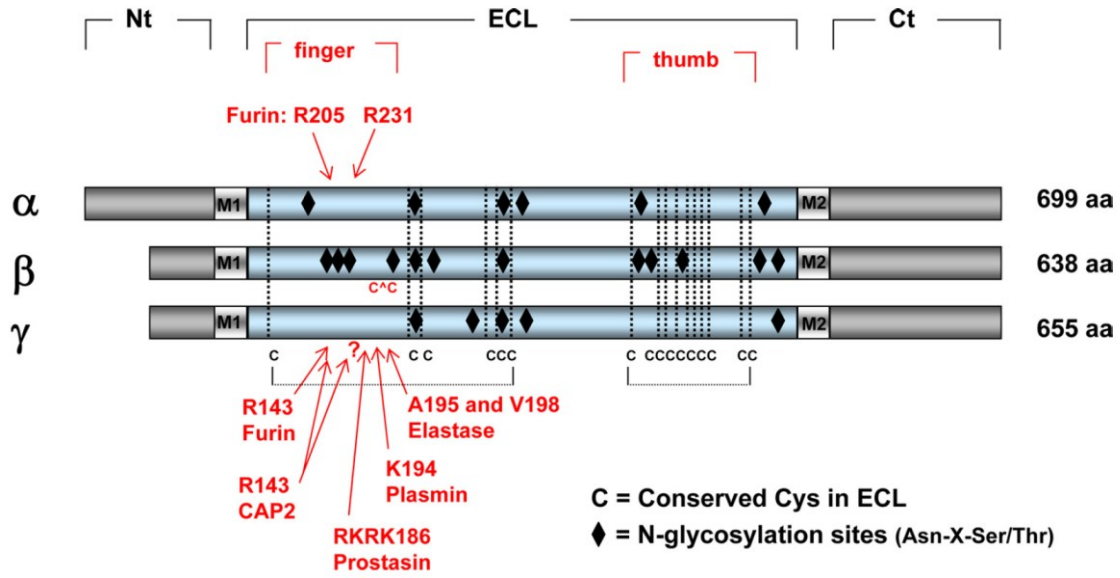

Figure 10: Linear models of the ENaC subunits [54].

Each of the three subunits contain a cytoplasmic N-terminal (Nt) and C-terminal (Ct) tail, two membrane-spanning segments (M1 and M2) and a large extracellular loop (ECL) that includes the predicted finger and thumb domains. The cleavage sites for the α subunit (cut by furin) and for the γ subunit (cut by furin, prostasin (CAP1), CAP2, elastase (neutrophil and pancreatic), and plasmin) are all located in the finger domain of this extracellular loop.
This comparison between the subunits also shows that the finger domain of the β subunit (i) does not contain the protease recognition motifs, (ii) that it has more sites where N-linked glycans can be attached (iii) and that it has one more cysteine pair compared to the other subunits.
aa = amino acids

For some candidate proteases, it has been experimentally shown that they proteolytically process the γ-subunit distal to the furin cleavage site. These include the soluble proteases kallikrein, chymotrypsin, trypsin, plasmin, neutrophil elastase, cathepsin B and S, but also the membrane-bound proteases "CAP1" (prostasin), "CAP2" (TMPRSS4) and "CAP3" (matriptase).

It is important to distinguish proteases that, like prostasin and tissue kallikrein, occur physiologically in the lumen of the distal tubule. In contrast, proteases such as plasma kallikrein or plasmin are only entering the urine when podocytes are damaged and proteinuria is present, as is the case in nephrotic syndrome. Finally, experimentally used proteases, such as trypsin or chymotrypsin, are unlikely to play a role in the activation of ENaC *in vivo*.

1.4 (Patho-)Physiological significance of urinary proteases

In addition to the excretion of albumin, which is the main protein of the plasma and a hallmark of proteinuria, proteases with comparable or even greater molecular mass are likewise expected to be abnormally filtered and released into the nephrotic urine. Proteases, also referred to as peptidases, belong to the hydrolase family of enzymes and catalyze the cleavage of proteins and peptides through breaking the peptide bond. By peptidase databases like MEROPS, proteases can be are grouped according to the amino acid residue forming the catalytic center, resulting in six major categories, designated as serine, threonine, cysteine, aspartic, glutamic and metallo-peptidases [55]. *In vivo*, proteases are widely distributed in both the intra- and extracellular compartments . They a broad spectrum of physiological functions such as cleavage of enzymes to activate the catalytically active center, signaling pathways, post-translational modifications and protein degradation [56, 57]. In the plasma, soluble proteases secreted from the liver are often organized in essential proteolytic networks such as the coagulation and fibrinolysis system, the complement system or the kinin system to name a few. These systems are often tightly regulated as cascades in which individual proteases become activated through sequential proteolytic cleavage by upstream enzymes.

It was found out, that proteinuria strongly correlates with the excretion of plasminogen. This gave the idea that also unnatural protease activity by cleavage of new substrates in the renal tubule system could occur and trigger pathological effects of nephrotic syndrome [58].

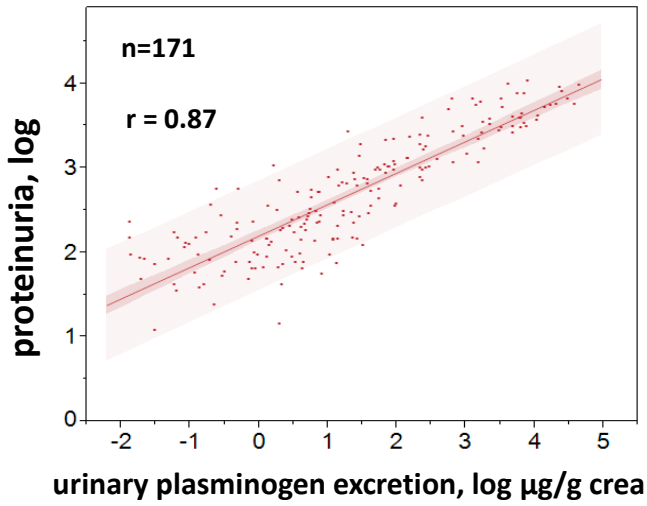

Figure 11: Correlation of plasmin(ogen)uria with proteinuria in n=171 patients with CKD [58]

Studies from both nephrotic mice and humans have revealed the excretion of serine proteases such as plasmin, plasma kallikrein or urokinase-type plasminogen activator (uPA) in urine samples [58-60]. Serine proteases are proteolytic enzymes that contain the amino acid serine in their catalytic centre and influence the regulation of various processes both physiologically and pathophysiologically.

The base-activated nucleophilic serine in the active site attacks the carbonyl carbon of the peptide bond so that a covalent intermediate is formed. The first part of the peptide or protein can be released. A water molecule can hydrolyze the covalent intermediate to release the second product so that the enzyme is regenerated in an active state. This reaction mechanism is depicted in following figure:

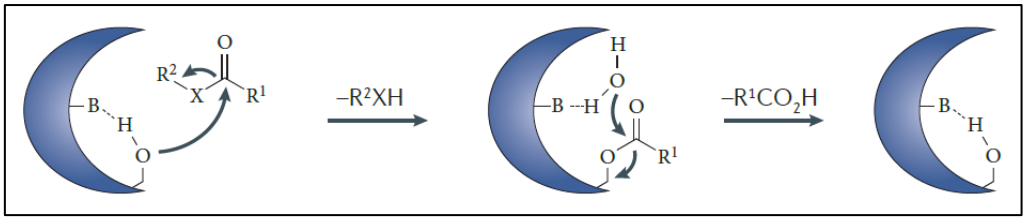

Figure 12: General reaction mechanism of serine hydrolases with serine proteases as subgroup [61].

'X' corresponds to a nitrogen, oxygen or sulphur atom

The specificity of serine proteases is defined by the amino acid side chains of the substrate which can bind to binding pockets of the enzyme by hydrophobic or ionic interactions. The nomenclature of certain sites is shown in following figure:

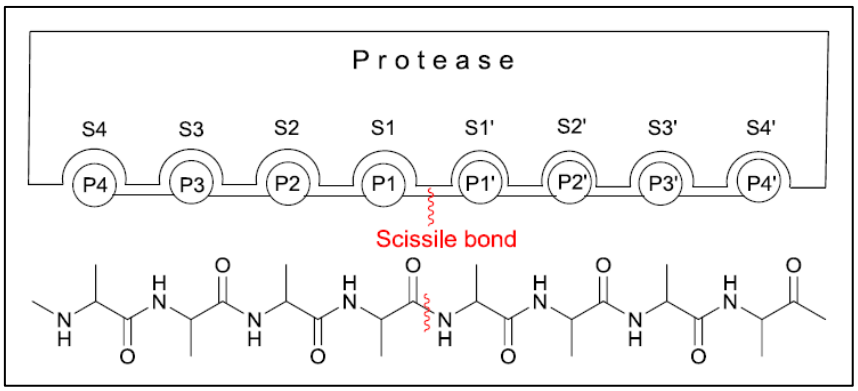

Figure 13: Nomenclature of protease specificities.

The active site of the enzyme consists of multiple binding pockets, each of which interacts with a single side chain of the substrate peptide. N-terminal to the cleaved "scissile bond" the substrate residues are numbered P1-Pn, and P1'-Pn' towards the C terminus. Correspondingly, the binding pockets of the enzyme are termed S1-Sn and S1'-Sn' in the same manner [62].

The specificity is especially influenced by the S1 site of the enzymes which can accommodate very different side chains determined by the amino acid groups in the binding pocket. In following figure, three typical serine protease families are shown:

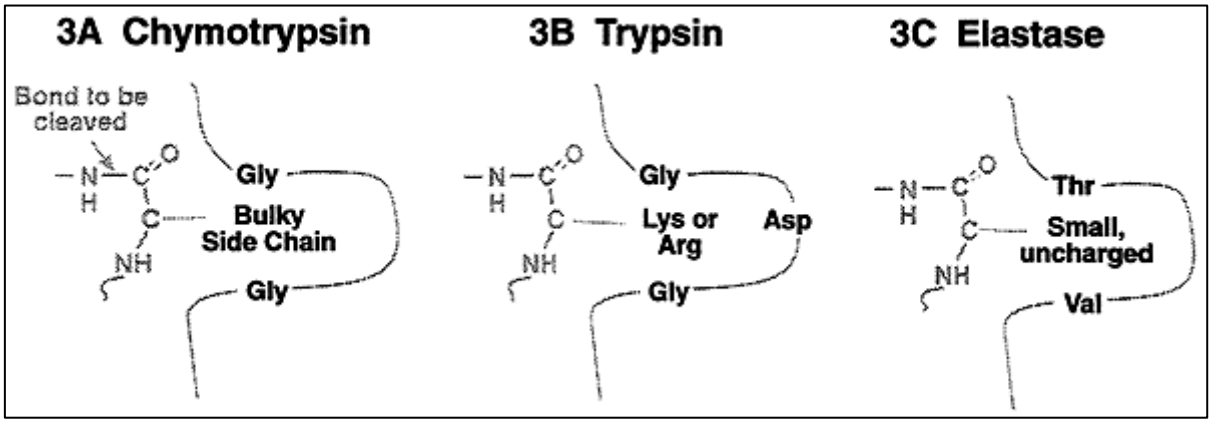

Figure 14: S1 binding pockets of typical serine protease families [63]

Many ENaC-cleaving serine proteases are trypsin-like serine proteases so that their cleavage sites come after a lysine or arginine. Chymotrypsin needs a bulky side chain, the phenylalanine and the elastases a valine side chain which is small and uncharged.

Interestingly, the newly appearing proteases in nephrotic urine often were present in their active forms, in contrast to plasma, where they normally circulate as inactive zymogens [36].

In a proteomic study examining nephrotic patients diagnosed with membranous glomerulonephritis, the urinary proteome was analyzed by measuring total urinary proteins by the method of nanoscale liquid chromatography tandem mass spectrometry [64]. The authors of this publication revealed that, based on gene ontology (GO) analysis of 249 identified proteins, a significant percentage of them were localized in the extracellular space (145 of 249) and 32 were classified to serine proteases. The Kyoto Encyclopedia of Genes and Genomes (KEGG) pathway annotation also revealed that the primary pathways linked to these proteins were the complement and coagulation cascades were the main pathways.

1.4.1 Possible candidates of extracellular proteases which could overactivate ENaC

In recent years, endoluminal activation of ENaC by improperly filtered serine proteases has been proposed as a mechanism for explaining sodium retention, consistent with the overfill theory. For that, the term “proteasuria” was introduced [36] to define the

increased excretion of active plasma proteases in the urine of patients with nephrotic syndrome. Robust data support the strong evidence that proteasuria is a key mechanism of sodium retention in patients with nephrotic syndrome.

Physiologically relevant serine proteases involved in ENaC regulation are for example furin, acting intracellularly, the membrane anchored prostasin, and soluble tissue kallikreins. Based on *in vitro* experiments, it was shown that ENaC can be proteolytically activated by aberrantly filtered serine proteases such as plasmin. This has been proposed as a key mechanism contributing to pathophysiologic sodium retention and edema formation [65, 66].

In vivo have further enforced this concept. It was discovered that nephrotic mice could be protected from proteolytic ENaC overactivation and resulting renal sodium retention when they were treated with a constant high enough level of serine protease inhibitor aprotinin which inhibits the relevant urinary serine proteases [38]. This finding has highlighted the high relevance of proteasuria as the excretion of active proteases into the urine and therefore as a key mechanism which is responsible for the very high sodium retention in nephrotic syndrome [36, 67].

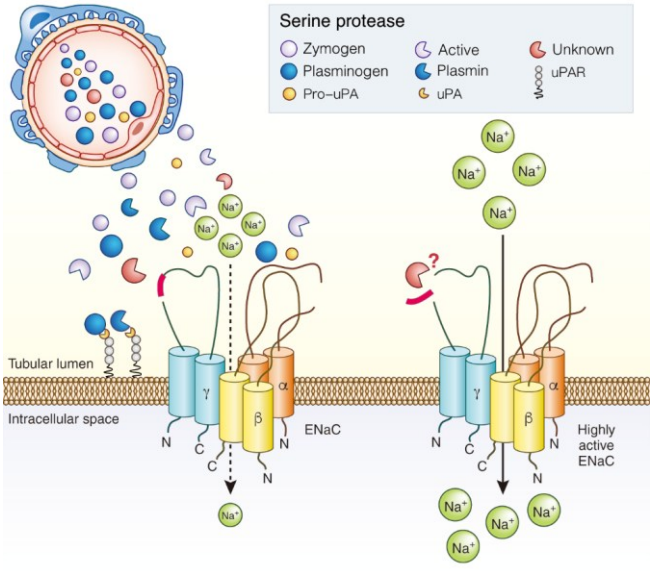

Figure 15: ENaC activation in nephrotic syndrome by newly filtered plasma proteases (modified from [36])

Many new serine proteases from the plasma reach the tubular lumen when the glomerular filtration barrier is damaged. In this more unregulated environment, they get often activated. Then it's thought that they can release the ENaC γ-subunit (depicted in red) by proteolytic cleavage so that the channel gets fully activated for high sodium retention. But the identity of the essential serine proteases for ENaC activation *in vivo* is still unknown.

For example, it proposed that new plasma serine proteases could form complexes with the membrane serine protease prostasin so that they cleave the gamma-subunit, releasing the inhibitory peptide. The removal of the inhibitory peptide from the gamma-subunit

promotes further increases in the open probability (Po) which can approaches to 1 as full activation when the channels are lacking the inhibitory tract in both the alpha- and gamma-subunits [36].

1.4.1.1 Plasmin(ogen)

The serine protease plasminogen is formed in the liver and is proteolytically activated to plasmin by the endothelial tissue-specific plasminogen activator (tissue-type plasminogen activator, t-PA). Plasmin is best known for its role in fibrinolysis of the blood. Plasminogen and plasmin are too large and too heavy (plasminogen 92kDa and plasmin 83kDa) to physiologically enter the urine. However, both proteins can be detected in the urine of nephrotic patients [68].

One possibility of activating plasminogen to plasmin in the tubular lumen is via membrane urokinase (urokinase-type plasminogen activator, uPA). It was also possible to show that plasmin can cut the γ subunit of ENaC and thus lead to increased sodium reabsorption. It has also already been shown that plasminogen does not protect against edema formation in the nephrotic syndrome in the experimental knock out mouse model [69]. It could be also shown in another mouse model with a urokinase-type plasminogen activator knock out, that ENaC activation in nephrotic syndrome is not reduced compared to wild-type control mice [60].

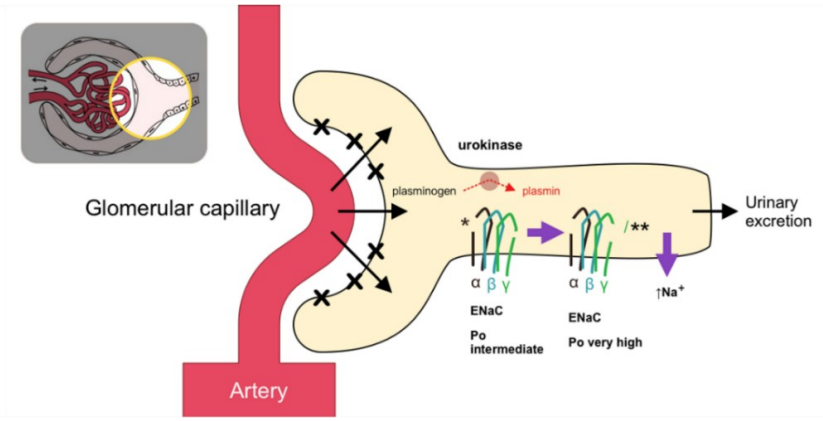

Figure 16: Role of plasmin in ENaC regulation during nephrotic syndrome[66]

The damaged glomerular filter system in NS leads to massive proteinuria, and therefore also to increased filtration of plasminogen from blood plasma to urine. After that, plasminogen is cleaved into its active form, plasmin, by urokinase-type plasminogen activator (uPA) in the tubular lumen. The active plasmin is then thought to proteolytically activate ENaC in the distal tubule, thereby

leading to very high open probability of the channel (Po) and so to increased sodium retention in NS.

1.4.1.2 Kallikreins

Kallikreins are serine proteases and can be divided into two groups: On the one hand in the tissue kallikreine and on the other hand in the plasma kallikreine. The tissue kallikrein is mainly formed in the colon and kidneys. It plays a role in various processes such as the regulation of pain perception, the inflammation cascade and the coagulation cascade by converting the inactive precursors of tissue hormones into active kinins. It can cause increased sodium resorption in the distal tubule by cleaving the extracellular γ-subunit of ENaC and therefore has an influence on blood pressure regulation [70].

In contrast, plasma kallikrein is larger and heavier (88 kDa instead of 35 kDa for tissue kallikrein). It arises from the precursor plasma prekallikrein, which is formed in the liver. After activation to plasma kallikrein, it has an influence on coagulation, among other things by splitting plasminogen into plasmin (Figure 17). Physiologically, plasma kallikrein and its precursors do not occur in the urine. However, it can be detected in the urine of patients with nephrotic syndrome, although it is still unclear how and by which protease plasma prekallikrein can be activated in the tubular lumen.

It has already been shown for plasma kallikrein on the basis of a knock-out mouse model that it is not essential for volume retention in nephrotic syndrome. In addition, there was no significant difference in ENaC activation compared to wild-type control mice.

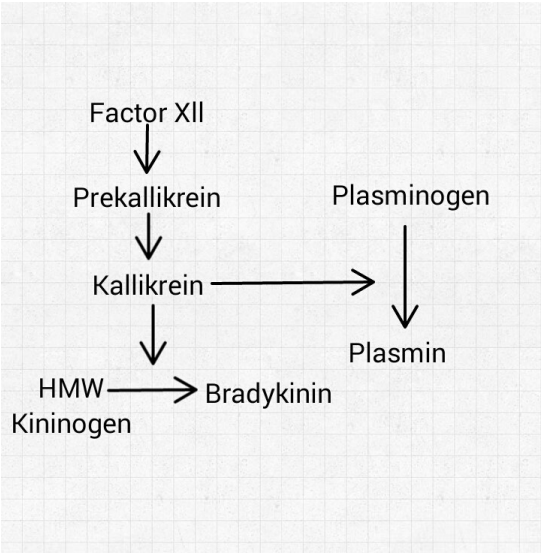

Figure 17: Activation pathways of kallikrein and its substrates [71]

1.4.1.3 Prostasin

Prostasin, also known as channel activating protease 1 (CAP1) or PRSS8 / Prss8, is an extracellular serine protease of the trypsin family, which was first published in 1994 by Yu et al [72]. It was discovered and described in prostate secretion. Prostasin is one of the few membrane-bound serine proteases. It is bound to the cell membrane via a glycosylphosphatidylinositol anchor (GPI anchor).

Prostasin influences ENaC activity at low plasmin concentrations. The following diagram illustrates the theory from *in vitro* experiments that prostasin acts as an enhancer of plasmin when plasmin is only present in low concentrations. There, it is activated by plasmin and can cut the γ subunit. As soon as plasmin is present in higher concentrations, prostasin no longer plays a decisive role.

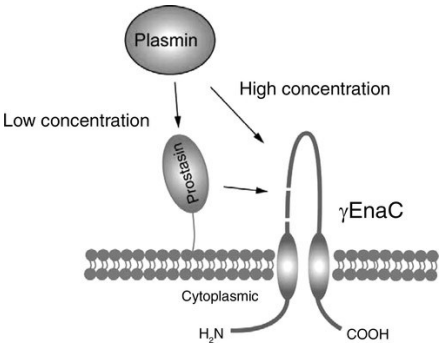

Figure 18: Scheme of the activation of the ENaC by plasmin via prostasin [73]

A knock-out of prostasin is not possible in the mouse model, because prostasin knock-out mice die from placental insufficiency or from dehydration shortly after birth because their epidermis is not fully and functionally developed [74]. However, it is possible to develop prostasin knock in mice that have no proteolytic function or in which prostasin occurs only as a zymogen. In addition to its relevance in epidermal and placental development, prostasin plays an important role in the activation of the ENaC [75].

Interestingly, prostasin mutants with changed amino acids within the catalytic triad were still able to induce ENaC activation, indicating that prostasin-mediated channel activation may occur independently of its enzymatic activity. However, replacement of the putative prostasin cleavage motif in the γ-subunit ($RKRK^{186}$ by four glutamine residues, $QQQQ^{186}$) prevented ENaC activation by both wild-type prostasin and the catalytically inactive S238A mutant, supporting the requirement of prostasin-dependent channel cleavage [48].

Thus, it remains unresolved by which exact mechanism a prostasin variant lacking catalytic function can nevertheless promote proteolytic processing and activation of ENaC, but it's thought that it is a scaffold function for recruiting another serine protease, like for the shown plasmin.

1.5 Protease inhibitors

1.5.1 Aprotinin

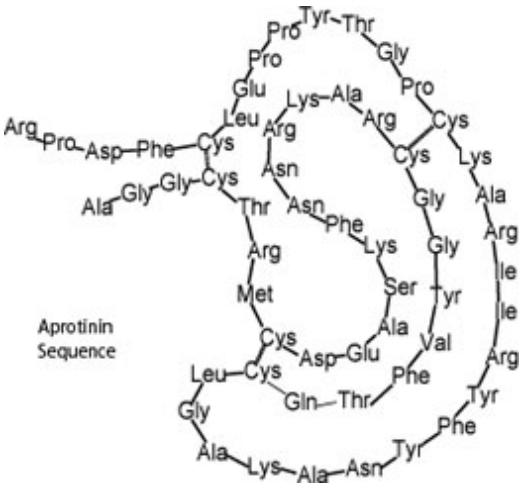

Figure 19: Aprotinin structure as a single peptide chain with three disulfide bonds

The drug aprotinin is a low-molecular-weight protein (6,5 kDa) derived from the bovine pancreas, therefore also known as bovine pancreatic trypsin inhibitor (BPTI) or basic pancreatic trypsin inhibitor. It functions as an antifibrinolytic agent that blocks the activity of trypsin as well as closely related proteolytic enzymes, for example plasmin. It's a broad-spectrum serine protease inhibitor isolated from bovine lung. It acts as a potent, reversible inhibitor of a wide range of serine proteases, including plasmin, kallikreins, and trypsin, by forming tight-binding complexes with their active sites. Its small size and stability make it suitable for *in vitro* and *in vivo* applications.

A study of our laboratory where nephrotic mice were treated with aprotinin, prevented sodium retention and edema completely [38]. This finding provides strong evidence that ENaC activation by proteasuria plays an essential role, and also proposes a promising treatment by targeting ENaC in sodium retention and edema in NS. However, aprotinin is a broad-spectrum inhibitor of serine protease and has strong side-effects for animals and patients [76]. Therefore, the optimal treatment would be targeting the specific over-filtered serine protease(s) responsible for ENaC activation in NS.

1.5.2 AEBSF

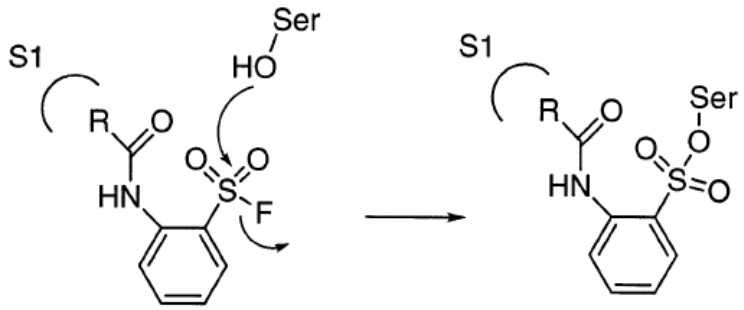

AEBSF (4-(2-Aminoethyl)benzenesulfonyl fluoride hydrochloride) is a water-soluble, irreversible serine protease inhibitor [77]. It specifically targets the active site serine residue of trypsin-like serine proteases, such as plasmin, thrombin, and kallikreins. AEBSF acts through a nucleophilic substitution mechanism. Its sulfonyl fluoride group ($–SO_2F$) reacts with the hydroxyl group of the catalytic serine residue in the active site of serine proteases, forming a stable sulfonyl-enzyme complex that permanently inactivates the enzyme.

Unlike aprotinin, AEBSF is a small molecule inhibitor that does not compete with protein substrates, making it ideal for functional assays and pull-down experiments. Its primary amino group ($–CH_2CH_2NH_2$) allows for directed coupling to NHS-activated surfaces, making it highly suitable for affinity purification applications. In our study, AEBSF was covalently coupled to magnetic beads to selectively capture and identify active serine proteases from nephrotic urine samples in pull-down proteomics experiments. In the functional protease activity profiling, it's a part of a class-specific inhibitor cocktail (alongside E-64, pepstatin A, and EDTA). This cocktail was added to urine samples incubated with the FRET-based pentapeptide substrate library. The reduction in fluorescence signal upon AEBSF addition directly quantified the contribution of serine proteases to the total urinary proteolytic activity.

1.5.3 E-64

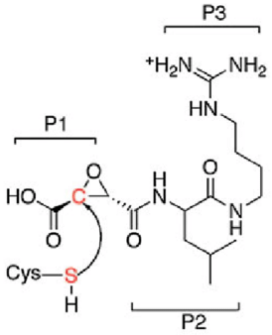

E-64 (N-(trans-Epoxysuccinyl)-L-leucine 4-guanidinobutylamide) is a potent, irreversible inhibitor of cysteine proteases [78, 79]. Its inhibitory action is based on the highly reactive epoxysuccinyl group, which forms a stable covalent thioether bond with the nucleophilic thiol group of the active site cysteine residue. By this mechanism, E-64 inactivates the enzyme permanently, in contrast to reversible inhibitors that only compete transiently for substrate binding.

In the experimental inhibitor cocktail, E-64 was used to measure the activity of cysteine proteases, such as cathepsins, which may be present in nephrotic urine due to inflammatory processes. Its irreversible mode of inhibition also allows for cumulative blockade of protease activity, which is advantageous when assessing the maximal inhibitory potential against cysteine proteases in complex mixtures such as urine samples. It also does not inhibit serine, aspartic, or metalloproteases, thereby ensuring high selectivity and minimizing off-target effects in complex biological samples.

1.5.4 Pepstatin A

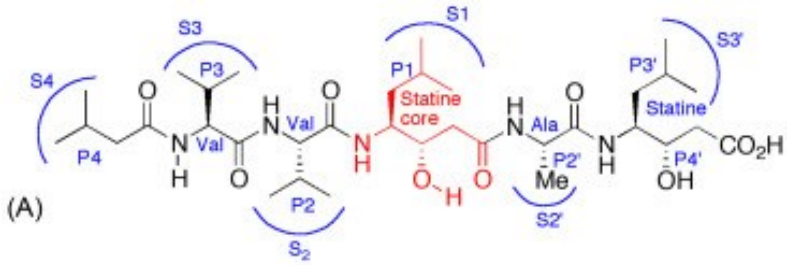

Pepstatin A is a highly specific and potent inhibitor of aspartic proteases, including pepsin, cathepsin D, and renin [80]. Structurally, it is a pentapeptide that contains the unusual amino acid statine, which mimics the transition state of peptide bond hydrolysis catalyzed by aspartic proteases. By occupying the active site in a stoichiometric fashion,

Pepstatin A prevents substrate access and thereby blocks proteolytic activity with high efficiency.

In the present study, its inclusion in the inhibitor cocktail ensured that proteolytic activity attributable to aspartic proteases was effectively blocked and its ratio to the total protease accitvity was calculated.

1.5.5 EDTA

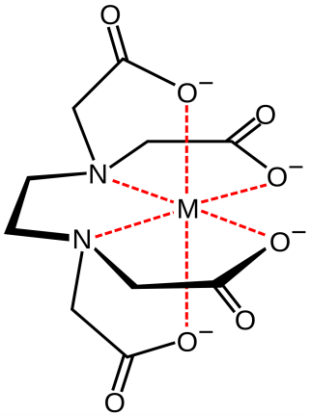

EDTA (Ethylenediaminetetraacetic acid) is a chelating agent that inhibits metalloproteases by binding essential divalent cations, such as Zn^{2+}, Ca^{2+}, and Mg^{2+}, required for their catalytic activity [81]. The removal of these metal ions leads to conformational changes in the active site, thereby preventing proteolytic cleavage of peptide bonds. EDTA effectively inactivates a broad range of metalloproteases, including matrix metalloproteinases (MMPs) and neprilysin.

In the context of the used inhibitor cocktail, EDTA served to specifically suppress metalloprotease-driven activity, to measure any contribution from metalloproteases to the total proteolytic activity.

1.6 Research aims:

So far, comprehensive and systematic information on urinary proteases in nephrotic syndrome were limited. In particular, data about their abundance, enzymatic activity, protease class specificity and molecular identity are still incomplete. To address this lack, the urinary protease landscape in nephrotic syndrome was examined in different comprehensive methods, using samples obtained from both human patients and mouse models with experimental nephrotic syndrome. First, the total and class-specific protease

activity is determined by an universal five amino acdid long peptide substrate library with flanked FRET pair (Mca (7-methoxycoumarin-4-acetamide) as a fluorophore and Dnp (dinitrophenyl) acting as a quencher) and the use of protease class-specific inhibitors.

The combination of the inhibitors in the cocktail, AEBSF for serine proteases, E-64 for cysteine proteases, pepstatin A for aspartic proteases and EDTA for metalloproteases, enables to quantify the class-specific protease activities in nephrotic urine. By comparing the total proteolytic activity in the absence of inhibitors to the residual activity in the presence of the cocktail or individual inhibitors, the observed enzymatic activity could be attributed to specific protease classes. This approach is essential to determine which protease classes contribute most significantly to proteasuria in nephrotic syndrome and to identify the specific protein groups from which pathways and cascades that are responsible for the observed enzymatic activity.

In another step, efforts were made to identify the identity of the urinary proteases in healthy and nephrotic humans and mice alike. To this end, a proteomic studies were done with a hypothesis-free (so-called shotgun method) and using probes such as the Kunitz-domain of aprotinin or AEBSF to pull-down proteases of interest.

The expression of several identified serine proteases were validated in urine and plasma samples by western blots, to see whether they are actually cleaved to their active form with the corresponding lower bands, often as heavy and light chains, and to which extent they appeared compared to the higher full length zymogen band and lower, inactive degradation product bands.

Finally, using peptide representing the region of the extracellular proteolysis of g-ENaC, specificity of the aprotinin sensitive proteolytic activity was investigated by the incubation of urine samples with the physiological γ-ENaC section for the second cleavage, with individually synthesized activity substrates which have tags of AMCA/AMC.

2 Materials & Methods

2.1 Collection of urinary samples from nephrotic subjects and mice

Spot urine samples were obtained from patients who showed previously untreated acute nephrotic syndrome at our university hospital from 2016 to 2017. The clinical features of these patients and the underlying causes of their nephrotic syndrome are listed in Table 1. The primary concerns were edema and body weight increase which are typical signs of increased sodium retention. The overhydration was assessed from each patient by bioimpedance spectroscopy using a body composition monitor (Fresenius) [58, 82]. Spot urine samples from healthy persons were also taken for comparison. The study followed the principles of the Declaration of Helsinki and was approved by the local ethics committee of the University of Tuebingen (259/2012MPG23). In a second cohort, spot urine samples from 3-month-old129S1/SvImJ wildtype mice were collected where experimental nephrotic syndrome was induced. In this mouse model, the nephrotoxic substance doxorubicin damages the glomerular endothelium and podocytes. This leads to proteinuria, hypoproteinemia and renal sodium retention [39, 45, 83]. For this purpose, spot urine samples were collected by bladder massage before doxorubicin injection and again 8 days after it when proteinuria had reached its maximum, accompanied by high sodium retention. All the mouse experiments followed the National Institutes of Health Guide for the Care and Use of Laboratory Animals and the German law for the welfare of animals and received consent from local authorities (Regierungspraesidium Tuebingen, approval number M5/16).

In addition, urine samples from two previously published mouse studies of experimental nephrotic syndrome were analyzed. In one model, nephrotic syndrome was induced by doxorubicin treatment in wild-type 129S1/SvImJ mice [68]. In the second model, podocin deficiency (encoded by Nphs2) was induced in B6 mice, either with or without additional plasminogen deficiency (B6-$Nphs2^{\Delta ipod}$ *and* B6-$Nphs2^{\Delta ipod}$ * $Plg^{-/-}$, respectively) [69]. Spot urine samples were obtained by bladder massage, collected before induction and between day 5 and 8 thereafter, a time window when proteinuria peaked with very high renal sodium retention.

Table 1: Characteristics of the healthy persons and nephrotic patients

Overhydration was determined using bioimpedance spectroscopy (BCM, Fresenius Medical Care, Germany, normal value 0±1 L/1.73m²). Medians with interquartile range. n.d. not determined, n.a. not applicable. BMI body mass index, MDRD-GFR glomerular filtration rate estimated from the Modification in Renal Diet study [84].

	healthy persons (n=10)	patients with acute nephrotic syndrome (n=10)
median age, years	43 (29; 53)	58 (39; 70)
gender distribution	50% ♀ / 50% ♂	40% ♀ / 60% ♂
BMI, kg /m²	22.7 (20.1; 24.1)	25.2 (24.1; 30.0)
MDRD-GFR, mL/min/ 1.73m2	>60	50 (17; 58)
albuminuria, mg /g crea	<20	7224 (4874; 9484)
edema	absent	present in 9/10
overhydration (OH), L/1.73m2	n.d.	+5.2 (+2.5; +6.5)
diagnoses	n.a.	diabetic-hypertensive nephropathy (n=4), minimal change glomerulopathy/focal-segmental glomerulosclerosis (n=4), membranous glomerulonephritis (n=1), immune complex glomerulonephritis (n=1)

2.2 General quantitaive measurements

2.2.1 Bradford protein assay

Urine samples were measured undiluted (before induction of NS) and were diluted 10-20 folds during increased proteinuria. Undiluted/diluted urine (2 µL) was added into a 1ml 1x Bradford working solution (Bio-Rad Laboratories, Germany) after dilution of the 5x stock solution with distilled water (dH2O) and was incubated at room temperature (RT) for 5 minutes. Absorbance was measured with a photometer ("GeneQuant pro UV/Vis Spectrophotometer" from Biochrom) at 595 nm. The photometer was calibrated with standard concentrations of bovine serum albumin (BSA), from 1-10 mg/ml. Distilled water (dH2O) was used as blank control. The ratio of urinary protein and urinary creatinine (urinary protein [mg/mL]/ creatinine [mg/dL]) was used as the parameter of proteinuria evaluation [mg/mg crea].

2.2.2 Creatinine Determination

The creatinine in urine samples was determined by using a creatinine kit (LT-CR 0121) from LT-SYS® (Labor + Technik) according to the Jaffé method in a modified form without protein depletion [122]. It's a kinetic color reaction in which creatinine forms a deep yellow complex with picric acid in the alkaline pH range. By determining the absorbance, it is possible to calculate the creatinine concentration, since it is proportional to the increase in absorbance in relation to the initial value.

10 µl of the sample/standard/dH_2O blank were mixed with 200 µl of the working solution in a 1 cm cuvette and immediately measured at 492 nm on a 96-well microtiter plate with an ELISA reader. The second measurement took place after an 8-minute incubation time. Two standard values and two blank values were determined for each series of measurements. For the handling, a multi-channel pipette was used for the addition of the working solution and 4-6 standard values and blank values should be determined.

The creatinine concentration was calculated from the respective absorbance differences as follows:

$$\Delta_{Absorption} = Absorption_{(t=8min)} - Absorption_{(t=0min)}$$

$$C_{Creatinine}[mg/dl] = (\Delta \text{Sample} - \Delta \text{Zero Value}) / (\Delta_{Standard} - \Delta \text{Zero Value}) * C_{Standard} * \text{Dilution Factor}$$

Since the test used is only linear up to a concentration of 300mg/dL in urine, higher concentrations had to be diluted with dH_2O and the dilution factor must be included in the calculation. According to the manufacturer protocol, the lower limit of detection is 0.03. For urine samples, a 1:20 dilution was used for the most urine samples. Only in the case of very low concentrations of creatinine in the urine (with an absorption ≤ 0.18), an 1:10 dilution was prepared and the measurement repeated.

2.3 Determination of urinary protease activity

The methods in this section are based on the first-author publication "Proteasuria in nephrotic syndrome-quantification and proteomic profiling" [68]

A biochemical assay was developed to quantify protease activity in urinary samples using a pentapeptide substrate library comprising 19^5 distinct peptides, collectively representing up to 2.47 million possible sequence variants (P-Check, Panatecs, Germany, Figure 20). This library was originally designed for the highly sensitive detection of protease impurities in protein-based raw materials employed for diagnostic assays [85]. Each peptide was labeled with the fluorophore MCA (7-methoxycoumarin-4-acetamide) and the quencher DNP (dinitrophenyl), thereby forming a FRET (fluorescence resonance energy transfer) pair that generates a fluorescent signal upon proteolytic cleavage (excitation/emission: 320 nm/405 nm). The complete substrate structure was defined as MCA-X-X-X-X-X-Lys(DNP)-D-Arg-NH_2, with X representing any of the 19 amino acids except cysteine. MALDI-TOF mass spectrometry determined an average molecular weight of approximately 1140 Da for the substrate.

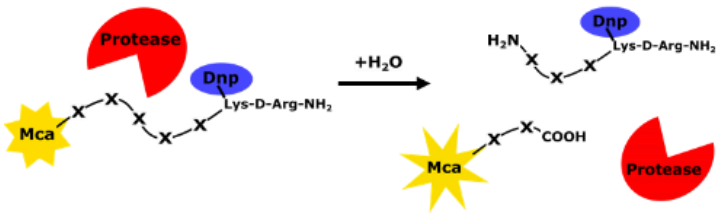

Figure 20: Reaction scheme of the universal peptide substrate library by any protease modified from first-authorship publication [68]

The substrate was designed to include nearly all possible combinations of a five–amino acid sequence, referred to as X. Each substrate included a FRET pair, consisting of Mca (7-methoxycoumarin-4-acetamide) as the fluorescent donor and Dnp (dinitrophenyl) serving as the

quencher. Proteolytic cleavage at any amide bond by a protease results in fluorescence emission of Mca at 405 nm.

The substrate library was prepared at a concentration of 1 mg/mL (877 µM) by dissolving it in 20 % DMSO. For the quantification of urinary protease activity, 20 µL of healthy or nephrotic human urine and 5 µL of diluted mouse urine (1:2 for healthy and 1:10 for nephrotic samples) were incubated with 10 µL of the substrate library, 6.5 µL of 10 % sodium azide to achieve a final concentration of 10 mM, and TBS buffer (25 mM Tris, 150 mM NaCl, pH 7.2) in a total volume of 100 µL at 37 °C for 48 h.
Fluorescence was recorded using a microplate reader at an excitation wavelength of 320 nm and emission at 405 nm (gain 80, Tecan Spark 10M). Protease activity was determined by comparing the fluorescence signal of samples without inhibitors to those treated with an inhibitor cocktail containing blockers of serine proteases (AEBSF, final concentration 2 mM for human and 1 mM for mouse samples), cysteine proteases (E-64, 56 µM), aspartic proteases (pepstatin A, 7.29 µM for human and 0.24 µM for mouse samples), and metalloproteases (EDTA, 8.97 µM). This inhibition-based approach proved more effective at suppressing total protease activity than thermal inactivation at 90 °C for 10 min.
Class-specific activity was calculated by comparing samples incubated with a single inhibitor, either one component of the inhibitor cocktail or the serine protease inhibitor aprotinin (15.36 µM), to untreated controls. Protease activity was measured in two independent batches of samples and substrates, and mean values were used for analysis. Finally, activities were normalized to urinary creatinine concentrations and expressed in relative units (1 RU = 1000 relative fluorescence units per mg creatinine).

2.4 Preparation of samples for mass spectrometry

The methods in this section are based on the first-author publication “Proteasuria in nephrotic syndrome-quantification and proteomic profiling” [68], except for the aprotinin approach in section 2.4.2.2

2.4.1 Non-targeted shotgun approach

Shotgun proteomics label-free quantification workflow: During sample preparation, proteins were extracted from biological samples and subsequently digested into peptides. The resulting complex peptide mixture was then separated using an HPLC system coupled online to a mass spectrometer. In the mass spectrometer, ionized peptides were resolved based on their mass-to-charge ratio. In a typical liquid chromatography–mass spectrometry (LC–MS) experiment, thousands of MS spectra were recorded. For quantification of peptide and protein abundances across samples, peptide elution profiles were detected and compared with corresponding peptides from other LC–MS runs. Finally, label-free quantification data were processed, statistically analyzed, and visualized using dedicated software tools.

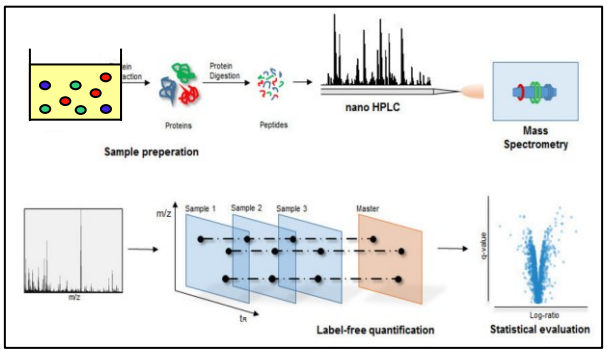

Figure 21: MS shotgun workflow from sample preparation to statistical evaluation [86].

Human urine samples containing 20 µg of total protein and mouse urine samples with 6 µg of total protein were precipitated with pre-cooled acetone at −20 °C for one hour. The precipitated proteins were pelleted by centrifugation at 15,000 g for 10 min, and the resulting pellets were air-dried for 30 min following removal of residual acetone. Each pellet was then resuspended in 30 µL of 50 mM ammonium bicarbonate (ABC, Sigma-Aldrich) supplemented with 4 µL of RapiGest (Waters). Subsequently, 1 µL of 100 mM dithiothreitol (DTT, Merck) was added, and samples were incubated at 60 °C for 10 min. Reduction was followed by alkylation with 1 µL of 300 mM 2-iodoacetamide (IAA, Merck) for 30 min at room temperature in the dark. Prior to overnight digestion at 37 °C, 1 µL of sequencing-grade trypsin (Serva, 0.5 µg/µL) was added. The reaction was terminated by addition of trifluoroacetic acid to a final concentration of 5 %. The acidified mixtures were centrifuged in polypropylene tubes with bottom springs (200 µL, SUPELCO) at 16,000 g for 15 min, and the resulting clear supernatants were collected for peptide purification prior to mass spectrometric analysis.

2.4.2 Serine protease purification by immobilized AEBSF/Aprotinin (pull down proteomics)

2.4.2.1 AEBSF approach

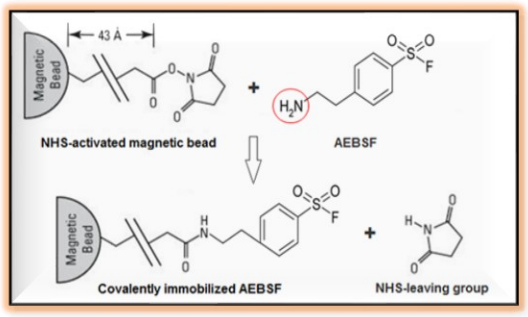

Figure 22: AEBSF scheme for coupling on magnetic beads (modified from company website [87])

To capture all active serine proteases covalently, AEBSF was immobilized via its primary amino group on NHS-activated magnetic beads (#88826, Pierce, Thermo Scientific) following the manufacturer's protocol for washing steps and solvent volumes. Coupling was carried out using an excess concentration of AEBSF (33.3 mM in PBS, 1 µL reagent per µL beads, 25 µL beads per subsequent urine sample) after bead activation with 1 mM HCl. The reaction proceeded for 1 hour at room temperature under continuous rotation. For negative controls, beads were incubated only with the solvent PBS instead of dissolved AEBSF.

Following coupling, the beads were washed sequentially with 0.1 M glycine (pH 2.0) and ultrapure HPLC water, after that quenched for 2 hours with 3 M ethanolamine (pH 9.0) to block remaining NHS groups and prevent nonspecific protein binding. Afterward, they were washed again with HPLC water and PBS and resuspended in PBS for subsequent use.

Prepared beads were incubated with urine samples for 30 min at room temperature on a rotating wheel. Each sample was diluted in IP Lysis/Wash Buffer (#88828, Pierce, Thermo Scientific) to a total volume of 500 µL. Protein input varied depending on sample availability and prior optimization experiments, ranging from 5–20 µg for healthy urine samples and 100–1000 µg for nephrotic urine samples.

2.4.2.2 Aprotinin approach

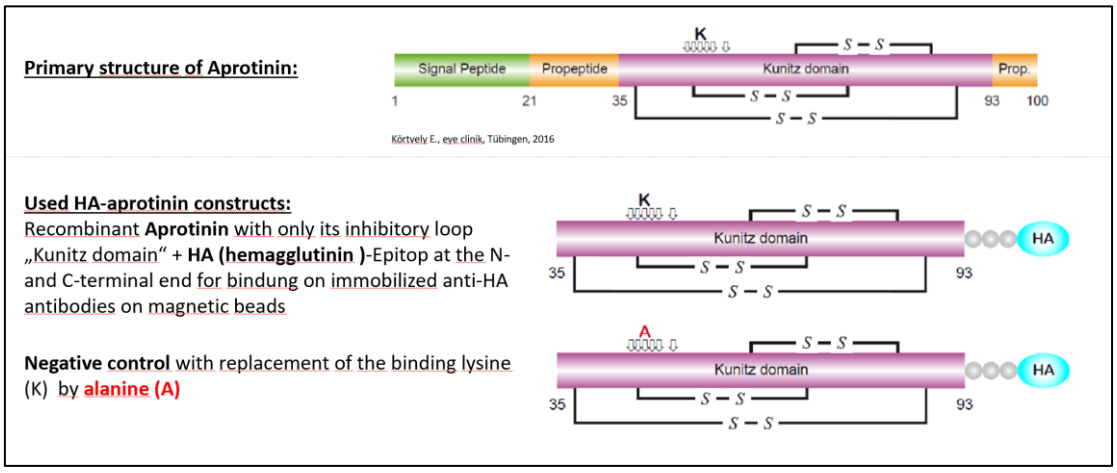

Figure 23: Schematic representation of the strategy for HA (hemagglutinin)-tag labelling of aprotinin

(A) Aprotinin as encoded by the corresponding gene of the house bark. Aprotinin is stabilized by three disulphide bridges. Arrows show the localisation of amino acids that are particularly important for the inhibitory function. Of central importance for the inhibitory effect is the amino acid residue lysine 50 [K]. The so-called Kunitz domain binds to the catalytic centre of the protease and thereby prevents the cleavage of the corresponding protease substrates. This binding is strong enough (Kd for many serine proteases in the nanomolar range) that it can also be used for the purification of inhibitor-protease complexes.

(B) Positive probe: The mature protein consists exclusively of the inhibitory loop (amino acids 35 to 93). An HA epitope is added to the construct expressed in E. coli at the C-terminus, which allows the protein (and the proteases bound to it) to be isolated from urine by immunoprecipitation. The inhibitor and the tag are linked by a movable "hinge sequence", so the tag, or epitope, remains readily accessible to anti-HA antibodies.

(C) Negative probe. This construct is almost identical to the previous one and serves as a negative control. It contains a point mutation (K A) at the critical site that leads to dysfunction of the inhibitor."

25 µL of Pierce Anti-HA magnetic beads were used per urine sample. Prior to sample incubation, the beads were preincubated with 2 µg of aprotinin probe. The protein amount was adjusted based on the sample type: for healthy samples, 5-50 µg of protein was used, whereas for nephrotic samples, 500 µg of protein was applied. The samples were incubated with the prepared beads for 60 minutes at room temperature on a rotating wheel.

2.4.3 Common steps of AEBSF/Aprotinin protocol

After washing the beads with PBS, the bound proteins were pre-digested and released by trypsin treatment following the protocol of Turriziani et al. [88]. For each sample, 60 µL of trypsin solution (5 µg/mL in urea buffer containing 2 M urea and 50 mM Tris–HCl, pH 7.5) were added, and digestion was carried out for 30 min in a thermomixer at 27 °C and 800 rpm. The resulting supernatant was separated from the beads, which were subsequently washed twice with 25 µL of 1 mM DTT in urea buffer. Both wash fractions were combined with the initial trypsin solution, and the digestion was continued overnight at room temperature without agitation. The following day, 20 µL of IAA were added for alkylation and incubated for 30 min in the dark. The reaction was terminated by addition of 1 µL TFA.

The resulting peptide mixtures were desalted and purified using C18 StageTips (#SP301, 200 µL tip, Thermo Scientific). Tips were activated with 20 µL of 80 % acetonitrile containing 5 % TFA (80/5 solution) and equilibrated with 20 µL of 0/5 solution before sample loading. Peptide solutions were applied in 40 µL units, washed with 20 µL of 0/5 solution, and eluted sequentially with 20 µL of 50/0 and 20 µL of 80/5 solution. The combined eluates were concentrated to a final volume of 5 µL using a SpeedVac concentrator.

LC–MS/MS analysis was performed on a NanoRSLC 3000 HPLC system (Dionex) coupled via a nano-spray ion source to a Q Exactive Plus mass spectrometer (Thermo Fisher Scientific). The trypsin digested peptides were automatically injected and loaded at a flow rate of 6 µL min^{-1} in 98 % buffer C (0.1 % TFA in HPLC-grade water) and 2 % buffer B (80 % acetonitrile and 0.08 % formic acid in HPLC-grade water) onto a nanotrap column (75 µm i.d. × 2 cm, Acclaim PepMap 100 C18, 3 µm, 100 Å; Dionex). After 5 min, peptides were eluted and separated on the analytical column (75 µm i.d. × 25 cm, Acclaim PepMap RSLC C18, 2 µm, 100 Å; Dionex) using a linear gradient from 2 % to 35 % buffer B in buffer A (2 % acetonitrile and 0.1 % formic acid in HPLC-grade water) at 300 nL min^{-1} over 82 min, followed by a brief gradient from 35 % to 95 % buffer B within 5 min.

The eluted peptides were analyzed on the Q Exactive Plus in data-dependent mode. Survey scans were acquired from m/z 335–1500 at a resolution of 70,000, and the ten most intense precursor ions exceeding 10,000 counts and carrying at least two charges

were selected for HCD fragmentation in the Orbitrap. Fragment spectra were recorded at 17,500 resolution with a normalized collision energy of 26. The lock-mass option was enabled and set to m/z 445.12002 [89]. Each precursor ion selected for fragmentation was dynamically excluded for 20 s to avoid repeated analysis.

2.5 Statistical analysis of proteomic data

The calculations in this section are based on the first-author publication "Proteasuria in nephrotic syndrome-quantification and proteomic profiling" [68]

Data following a normal distribution were expressed as arithmetic means with standard error, whereas non-normally distributed data were presented as geometric means with interquartile ranges. Statistical differences between healthy and nephrotic groups were evaluated using the Wilcoxon rank-sum test.

Protein identification and label-free quantification (LFQ) were carried out using MaxQuant (version 1.6.1.0). Trypsin/P was defined as the proteolytic enzyme, and peptide as well as protein false-discovery rates were set to 1 %. Only unique peptides were considered for quantification. Cysteine carbamidomethylation was specified as a fixed modification, while methionine oxidation and protein N-terminal acetylation were included as variable modifications. One missed cleavage per peptide was allowed. The initial precursor ion mass tolerance was set to 6 ppm, with a enabled first search tolerance of 10 ppm. Fragment ion mass tolerance was set to 0.5 Da. Peptide and protein identification was performed against the SwissProt proteome database (Release 2014_04) for human samples and the UniProt proteome database (Release 2018_01, ID UP000000589) for mouse samples. Common contaminants such as keratins were automatically detected by searching against the contaminant database. For protein quantification, only unique peptides with a minimum of two per protein and a length of at least seven amino acids were accepted. LFQ settings included a minimum LFQ count of 4 and activation of the "re-quantify" option. Matching between runs was set with a time window of 0.7 min, and the fast LFQ option was disabled.

Statistical analysis of LFQ data was performed with Perseus software (version 1.6.2.3, http://www.perseus-framework.org. Datasets were first filtered to remove potential contaminants, peptides identified only by site, or reverse sequences. For quantitative

analysis, proteins were retained only if valid LFQ values were available in at least half of the samples (≥6 of 10 human samples and ≥2 of 4 mouse samples for AEBSF purification, or ≥3 of 6 for acetone purification). Missing values after filtering were imputed from a normal distribution (width = 0.8, downshift = 1.8) across the entire matrix. Significantly enriched proteases were determined using volcano plot analysis (FDR = 0.05, s_0 = 0.1). Proteases were identified according to EC classification 3.4.x.x for peptidases acting on peptide bonds, annotated with enzymatic information from UniProt, and categorized based on their catalytic residues (serine, threonine, cysteine, aspartic, glutamic, and metallo-peptidases).

To analyze potential normalization effects within LFQ quantification, the corresponding raw intensity values (extracted ion current, XIC) from the same MaxQuant calculation runs were analyzed in parallel using identical volcano plot settings. Additional MaxQuant runs were performed using LFQ values without normalization.

2.6 Western Blots of plasma/urinary/kidney proteases

2.6.1 SDS-PAGE (1D gels):

The gel chamber used was the "Mini-PROTEAN® Tetra Cell" and the power supply utilized the "PowerPac™ Basic Power Supply", both from Bio-Rad. Protein separation was monitored using the "Amersham™ ECL Plex Markers (full range), RPN 850E" from GE Healthcare

Recipe for two 8%/12% gels:

Separation gel (8%/12%):

- 9.2/6.4 mL H2O (Millipore)
- 5.2/8 mL "30% Acrylamide/Bis Solution, 29:1" (Bio-Rad)
- 5.2 mL 1.5 M TRIS (Tris(hydroxymethyl)-aminomethane, pH 8.8)
- 0.2 mL 10% SDS solution
- 0.2 mL 10% APS (Ammonium persulfate) solution
- 0.012/0.008 mL TEMED (Tetramethylethylenediamine)

Stacking gel:

2.8 mL H2O (Millipore)

0.66 mL "30% Acrylamide/Bis Solution, 29:1"

0.5 mL 0.5 M TRIS (pH 6.8)

0.2 mL 10% SDS solution

0.2 mL 10% APS solution

0.008 mL TEMED

Up to two gels can be placed in a single gel chamber. The chamber was filled with 1x Running Buffer and the sample wells were loaded with "samples in 1x Laemmli buffer" Empty wells were filled with 1x Laemmli buffer to ensure a proper running front.

The electrophoresis run was initiated at 200 V for 10 min, with the chamber surrounded by ice to maintain temperature. Gels were allowed to run until the bromophenol blue dye reached the front (~1 hour at 100 V).

2.6.2 Western Blot procedure:

The gel chamber used for blotting was the "Mini Trans-Blot® Cell" from Bio-Rad for Mini-sized gels and the xxx for Midi-size, and the blotting membrane was the Nitrocellulose Blotting Membrane "Amersham™ Protran™ 0.2 µM NC" from GE Healthcare.

The nitrocellulose membrane was soaked in 1x transfer buffer also the swams, blotting paper and the gel before stacking one top to each other. Firstly, the sponges and then the papers are covering gel and membrane from the outside and they are oriented on the transfer plate in that way that the negatively charged proteins runs toward the anode and to the membrane where they are blotted.

Blotting conditions were set to 100 V for 1 hour, with a cold pack and magnetic stirrer to maintain temperature.

2.6.3 Total protein staining, for fluorescence membranes

After protein transfer, membranes were briefly rinsed in distilled water and incubated for 5 min in “Revert™ 700 Total Protein Stain for Western Blot Normalization” solution from LI-COR (15–30 mL, depending on membrane size) with gentle agitation. When processing multiple membranes simultaneously, all were incubated together in the same staining solution to ensure uniform staining. The solution was then completely decanted, and the membranes were washed twice for 30 s each in 15–30 mL of “REVERT Wash Solution”, followed by a short rinse in distilled water. Stained membranes were scanned in the 700 nm channel (intensity 2.0) using the “Odyssey Imaging” scanner system from

LI-COR. After scanning, membranes were briefly rinsed again in water and incubated for up to 10 min in 15–30 mL of "REVERT Reversal Solution" with gentle shaking, or until the visible stain was removed, typically within 5 min. Finally, membranes were washed in distilled water before subsequent membrane blocking.

2.6.4 Blocking and antibody treatment of the blotted membrane

For all subsequent steps, 10-15 mL of each solution was used per membrane.

Free protein binding sites on the membrane were blocked using "Intercept® (TBS) Blocking Buffer" for 1 hour in a closed container on a tumbling shaker. The membrane was then washed with TBS-Tween for 5 minutes on a shaking plate.

Primary antibody incubation with Blocking-Buffer and addition of one of the listed antibodies (the exact amounts are shown in the respective figure captions):

-Plasmin(ogen): „Anti-Plasminogen antibody ab6189" from abcam®; goat polyclonal; recognizes human plasminogen and plasmin

-Plasma kallikrein: „Anti Human Prekallikrein, Clone 20E7" from Molecular® Innovations; mouse monoclonal; recognizes the light chain of human prekallikrein

-Urokinase: "Human Urokinase Plaminogen Activator (uPA) Antibody A7611.1" from Immundiagnostik; goat polyclonal; recognizes human urokinase plasminogen activator (uPA)

Incubation: Overnight, 4 °C, closed box on a tumbling shaker

Washing with TBS-Tween: 4x5 min, strong shaking

Secondary antibody incubation

The membrane was incubated with Blocking Buffer (75 %) and TBS-T (25 %), along with one of the following secondary antibodies:

„Rabbit Anti-Goat IgG H&L (HRP) ab6741" from abcam®; rabbit polyclonal_for plasmin(ogen), urokinase:

"goat anti-mouse IgG-HRP: sc-2005" from Santa Cruz Biotechnology; host goat_ for plasma kallikrein

The incubation was performed for 1 hour in a closed, light-protected container on a tumbling shaker, followed by four washes with TBS-Tween and two washes with TBS, each for 5 minutes

2.6.5 Chemiluminescent/Fluorescent development

As imaging system., the “ChemiDoc™ Touch Imaging System” device from Bio-Rad was used

The TBS-stored membrane was put one a transparent film and overlayed by a 1:1-mixture of the ECL substrate components “Clarity Western Peroxide Reagent” and “Clarity Western Luminol/Enhancer Reagent” (~1.5 ml for completely covering of one membrane), both from the “Clarity™ Western ECL Substrate” kit from Bio-Rad.

After incubation of ~ 5 min, the film with the membrane was put on the chemi/UV/stain-free tray and the tray on the imaging bed of the device. After closure of the transilluminator drawer, different settings were performed on the touch screen: Image size, chemiluminescence application, auto-exposure or manual exposure time and resolution settings. Also one photograph of each membrane was recorded to create an later intermediate overlay in the image editing with the recordings, positioned in the same way. So, the height of the marked ladder bands could be detected. After that, the images could be acquired and exported to USB drive or network system.

For further image editings, Bio-Rad’s “ImageLab™ Touch Software” (removal of red areas which stands for overexposing) was used for chemiluminescene recordings.

For fluorescence recordings, secondary antibodies from LI-COR with IRDye® tags were used, in the standard case for rabbit antibodies the antibody „IRDye® 800CW Donkey anti-Rabbit”, #926-32213 and for goat antibodies the antibody “IRDye® 680LT Donkey anti-Goat IgG, #926-68024. The recording of the membranes were performed by the scanner system “LI-COR Odyssey® Imagers” and the digital images were analyzed and exported by the software “Image Studio™”.

2.7 HPLC separation and fluorescene detection of γ-ENaC by AMCA substrate + quantification of proteolytic activity by AMC substrates

The methods in this section are based on the first-author publication "Proteolytic Activity against the Distal Polybasic Tract of the Gamma Subunit of the Epithelial Sodium Channel ENaC in Nephrotic Urine" [90]

2.7.1 Synthesis of peptides encompassing the polybasic tract of γ-ENaC

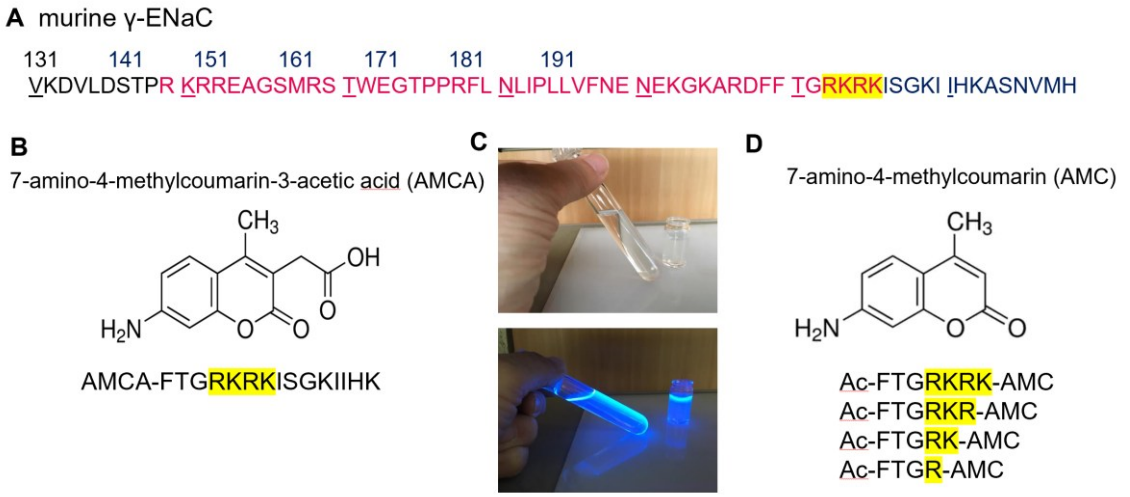

Figure 24: Design of peptide substrates containing the distal polybasic tract of γ-ENaC modified from first-authorship publication [90]

A Amino acid sequence of murine γ-ENaC representing the inhibitory peptide spanning positions 140 to 186. Two polybasic motifs are present, RKRR at positions 140–143 and RKRK at positions 183–186, the latter highlighted in yellow. Cleavage at the proximal polybasic site γ-ENaC^{140_143} represents an intracellular maturation step mediated by the serine protease furin within the Golgi apparatus, whereas cleavage at the distal polybasic site γ-ENaC^{183_186} occurs under physiological conditions and presumably also during pathophysiological states[91].
B Schematic design of a peptide substrate covering amino acid positions 180–194 of murine γ-ENaC, N-terminally labeled with the fluorophore 7-amino-4-methylcoumarin-3-acetic acid (AMCA). Proteolytic cleavage products of this substrate can be detected by HPLC as distinct peaks with different retention times.
C Fluorescence emission of AMCA-FTGRKRKISGKIIHK measured at excitation/emission wavelengths of 350/450 nm.
D Design of peptide substrates with a C-terminally conjugated 7-amino-4-methylcoumarin (AMC), enabling detection of multiple cleavage events within the polybasic tract. Release of free AMC was quantified using a fluorescence plate reader at 380/460 nm.

A fluorescent peptide substrate corresponding to the amino acid sequence 180–194 of murine γ-ENaC (FTGRKRKISGKIIHK) was synthesized by solid-phase peptide

synthesis using the standard Fmoc/tBu protocol [92]. After deprotection of the N-terminal Fmoc group with 20 % piperidine in dimethylformamide (DMF), the fluorophore 7-amino-4-methylcoumarin-3-acetic acid (AMCA) was coupled in threefold molar excess using the N,N′-diisopropylcarbodiimide/HOBt activation method for 3 h in the dark. The resin was subsequently washed with DMF, isopropanol, and diethyl ether and then air-dried. Final deprotection was performed with the mixture TFA/triisopropylsilane/water (92.5:5:2.5) for 2 h at room temperature, and finally the peptide was precipitated in cold diethyl ether.

Acetylated AMC-coupled peptides representing different cleavage sites within the polybasic tract were synthesized in an analogue way. The peptides Fmoc-FTGR, FTGRK, FTGRKR, and FTGRKRK were assembled on acid-labile TCP resin (Intavis, Tübingen, Germany) using the standard Fmoc/tBu protocol with TBTU as coupling reagent [93, 94]. After Fmoc deprotection with 20 % piperidine in DMF, acetylation was carried out using acetic anhydride in pyridine for 30 min. The protected peptides were released from the dried resin by three successive 20-min treatments with dichloromethane/1,1,1,3,3,3-hexafluoro-2-propanol (8:2 v/v) at room temperature. The filtrates were combined, evaporated under reduced pressure, and the resulting oily residues were lyophilized from tert-butanol/water getting white solid substrates: Ac-FTGR-OH (I), Ac-FTGRK-OH (II), Ac-FTGRKR-OH (III), and Ac-FTGRKRK-OH (IV).

Peptides I and III were coupled for 18 h with H-Lys(Boc)-AMC (IRIS Biotech, Germany), while peptides II and IV were coupled with H-Arg-AMC·HCl (IRIS Biotech) in solution using O-benzotriazol-1-yl-N,N,N′,N′-tetramethyluronium tetrafluoroborate and N-methylmorpholine in DMF as the coupling system. After evaporation under vacuum, the oily residues were treated with TFA/triisopropylsilane/water (92.5:5:2.5) for 2 h at room temperature, and the final peptides were precipitated as amorphous solids upon addition of diethyl ether.

Crude AMCA- and AMC-coupled peptides were further purified by preparative reversed-phase HPLC on a Reprosil-Pur Basic C18 column (5 µm, 250 × 10 mm; Dr. Maisch, Tübingen, Germany) using a linear gradient from 0 to 70 % acetonitrile in water containing 0.05 % TFA. Purity was confirmed by analytical RP-HPLC, and peptide identity was verified by electrospray ionization mass spectrometry (ESI-MS) and MALDI-TOF-MS. All peptides exhibited purities of ≥95 % as determined by analytical

HPLC. AMCA-coupled γ-ENaC$_{180–194}$ was dissolved in HPLC-grade water at 1 mg/mL, whereas AMC-coupled peptides were dissolved in 30 µL DMSO and diluted with HPLC water to a final concentration of 2 mg/mL.

2.7.2 Analysis of proteolytic activity against the polybasic tract of γ-ENaC using HPLC and MALDI-TOF

5 µL of human urine or 5 µL of mouse urine (diluted 1:10 in PBS) were incubated with 5 µL of AMCA-coupled γ-ENaC$_{180–194}$ substrate (0.1 µg/mL; corresponding to 50 fmol, diluted 1:10,000 in PBS) in a total volume of 100 µL, adjusted with PBS. Incubations were carried out overnight at 37 °C under gentle agitation. To inhibit serine protease activity, parallel reactions were co-incubated with 5 µL of aprotinin (0.2 mg/mL; stock 2 mg/mL in PBS, diluted 1:10). All reactions were performed in low protein-binding tubes (Sarstedt, Germany). The enzymatic reaction was terminated by addition of 10 µL of 2.5 % TFA.

From each reaction sample, 20 µL of the resulting solution were mixed with 80 µL of solvent A (HPLC-grade water containing 0.055 % TFA) and the full 100 µL were injected loaded on a reversed-phase HPLC column (ReproSil 100 C18, 5 µm, 250 × 2 mm, #r15.96.s2502; Dr. Maisch, Tübingen, Germany) connected to a Merck-Hitachi L-6200 HPLC pump. Separation was achieved using a linear gradient from 95 % solvent A / 5 % solvent B (80 % acetonitrile, 20 % HPLC water, 0.047 % TFA) to 20 % A / 80 % B over 45 min at a flow rate of 3 mL min^{-1}. Fluorescence detection was performed with a Shimadzu RF-10XL detector using excitation at 350 nm and emission at 450 nm, with chromatograms recorded at an attenuation setting of 8.

In addition to the main peak corresponding to the intact substrate, newly emerging peaks appearing at approximately 17–18 min indicated proteolytic cleavage products of varying size. The respective eluate fractions were directly collected for mass determination, and 1 µL per sample was mixed with 1 µL of the matrix substance gentisic acid (2,5-dihydroxybenzoic acid, DHB) on a gold target. The resulting peptide fragments were analyzed by MALDI-TOF-MS using a Reflex™ IV mass spectrometer (Bruker Daltonik, Germany; method scheme shown in Figure 25). Obtained mass spectra were processed with the Mascot Search Results software (Matrix Science) using peptide mass

fingerprinting (PMF) and compared to the calculated masses of the intact substrate and all theoretical cleavage products (see Table 2 of all possible digested fragments).

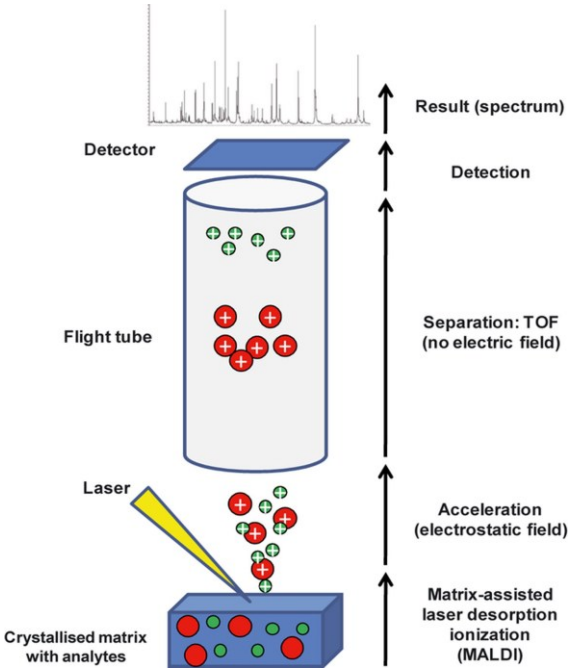

Figure 25: MALDI detection of digested HPLC fragments [95]

Table 2: Masses of the possible digested fragments of the AMCA-FTGRKRKISGKIIHK substrate

AMCA-coupled γ-ENaC fragments	Mass, Da
AMCA-FTGRKRKISGKIIHK (full length)	1983,2
AMCA-FTGRKRKISGKIIH	1855,2
AMCA-FTGRKRKISGKII	1718,1
AMCA-FTGRKRKISGKI	1605,0
AMCA-FTGRKRKISGK	1492,0
AMCA-FTGRKRKISG	1363,9
AMCA-FTGRKRKIS	1306,8
AMCA-FTGRKRKI	1219,8
AMCA-FTGRKRK	1106,7
AMCA-FTGRKR	978,6
AMCA-FTGRK	822,5
AMCA-FTGR	694,4
AMCA-FTG	538,3
AMCA-FT	481,3
AMCA-F	380,3

2.7.3 Quantitation of urinary protease activity against the polybasic tract of γ-ENaC using AMC-coupled substrates

For quantification of urinary protease activity, 5 µL of human urine or 5 µL of diluted mouse urine (1:10 in PBS) were incubated with 5 µL of AMC-coupled substrates (0.2 mg/mL; 1:10 dilution in PBS) and 5 µL of the serine protease inhibitor aprotinin (2 mg/mL in PBS) in a total reaction volume of 100 µL. Incubations were performed in black microtiter plates at 37 °C for 2 h. Fluorescence was recorded on a microplate reader with excitation at 380 nm and emission at 460 nm (gain 80; Tecan Spark 10M, Germany). Aprotinin-sensitive protease activity was calculated as the difference in fluorescence signal between samples incubated without and with aprotinin. Finally, the urinary protease activity values were normalized to urinary creatinine concentration (0.1 × mg/dL) and expressed as relative fluorescence units (RFU).

2.7.4 Data analysis and statistics for AMCA-/AMC-coupled substrates

Data are presented as arithmetic means with standard error. The relative abundance of individual cleavage products was determined by calculating the area under the curve (AUC) for each peak and dividing it by the total chromatographic area of the respective sample. Differences in the mean distribution of cleavage products between healthy and nephrotic groups were assessed using the Chi-squared test. Proteolytic activity differences between native and aprotinin-treated samples were analyzed by paired t-test, while comparisons between healthy and nephrotic groups were performed using an unpaired t-test (see Table 5). Activity values were additionally evaluated by one-sample rank-sum testing.

3 Results

3.1 Total protease activity in healthy and nephrotic urine

The results in this section are based on the first-author publication "Proteasuria in nephrotic syndrome-quantification and proteomic profiling" [68]

3.1.1 Proteinuria and proteasuria in human and mouse urine samples

First, the concentration of proteins in the urine samples was measured to assess the level of proteinuria, which reflects the amount of protein excreted in the urine and which can indicate potential kidney dysfunction. Measuring protein levels in this way provides a direct insight into the severity of protein loss, which is a hallmark of nephrotic syndrome. This measurement was normalized to the creatinine concentration. This normalization process is crucial because it accounts for any differences in urine volume, ensuring that the results remain consistent and comparable across all samples, regardless of individual variations in hydration status or urine output.

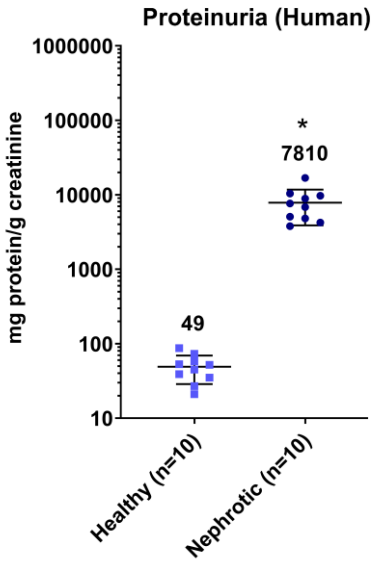

Figure 26: Urinary protein excretion from spot human urine samples normalized for creatinine

modified from first-authorship publication [68]

Arithmetic means ± SEM. * indicates significant difference between healthy and nephrotic samples.

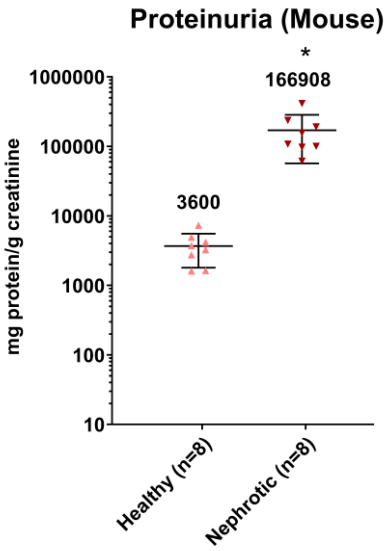

Figure 27: Urinary protein excretion from spot mouse urine samples normalized for creatinine

modified from first-authorship publication [68]

Arithmetic means ± SEM. * indicates significant difference between healthy and nephrotic samples.

There was typically minimal protein excretion in healthy individuals, but in nephrotic syndrome, massive protein loss into the urine could be detected. In the urine samples from 10 patients with acute nephrotic syndrome, proteinuria increased significantly by 159-fold compared to healthy people (Figure 26). In mice, the urinary protein excretion also increased strongly 46-fold from 3600 ± 649 mg/g crea at healthy state to 166,908 ± 39,341 mg/g crea at nephrotic state, on day 8 after doxorubicin induction (Figure 27). The Mann-Whitney-Test was always highly significant.

The reason for this high number is that among the newly arising plasma proteins, albumin and IgG ‘s were by far the most excreted ones which could newly enter the urine as dominant plasma protein due to much higher cut-off range of the damaged filter system. But also new, active proteases entered the filtrate as we can see in the following activity results. The total protease activity was measured with a universal peptide substrate library which comprised a variety of 19^5 different possible pentapeptides.

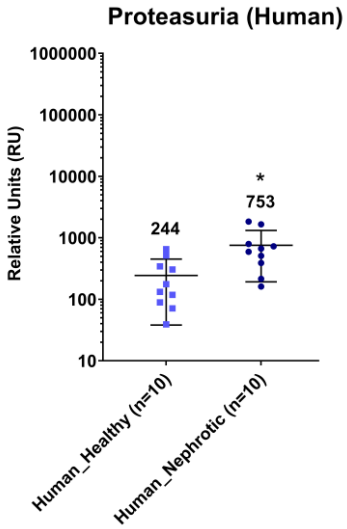

Figure 28: Total urinary protease activity from human spot urine, determined with the universal peptide substrate

modified from first-authorship publication [68]

1 relative unit (RU) = 1000 RFU (relative fluorescence units)/mg creatinine

Arithmetic means ± SEM. * indicates significant difference between healthy and nephrotic samples

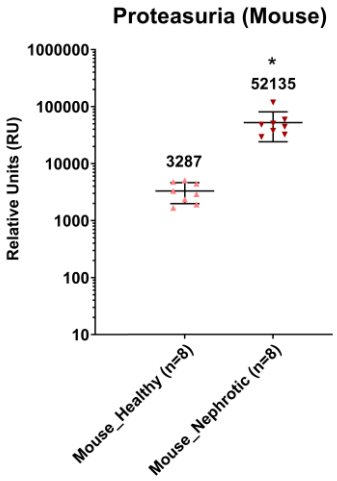

Figure 29: Total urinary protease activity mouse spot urine, determined with the universal peptide substrate

modified from first-authorship publication [68]

1 relative unit (RU) = 1000 RFU (relative fluorescence units)/mg creatinine

Arithmetic means ± SEM. * indicates significant difference between healthy and nephrotic samples

Here, there was also a significant increase from healthy samples to nephrotic by 3.09 fold from 244±65 RU to 753±178 in the mean values of the human samples, and by 15.86 fold in mouse samples from 3287 ± 465 RU at baseline to 52,135 ± 9958 RU in the nephrotic state (Figure 28 + Figure 29). But the increase was not as high as it was expected by the proteinuria results. The presumable reason is that the protease activity was already quite high in the healthy samples because of physiological protease activity like from urokinase and tissue kallikrein, but also many other renal proteases. And as already said, the protein content of nephrotic samples was especially increased by non-enzymatic proteins like albumin and IgG.

3.1.2 Inhibition of specific protease classes

After adding various protease inhibitors specific for different protease classes, the percentage of overall protease activity inhibition and the class specific activity in percentage to the total activty was calculated. To determine this percentage, the measurement considered 100% inhibition as the difference between the total protease activity (observed in the absence of any inhibitors) and the minimal activity remaining when all inhibitors were present. This approach allowed for a standardized calculation, where the inhibitory effect of each class-specific inhibitor could be calculated as percentage share relative to the complete inhibition of the protease activity.

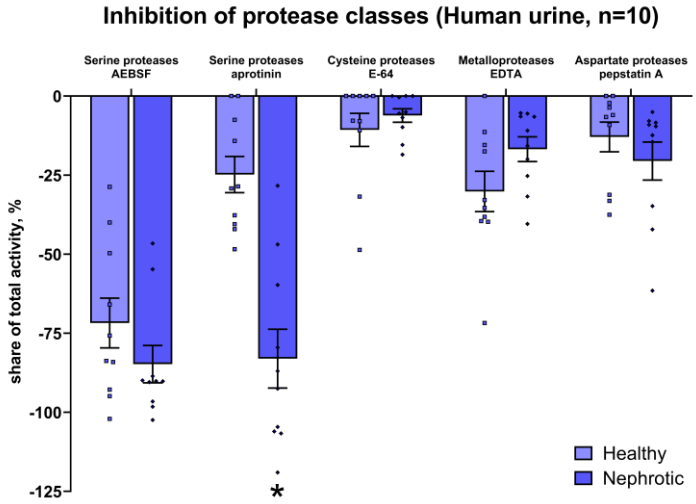

Figure 30: Percentage of inhibition of total protease activity in human urine samples modified from first-authorship publication [68]

Various protease inhibitors specific for different protease classes were used. Arithmetic means ± SEM. * indicates significant difference between healthy and nephrotic samples.

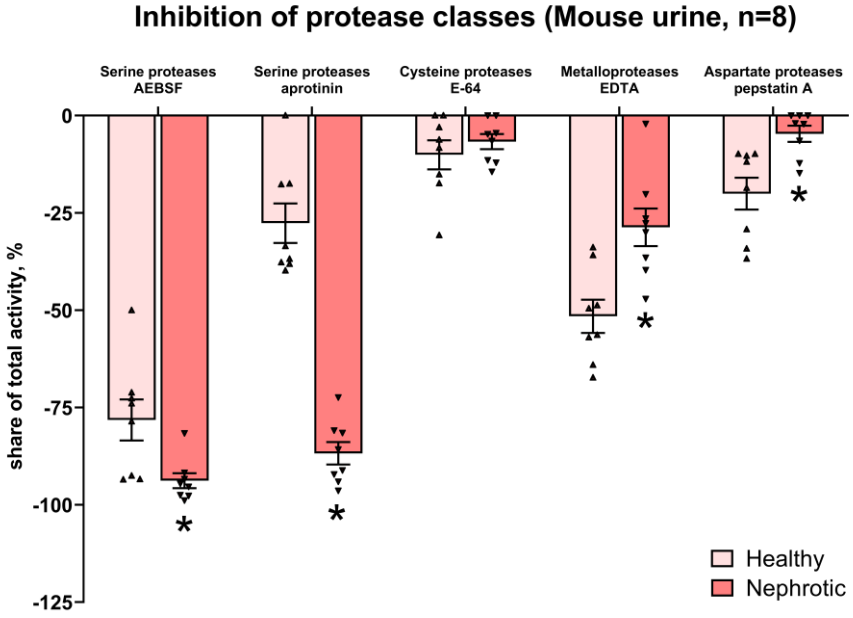

Figure 31: Percentage of inhibition of total protease activity in mouse urine samples modified from first-authorship publication [68]

Various protease inhibitors specific for different protease classes were used. Arithmetic means ± SEM. * indicates significant difference between healthy and nephrotic samples.

In human samples, the mean total activity was 7290 ± 427 in the healthy state and 17114 ± 1121 RFU in the nephrotic state, and in mouse samples 10009 ± 556 (dilution factor 8 = DF 8) and 12999 ±5 32 RFU (DF 40), respectively. The corresponding minimal activities in human samples were 5189 ± 295 (healthy state) and 7666 ± 569 RFU (nephrotic state) and in mouse samples 5844 ± 262 (DF 8) and 3791 ± 137 RFU (DF 40), respectively.

The serine protease inhibitor AEBSF suppressed most of the urinary protease activity in both nephrotic and healthy human samples (85±6% and 72±8%, respectively, Figure 30+ Figure 31). The next strongest effect was measured by EDTA, which blocks metalloproteases through metal ion chelation, with 17±4% and 30±6%, respectively. It tended to have a higher proportion in the healthy state. This was followed by pepstatin A for inhibition of aspartate proteases and E-64 for cysteine proteases, whereby E-64 also

showed a slightly higher share in the healthy samples. The sum of all inhibitor shares exceeded 100%, indicating that some of the inhibitors were highly overlapping.
In healthy urine, the serine protease inhibitor aprotinin reduced the activity only by 25±6%, whereas this fraction markedly increased to 83±9 % in nephrotic urine. This shows that aprotinin specific proteases got a much higher proportion with the newly entered proteases from the plasma.
Similarly in nephrotic mice, AEBSF inhibition represented the largest share of urinary total protease activity, and it was even significantly higher under nephrotic conditions. It was also followed by EDTA, which had a significant higher proportion in the health state, as it could also be seen as a trend in human samples. Aspartate proteases were also present in a significantly higher proportion. As well, the activity of aprotinin-sensitive proteases in nephrotic urine were much higher in a significant way compared to healthy urine samples. The sum of shares exceeded 100 percent again, as it was already observed in the results with human samples, indicating that the inhibitor specificity overlapped.

3.2 Protease identification by proteomics approaches

The results in this section are based on the first-author publication "Proteasuria in nephrotic syndrome-quantification and proteomic profiling" [68], except for the aprotinin approach in section 3.2.2.2

3.2.1 Mass spectrometry analysis of all urinary proteases identified by a non-targeted shotgun approach

3.2.1.1 Visualisation of the distribution of all detected proteins by venn diagrams

All individual proteins, including the proteases, were identified in healthy and nephrotic urine from both humans and mice by tandem mass spectrometry using an unbiased shotgun approach. This comprehensive proteomic analysis enabled the identification of all detectable urinary proteins, including distinct subsets of proteases and serine proteases, across both species and disease states. To provide an initial overview of their distribution, Venn diagrams were generated illustrating the overlap and exclusivity of proteins between healthy and nephrotic samples. These diagrams summarize the total

number of all detected proteins as well as the subset of proteases and serine proteases, thereby giving a first visual insight into the extent of proteomic changes associated with the nephrotic syndrome.

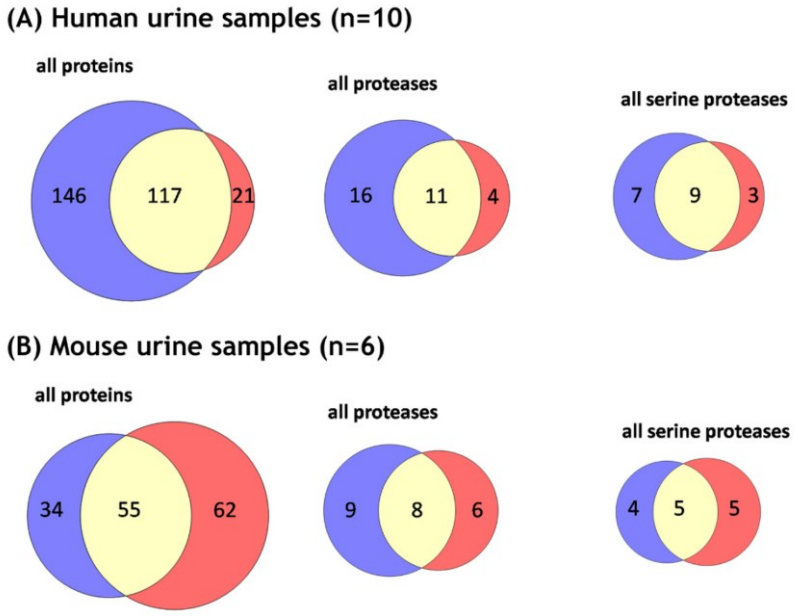

Figure 32: Venn diagrams with amount and distribution of all detected proteins, proteases and serine proteases

adopted from first-authorship publication [68]

in (A) human and (B) murine urine samples in the healthy (blue segments) and nephrotic state (red segments) and the overlapping yellow segments with proteins detected in both sample groups

The illustrated Venn diagrams (Figure 32) are comparing the presence of different proteins and proteases in human and mouse urine samples. Each panel (A and B) presents three Venn diagrams representing different categories: "all proteins," "all proteases," and "all serine proteases. The blue section indicates all proteins and proteases that were predominantly present in urine of healthy human and mouse samples. Red represents the number of proteins and proteases mainly detected in urine of nephrotic samples. Yellow as intersection encodes for the number of proteins and proteases which were expressed in similar quantities in urine of both healthy and nephrotic samples.

In the urine samples of healthy and nephrotic humans, a total of 284 proteins were identified, including 31 proteases of which 19 were serine proteases. In the corresponding

mouse samples, 151 proteins were measured overall, including 23 proteases of which 14 were serine proteases.

Some of these proteases appeared exclusively in only the healthy or nephrotic samples from either humans or mice. In the human urine samples (n=10), out of a total of 284 proteins identified, 146 proteins were exclusive to healthy samples, while 21 were unique to nephrotic samples. A significant number, 117 proteins, were common to both sample types, indicating that a substantial portion of urinary proteins were unaffected by nephrotic conditions. Within the protease subset, 16 proteases were specific to healthy samples, and 4 were unique to nephrotic samples. Eleven proteases were shared between both conditions. The smallest set of all serine proteases included 7 serine proteases specific to healthy samples and 3 unique to nephrotic samples. 9 serine proteases were common to both conditions.

For mouse samples, a total of 151 proteins were identified. Of these, 34 were exclusive to healthy samples, 62 were specific to nephrotic samples, and 55 proteins were shared between both conditions. This larger proportion of nephrotic-specific proteins, compared to human samples, suggests that nephrotic syndrome might induce more significant protein expression changes in mice. In the protease subset, 9 proteases were unique to healthy samples, while 6 were exclusive to nephrotic samples. Only 8 proteases were found in both conditions. In the smallest group, 4 serine proteases were specific to healthy samples, and 5 were unique to nephrotic samples. 5 serine proteases were common across both conditions. This pattern mirrors the human samples, with distinct serine protease profiles associated with nephrotic syndrome.

In general, human samples showed a larger proportion of proteins and proteases that were unaffected by nephrotic conditions, as seen in the overlapping yellow areas. In contrast, mouse samples demonstrated a greater number of nephrotic-specific proteins and proteases, particularly evident in the "all proteins" category. This difference might indicate species-specific responses to nephrotic syndrome, with mouse samples showing a broader protein profile changes. Additionally, both species showed some serine proteases associated with nephrotic conditions, suggesting that these serine proteases could be a sensitive marker for nephrotic syndrome across species.

3.2.1.2 Bioinformatic analysis of aberrantly filtered proteins in nephrotic syndrome using the GO and KEGG databases

Using the Gene Ontology (GO) and Kyoto Encyclopedia of Genes and Genomes (KEGG) databases in the software tool ShinyGO v0.61, the proteins newly appeared in nephrotic urine could then be bioinformatically analyzed for the GO terms with the lowest FDR values (=probability of error) in the three main categories (see Table 3) and the common signaling pathways were examined. The FDR values indicate the probability of false positives in enrichment analysis, where lower FDR values represent higher confidence in the identified pathways.

In human urine, proteins with the GO designation “Acute inflammatory response (n=22)” were most strongly represented in the GO main category “Biological Process”, followed by “Protein activation cascade (n=19)”, “Platelet degranulation (n =18)” and “Complement activation (n=15)”. In mouse urine, the term “Acute inflammatory response” was also present but with a lower significance of 13.73. For mice, the strongest representation in this category was the “Protein activation cascade” with a -log(FDR) of 33.64, higher than the 25.65 value observed in human samples. Other terms such as “Complement activation” and “Regulation of proteolysis” showed relatively similar significance in both species, though slightly less in mice, indicating that while inflammatory and proteolytic responses were significant in both, they appeared to be more prominent in humans.

Under the GO category "Cellular Component", extracellular GO terms dominated, with “Extracellular space” and “Extracellular region part” showing high -log(FDR) values of 37.04 and 35.66, respectively. Interestingly, in mouse samples, these extracellular terms were even more pronounced, with “Extracellular space” reaching 59.67 and “Extracellular region part” 61.13. This indicates that proteins in mouse urine were more strongly associated with extracellular components, which might reflect a higher presence or secretion of extracellular proteins in nephrotic mouse models. Conversely, certain terms, such as "Blood microparticle," were much less represented in mice (7.29) compared to humans (49.69), suggesting species-specific differences in the cellular origin of urine proteins.

In the GO category "Molecular Function", proteins of protease inhibition (n=19) were found most frequently and serine proteases (n=7) as the most common protease class.

Human urine samples showed a high presence of proteins involved in “Endopeptidase inhibitor activity” and related peptidase inhibitor functions, with -log(FDR) values around 21.98. In mice, these inhibitor activities were similarly significant, with values reaching up to 25.00 for "Endopeptidase inhibitor activity" and 24.78 for "Peptidase inhibitor activity." This strong representation in both species suggests a conserved role of protease inhibition in urinary protein profiles related to nephrotic syndrome. Additionally, the term "Serine-type endopeptidase inhibitor activity" was somewhat lower in significance for mice (18.40) compared to humans (20.68), indicating a minor difference in the prevalence of this specific protease class in urinary samples between the species.

Table 3: Dominant GO terms of Biological Process, Cellular Component and Molecular Functions

with -log(FDR), in human and mouse

Biological Process			Cellular Component			Molecular Function		
GO term	-log(FDR) (human)	-log(FDR) (mouse)	GO term	-log(FDR) (human)	-log(FDR) (mouse)	GO term	-log(FDR) (human)	-log(FDR) (mouse)
Acute inflammatory response	26.58	13.73	Blood microparticle	49.69	7.29	Endopeptidase inhibitor activity	21.98	25.00
Protein activation cascade	25.65	33.64	Extracellular organelle	45.03	---	Peptidase inhibitor activity	21.98	24.78
Platelet degranulation	22.59	---	Extracellular exosome	45.03	---	Endopeptidase regulator activity	21.98	24.78
Complement activation	19.79	20.89	Extracellular vesicle	45.03	---	Peptidase regulator activity	20.71	23.36
Negative regulation of endopeptidase activity	19.08	23.05	Extracellular space	37.04	59.67	Serine-type endopeptidase inhibitor activity	20.68	18.40
Regulation of proteolysis	19.08	20.19	Extracellular region part	35.66	61.13	Enzyme inhibitor activity	20.58	21.90
Negative regulation of peptidase activity	18.86	22.60	Extracellular region	31.83	59.04	Enzyme regulator activity	12.65	15.96
Proteolysis	18.00	21.03	Vesicle	30.86	---	Molecular function regulator	8.49	11.29
Regulation of protein activation cascade	17.99	5.46	Collagen-containing extracellular matrix	22.11	13.40	Phosphatidylcholine-sterol O-acyltransferase activator activity	5.39	3.32
Inflammatory response	17.99	12.71	Vesicle lumen	21.63	---	Serine-type endopeptidase activity	5.03	5.46

In the KEGG database analysis, the identified urinary proteins were further assigned to functional signaling and metabolic pathways to determine their potential biological relevance in nephrotic syndrome. The Kyoto Encyclopedia of Genes and Genomes (KEGG) is a comprehensive database that integrates genomic, chemical, and systemic functional information and enables the mapping of proteins to specific biochemical and signaling cascades. Using the bioinformatic software tool “ShinyGO v0.61”, all proteins that newly appeared or were significantly enriched in nephrotic urine were analyzed for pathway enrichment, and the resulting false discovery rate (FDR) values were automatically calculated to assess statistical significance.

Based on this analysis, a strong enrichment of proteins belonging to the complement and coagulation cascades was observed in both human and mouse samples, showing the most significant FDR values of all pathways (FDR = 4.9×10^{-25} for human, FDR = 2.9×10^{-45} for mouse). These pathways were visualized within the KEGG metabolic network using the integrated graph function of ShinyGO, which highlights the detected urinary proteins directly in the canonical KEGG pathway maps (Figure 33). In this graphical representation, the identified proteins were automatically marked in red, thereby allowing immediate visual correlation of detected urinary proteins with their respective positions in the complement and coagulation cascades.

Highly enriched proteins in the nephrotic human samples included plasminogen (PLG) and various complement factors (highlighted in red). A similar picture was found in the mouse samples, with the difference that coagulation factor XII and thrombin were also present and other inhibitors such as complement factor I (CFI) and C4-binding protein (C4BP).

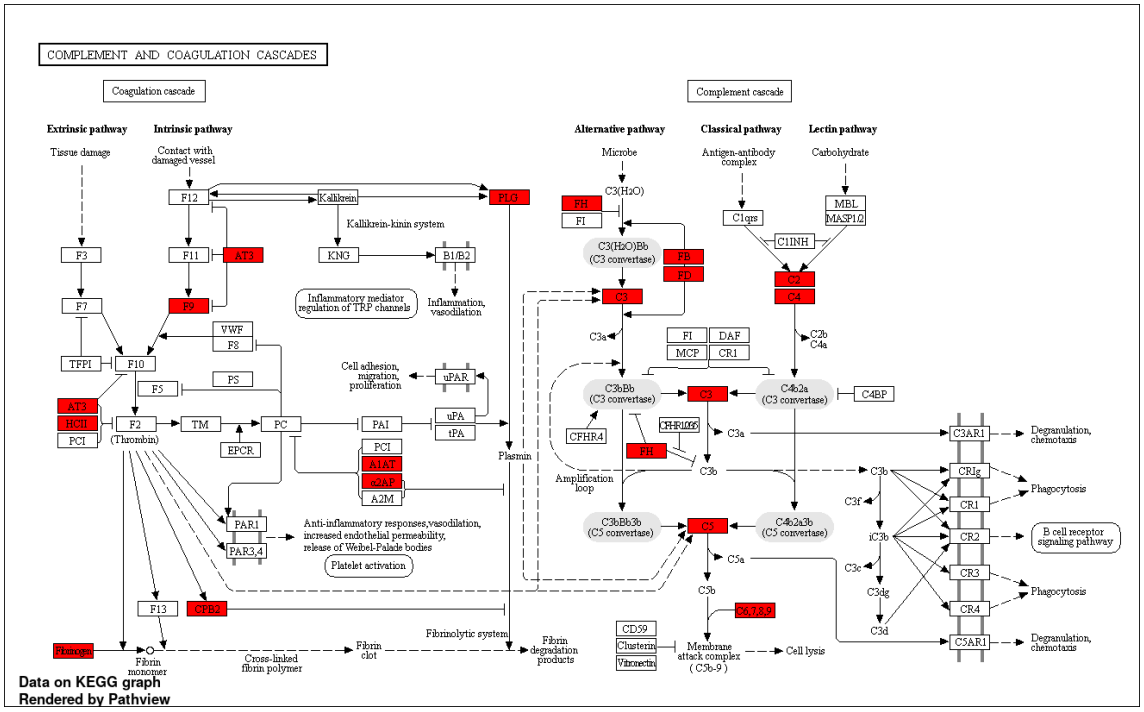

Figure 33: Detected and higlighted proteins in the graph "Complement and Coagulation Cascades", in nephrotic human urine

These proteases might play an important role in the pathophysiological processes underlying nephrotic syndrome. Their increased urinary presence and activity suggest a contribution to both local and systemic inflammatory mechanisms. They also might play an important role in the pathophysiological process of the NS, like proteases in the overactivation of the epithelial sodium channel (ENaC) in the distal tubule, which needs to be validated by targeted experiments, e.g. with knockout mice.

3.2.1.3 Hierarchical clustering of all proteases in human and mouse urine samples

To further investigate more detailed differences in protease expression profiles between healthy and nephrotic conditions, hierarchical clustering was performed on all proteases detected in human and mouse urine samples. This analysis used logarithmically transformed label-free quantification (LFQ) values and Euclidean distance with average linkage to evaluate similarities between the samples. The heatmaps generated from this analysis visually depict the intensity of protease expression on a color scale ranging from green (low intensity) to yellow and red (high intensity), facilitating the identification of protease clusters with similarities in expression patterns associated with health or disease status.

As shown in Figure 34, a clear separation between heathy and nephrotic samples from humans and mice could be observed. Nephrotic samples displayed a prominent group with many high molecular weight proteases, specifically those involved in the coagulation and complement cascades. These proteases, such as plasminogen and prothrombin, are key players in the body's immune response, coagulation, and inflammatory processes, and their upregulation in nephrotic conditions suggests a heightened activation of these pathways as part of the disease pathology. In contrast, healthy samples showed a prevalence of proteins with low molecular weight, including proteases which are locally secreted into the tubule system, such as kallikrein-1, neprilysin and urokinase-type plasminogen activator. These enzymes play essential roles in normal kidney function, including regulation of fluid balance and local tissue remodeling, indicating that their downregulation in nephrotic syndrome might contribute to kidney dysfunction and impaired physiological homeostasis (Figure 34).

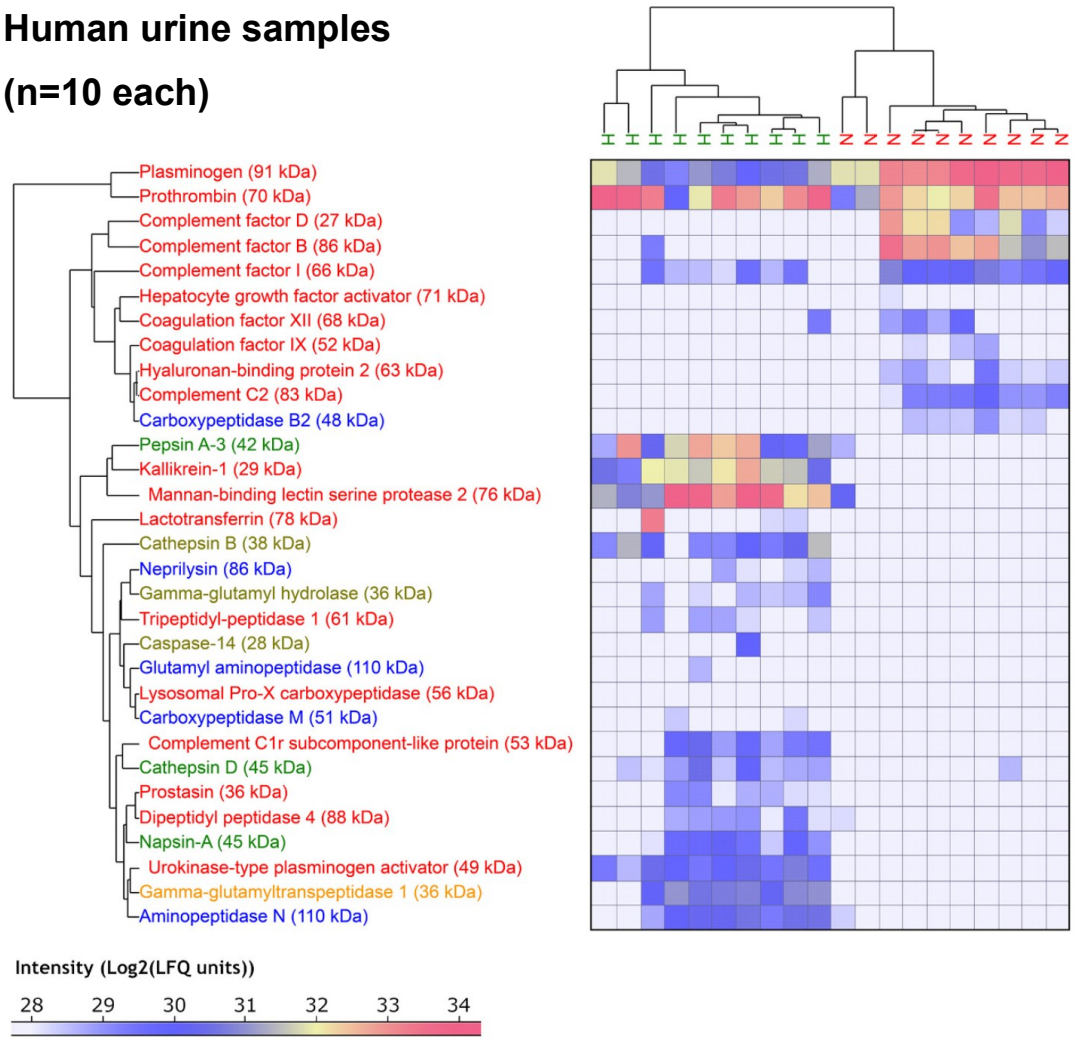

Figure 34: Hierarchical clustering of all proteases in human urine samples (n=10 each, of healthy and nephrotic samples), identified by shotgun approach adopted from first-authorship publication [68]

Serine proteases are highlighted in red, metalloproteases in blue, aspartate proteases in green, cysteine proteases in yellow-green and threonine proteases in orange. Nephrotic samples were characterized by a cluster of high molecular proteases from the coagulation and complement cascade (upper right cluster). In contrast, healthy samples were characterized by proteases with a low molecular weight that are locally expressed (lower left cluster).

H = healthy samples, N = nephrotic samples; intensity values in the legend are shown as log2(LFQ units)

The same analytical method was applied to mouse samples leading to clustering results that showed similar patterns to that observed in the human samples (Figure 35).

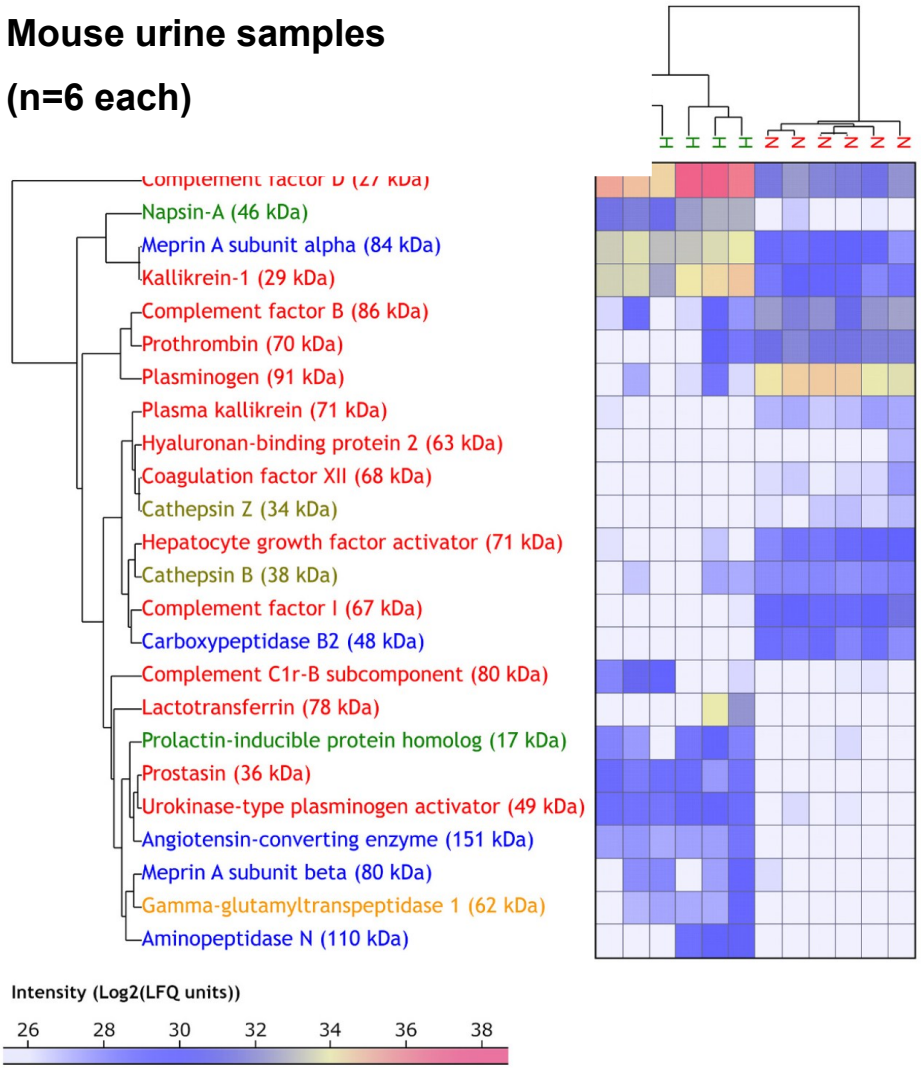

Figure 35: Hierarchical clustering of all proteases in mouse urine samples (n=6 each, of healthy and nephrotic samples), identified by shotgun approach adopted from first-authorship publication [68]

Serine proteases are highlighted in red, metalloproteases in blue, aspartate proteases in green, cysteine proteases in yellow-green and threonine proteases in orange. Nephrotic samples were characterized by a cluster of high molecular proteases from the coagulation and complement cascade (upper right cluster). In contrast, healthy samples were characterized by proteases with a low molecular weight that are locally expressed (lower left cluster).

H = healthy samples, N = nephrotic samples; intensity values in the legend are shown as log2(LFQ units)

Both human and mouse models showed a clear increase in protease activity and high abundance of newly appearing proteases in nephrotic samples compared to the healthy ones. Coagulation proteins like plasminogen and prothrombin, along with complement system proteins, were newly measured in both species, which are involved in immune response, coagulation and protein degradation. This indicates that these processes were heavily affected in nephrotic syndrome. But also proteases involved in protein degradation (e.g., cathepsins, aminopeptidases) were generally upregulated in nephrotic conditions, which suggests an increase in protein breakdown in the kidney.

In both the human and mouse urine samples, there were a few proteases that appear to have higher intensities in the healthy samples compared to the nephrotic samples. This might indicate that these proteases had more active roles in normal physiological processes, or their activity could be suppressed or overwhelmed in nephrotic conditions due to the disease pathology. Normal tissue remodeling and fluid regulation (through enzymes like urokinase, prostasin and meprin A) were more active in healthy kidneys. In nephrotic syndrome, the loss of these enzymes' activity might contribute to the dysregulation of fluid balance and the degradation of normal tissue structure, leading to further kidney dysfunction.

There were also species-specific differences, such as the higher expression of angiotensin-converting enzyme and lactotransferrin in mouse samples, which were not as prominent in humans. This suggests that the underlying pathology might vary slightly across species.

3.2.1.4 Volcano plots of all proteases differentially excreted in human and mouse urine samples

Next, the significant differences of the protease excretion were examined by volcano plots the mean differences of the LFQ values of each protease from healthy and nephrotic groups were calculated. In nephrotic samples, six serine proteases and one metalloprotease showed significantly higher excretion, including the coagulation factors plasminogen, Hyaluronan-binding protein 2 (HABP2) and coagulation factor IX and complement factors B, D and C2 (volcano plot A in Figure 36). Conversely, healthy samples contained significantly higher amounts of eight serine proteases (e.g. urokinase-

type plasminogen activator, Kallikrein-1 and prostasin), four metalloproteases like carboxypeptidase B2, three aspartate proteases, two cysteine proteases and two omega proteases. The exact identites of the differentially excreted proteases are provied in the figure legend. In mice, similar results were obtained (B-graph). Here, among the significant serine proteases in nephrotic urine, prothrombin, coagulation factor XII and complement factor I emerged as new ones compared to the human samples, and C2, coagulation factor IX, HABP2 and complement factor B were not significant.

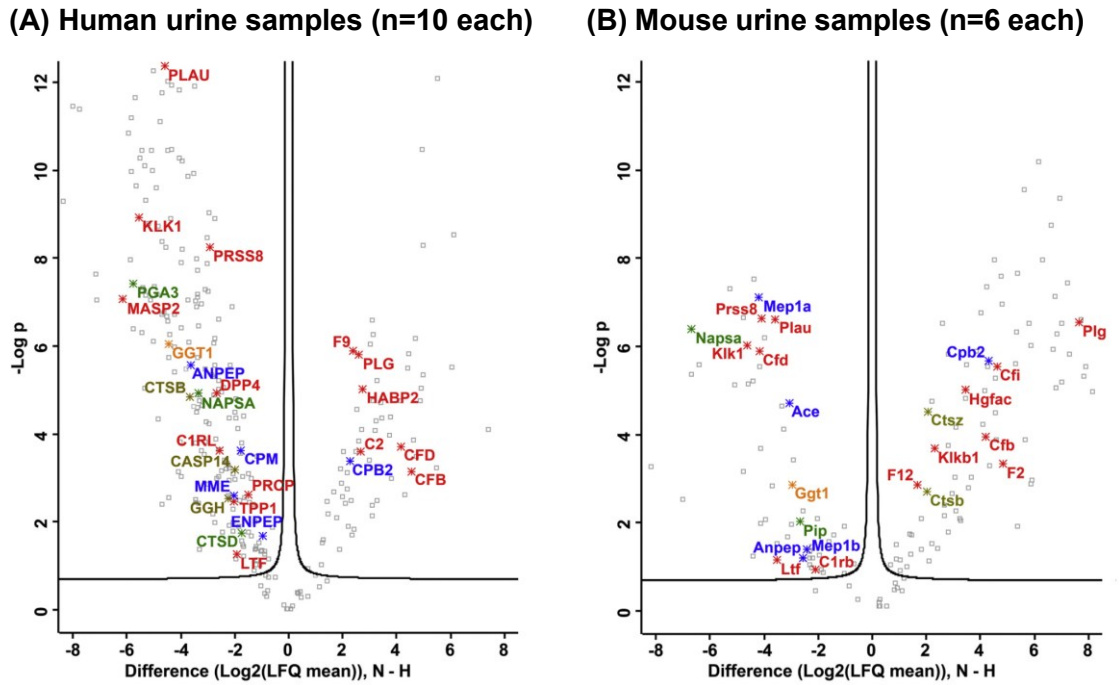

Figure 36: Volcano plots of all proteases differentially excreted in urine samples, shotgun approach

from healthy persons and nephrotic patients (A, n=10 each) as well as healthy and nephrotic mice (B, n=6 each)

adopted from first-authorship publication [68]

Gene name abbreviations, written out as full protein names (sorted by alphabet, first the classes, then the gene names):

(A, human): Aspartic proteases (green): CTSD = Cathepsin D, NAPSA = Napsin-A, PGA3 = Pepsin A-3 + Pepsin A-4 + Pepsin A-5; **Cysteine proteases (olive green):** CASP14 = Caspase-14, CTSB = Cathepsin B; **Metalloproteases (blue):** ANPEP = Aminopeptidase N, CPB2 = Carboxypeptidase B2, CPM = Carboxypeptidase M, ENPEP = Glutamyl aminopeptidase, GGH = Gamma-glutamyl hydrolase, MME = Neprilysin; **Threonine proteases (orange):** GGT1 = Glutathione hydrolase 1 proenzyme + Putative glutathione hydrolase 3 proenzyme; **Serine proteases (red):** C1RL = Complement C1r subcomponent-like

protein, C2 = Complement C2, CFB = Complement factor B, CFD = Complement factor D, DPP4 = Dipeptidyl peptidase 4, F9 = Coagulation factor IX, HABP2 = Hyaluronan-binding protein 2, KLK1 = Kallikrein-1, LTF = Lactotransferrin, MASP2 = Mannan-binding lectin serine protease 2, PLAU = Urokinase-type plasminogen activator, PLG = Plasminogen, PRCP = Lysosomal Pro-X carboxypeptidase, PRSS8 = Prostasin, TPP1 = Tripeptidyl-peptidase 1

(B, mouse): Aspartic proteases (green): Napsa = Napsin-A, Pip = Prolactin-inducible protein homolog; **Cysteine proteases (olive green):,** Ctsb = Cathepsin B, Ctsz = Cathepsin Z; **Metalloproteases (blue):** Ace = Angiotensin-converting enzyme, Anpep = Aminopeptidase N, Cpb2 = Carboxypeptidase B2, Mep1a = Meprin A subunit alpha, Mep1b = Meprin A subunit beta; **Threonine proteases (orange):** Ggt1 = Glutathione hydrolase 1 proenzyme, **Serine proteases (red):** C1ra = Complement C1r-A subcomponent, C1rb = Complement C1r-B subcomponent, Cfb = Complement factor B, Cfd = Complement factor D, Cfi = Complement factor I, F2 = Prothrombin, F12 = Coagulation factor XII, Hgfac = Hepatocyte growth factor activator, Klk1 = Kallikrein-1, Klkb1 = Plasma kallikrein, Ltf = Lactotransferrin, Plau = Urokinase-type plasminogen activator, Plg = Plasminogen, Prss8 = Prostasin

H = healthy samples, N = nephrotic samples.

This differential excretion of proteases underscores the pathogenic role of certain protease classes in nephrotic syndrome. The significant increase in serine proteases in nephrotic urine, particularly those involved in coagulation and complement activation, suggests that these enzymes may contribute to the disruption of kidney function by promoting inflammation and protein degradation. Meanwhile, the higher levels of various proteases in healthy samples suggest they are more critical in maintaining homeostasis, and their reduction in nephrotic syndrome may lead to a loss of regulatory functions in the kidney.

3.2.2 Differentially excreted active serine proteases in health and nephrotic syndrome

3.2.2.1 AEBSF approach

Because serine proteases were the largest subgroup among all detected proteases and their proteolytic activity could play a pathological role like in the overactivation of the sodium channel ENaC, the proteomics approach was further refined by using precipitation beads where the small serine protease inhibitor AEBSF was covalently coupled onto the bead surface. After that, these beads were pre-incubated with the urine samples so that the reactive sulfonyl fluoride group of AEBSF could covalently bind to the catalytic serine

residue in the active site of the target proteases. In nephrotic urine of humans (Figure 37 (A)), there are eight serine proteases and which had a significantly higher abundance in nephrotic samples. Only one metalloprotease was additionally detected, which was expected for the higher binding specificity of active serine proteases. On the other hand, the healthy urine showed seven significantly enriched serine proteases and additionally, six metalloproteases, three aspartate proteases and one omega protease. Similar patterns were observed in mice, and nearly all serine proteases found in nephrotic human urine were also significantly enriched here (Figure 37 (B)).

When this experimental approach was repeated only by the difference of using blank beads without AEBSF, the most serine proteases were detected again compared to AEBSF-containing beads or even using the shotgun approach without any beads. This could be explained by an adsorption effect where the proteins bind unspecifically on the bead surface, and were also enriched in that way. But as assumed for this background effect, the LFQ values were not identical but lower for beads without AEBSF for highly actice serine protease, and so the differences of each protease could be calculated. Positive differences between AEBSF-coupled beads with “without AEBSF”-beads indicated purification of serine proteases in a higher active form as it required good accessibility of their active site with the serine residue for covalent reaction with AEBSF (Table 4).

In urine samples of healthy humans, proteases such as urokinase-type plasminogen activator or aminopeptidase N showed a higher abundance in the active state which represent proteoloytic processes in the healthy tubule system. Also in healthy mice, there were several other renally expressed proteases in the active state such as kallikrein-1. In contrast, nephrotic urine from both species contained many actives proteases from the coagulation and complement cascade. Plasminogen/plasmin was by far the most active protease, followed by hyaluronan-binding protein 2 and complement factor B (Table 4).

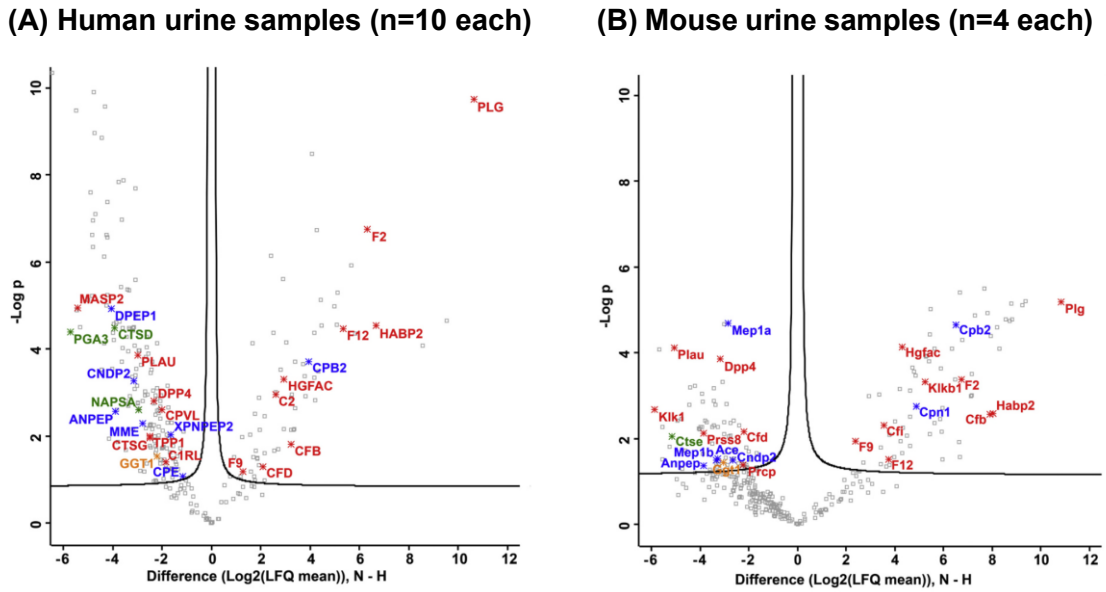

Figure 37: Volcano plots of active proteases differentially excreted in urine samples, AEBSF approach

from healthy persons and nephrotic patients (A, n=10 each) as well as healthy and nephrotic mice (B, n=4 each)

adopted from first-authorship publication [68]

Proteases were identified using beads conjugated with the serine protease inhibitor AEBSF which binds covalently to the serine of the active site. In addition, proteases of other classes were also detected, most probably by an absorbing effect of the beads.

Gene name abbreviations, written out as full protein names (sorted by alphabet, first the classes, then the gene names):

(A, human): Aspartic proteases (green): CTSD = Cathepsin D, NAPSA = Napsin-A, PGA3 = Pepsin A-3; **Metalloproteases (blue):** ANPEP = Aminopeptidase N, CNDP2 = Cytosolic non-specific dipeptidase, CPB2 = Carboxypeptidase B2**,** CPE = Carboxypeptidase E, DPEP1 = Dipeptidase 1, MME = Neprilysin, XPNPEP2 = Xaa-Pro aminopeptidase 2; **Threonine proteases (orange):** GGT1 = Glutathione hydrolase 1 proenzyme + GGT3P = Putative glutathione hydrolase 3 proenzyme; **Serine proteases (red):** C1RL = Complement C1r subcomponent-like protein, C2 = Complement C2, CFB = Complement factor B, CFD = Complement factor D, CPVL = Probable serine carboxypeptidase CPVL, CTSG = Cathepsin G, DPP4 = Dipeptidyl peptidase 4, F2 = Prothrombin, F9 = Coagulation factor IX, F12 = Coagulation factor XII, HABP2 = Hyaluronan-binding protein 2, HGFAC = Hepatocyte growth factor activator, MASP2 = Mannan-binding lectin serine protease 2, PLAU = Urokinase-type plasminogen activator, PLG = Plasminogen, TPP1 = Tripeptidyl-peptidase 1

(B, mouse): Aspartic proteases (green): Ctse = Cathepsin E; **Metalloproteases (blue):** Ace = Angiotensin-converting enzyme, Anpep = Aminopeptidase N, Cndp2 = Cytosolic non-specific dipeptidase, Cpb2 = Carboxypeptidase B2, Cpn1 = Carboxypeptidase N catalytic chain, Mep1a = Meprin A subunit alpha, Mep1b = Meprin A subunit beta; **Threonine proteases (orange):** Ggt1 = Glutathione hydrolase 1

proenzyme; **Serine proteases (red):** Cfb = Complement factor B, Cfd = Complement factor D, Cfi = Complement factor I, Dpp4 = Dipeptidyl peptidase 4, F2 = Prothrombin, F9 = Coagulation factor IX, F12 = Coagulation factor XII, Habp2 = Hyaluronan-binding protein 2, Hgfac = Hepatocyte growth factor activator, Klk1 = Kallikrein-1, Klkb1 = Plasma kallikrein, Plau = Urokinase-type plasminogen activator, Plg = Plasminogen, Prcp = Lysosomal Pro-X carboxypeptidase, Prss8 = Prostasin
H = healthy samples, N = nephrotic samples.

Table 4: Active serine proteases in the urine of humans and mouse in health and nephrotic syndrome

adopted from first-authorship publication [68]

Difference of the LFQ values (ΔAEBSF) between AEBSF-coupled (+AEBSF) and uncoupled negative (-AEBSF) beads. Positive values of ΔAEBSF indicate higher detection by AEBSF-containing beads corresponding to the active form of each protease. Mean LFQ values/10^6 ± SEM; the serine proteases are sorted according to the ΔAEBSF mean values of the human nephrotic samples; # indicates significant deviation from 0, * indicates significant difference between healthy and nephrotic, n.d. = not detected

	Human (n=10 each), mean values/10^6 ± SEM					
	Healthy samples			**Nephrotic samples**		
Protease name	**+AEBSF**	**-AEBSF**	**ΔAEBSF**	**+AEBSF**	**-AEBSF**	**ΔAEBSF**
Plasminogen	1.7 ± 0.7	1.0 ± 0.6	0.65 ± 0.27#	1995.7 ± 503.5	846.9 ± 207.1	1148.8 ± 337.8#*
Hyaluronan-binding protein 2	0.77 ± 0.10	0.62 ± 0.08	0.15 ± 0.11	260.2 ± 78.7	196.7 ± 75.0	63.5 ± 35.5
Complement factor D	19.4 ± 8.3	16.6 ± 7.8	2.9 ± 1.1#	67.8 ± 22.0	44.3 ± 14.3	23.6 ± 11.5
Coagulation factor XII	0.84 ± 0.26	0.57 ± 0.11	0.27 ± 0.27	63.1 ± 18.4	42.8 ± 16.0	20.3 ± 10.4*
Complement factor B	2.9 ± 1.3	2.0 ± 1.0	0.94 ± 0.38#	62.1 ± 29.6	49.8 ± 21.0	12.3 ± 13.3
Hepatocyte growth factor activator	1.1 ± 0.2	0.80 ± 0.10	0.27 ± 0.21	14.5 ± 6.5	8.8 ± 6.3	5.7 ± 2.0#*
Urokinase-type plasminogen activator	28.6 ± 6.9	22.0 ± 6.1	6.6 ± 3.3	4.0 ± 1.4	2.3 ± 1.0	1.7 ± 0.5#
Mannan-binding lectin serine protease 2	225.2 ± 86.5	228.6 ± 105.5	-3.4 ± 23.4	7.0 ± 4.1	5.5 ± 2.5	1.5 ± 2.7
Tripeptidyl-peptidase 1	11.9 ± 2.7	10.3 ± 2.9	1.6 ± 0.9	3.7 ± 1.9	3.1 ± 1.5	0.62 ± 0.5
Dipeptidyl peptidase 4	10.5 ± 2.0	6.9 ± 1.9	3.6 ± 1.0#	2.5 ± 0.8	2.1 ± 0.6	0.41 ± 0.33*
Complement C1r subcomponent-like protein	19.9 ± 6.3	17.0 ± 6.9	1.7 ± 1.0	4.9 ± 2.6	4.9 ± 2.2	-0.04 ± 0.10
Probable serine carboxypeptidase CPVL	5.4 ± 2.4	3.7 ± 1.5	1.0 ± 0.49	0.74 ± 0.21	0.78 ± 0.19	0.05 ± 0.11
Cathepsin G	3.6 ± 1.6	2.4 ± 1.1	2.0 ± 3.3	0.85 ± 0.24	1.0 ± 0.2	-0.18 ± 0.71

Coagulation factor IX	1.0 ± 0.3	0.74 ± 0.16	0.28 ± 0.29	3.9 ± 2.0	4.7 ± 2.3	-0.71 ± 0.44
Complement C2	1.0 ± 0.3	0.42 ± 0.05	0.56 ± 0.27	8.6 ± 3.7	9.5 ± 3.9	-0.94 ± 1.5
Prothrombin	0.60 ± 0.10	0.57 ± 0.10	0.03 ± 0.10	99.3 ± 36.2	115.4 ± 38.7	-16.1 ± 8.5
Plasma kallikrein	n.d.	n.d.	n.d.	n.d.	n.d.	n.d.
Kallikrein-1	n.d.	n.d.	n.d.	n.d.	n.d.	n.d.
Lysosomal Pro-X carboxypeptidase	n.d.	n.d.	n.d.	n.d.	n.d.	n.d.
Prostasin	n.d.	n.d.	n.d.	n.d.	n.d.	n.d.
Complement factor I	n.d.	n.d.	n.d.	n.d.	n.d.	n.d.

	Mouse (n=4 each), mean values/10^6 ± SEM					
	Healthy samples			**Nephrotic samples**		
Protease name	**+AEBSF**	**-AEBSF**	**ΔAEBSF**	**+AEBSF**	**-AEBSF**	**ΔAEBSF**
Plasminogen	6.0 ± 1.5	4.8 ± 0.6	1.2 ± 1.7	13736.4 ± 6923.3	5925 ± 1395.1	7811.4 ± 5620.8*
Hyaluronan-binding protein 2	5.3 ± 1.2	24.4 ± 18.7	-19 ± 19.4	3385.7 ± 1686.3	934.8 ± 376.1	2450.9 ± 1327.2*
Complement factor D	1229.1 ± 263.3	1141.7 ± 144.2	87.4 ± 146.1	282.0 ± 93.5	336.4 ± 18.3	-54.4 ± 76.3
Coagulation factor XII	7.6 ± 2.7	5.2 ± 1.3	2.3 ± 1.9	156.1 ± 62.6	70.8 ± 29.5	85.3 ± 36.3
Complement factor B	87.0 ± 69.7	32.5 ± 17.6	54.5 ± 52.1	8490.2 ± 4611.2	4300.6 ± 1435.6	4189.6 ± 3311.8
Hepatocyte growth factor activator	4.5 ± 1.0	7.1 ± 2.2	-2.6 ± 2.1	83.5 ± 10.7	44.2 ± 22.0	39.3 ± 15.4*
Urokinase-type plasminogen activator	444.2 ± 172.0	170.3 ± 46.0	273.9 ± 137.2	11.4 ± 1.9	3.6 ± 1.1	7.7 ± 2.5*
Mannan-binding lectin serine protease 2	n.d.	n.d.	n.d.	n.d.	n.d.	n.d.
Tripeptidyl-peptidase 1	n.d.	n.d.	n.d.	n.d.	n.d.	n.d.
Dipeptidyl peptidase 4	62.5 ± 6.5	35.3 ± 16.5	27.2 ± 12.4	7.2 ± 1.3	7.1 ± 1.8	0.09 ± 1.7
Complement C1r subcomponent-like protein	n.d.	n.d.	n.d.	n.d.	n.d.	n.d.
Probable serine carboxypeptidase CPVL	n.d.	n.d.	n.d.	n.d.	n.d.	n.d.
Cathepsin G	n.d.	n.d.	n.d.	n.d.	n.d.	n.d.
Coagulation factor IX	4.2 ± 0.7	4.8 ± 1.1	-0.60 ± 0.57	27.0 ± 10.2	19.3 ± 12.9	7.7 ± 8.3
Complement C2	n.d.	n.d.	n.d.	n.d.	n.d.	n.d.
Prothrombin	9.2 ± 3.7	11.3 ± 3.0	-2.1 ± 1.0	930.5 ± 382.9	965.3 ± 420.4	-34.8 ± 85.3
Plasma kallikrein	8.4 ± 3.0	4.7 ± 1.5	3.7 ± 4.1	324.7 ± 111.0	123.1 ± 15.3	201.6 ± 107.7
Kallikrein-1	1390.4 ± 828.8	1047.7 ± 494.1	342.7 ± 397.3	19.2 ± 10.1	17.6 ± 7.3	1.6 ± 2.8
Lysosomal Pro-X carboxypeptidase	36.0 ± 12.0	19.4 ± 7.6	16.6 ± 10.7	6.4 ± 1.6	8.3 ± 2.2	-1.9 ± 2.7
Prostasin	114.1 ± 41.1	69.6 ± 28.7	44.5 ± 19.9	5.7 ± 1.2	11.9 ± 2.6	-6.3 ± 1.8#
Complement factor I	13.6 ± 4.0	7.0 ± 1.5	6.5 ± 3.8	152.3 ± 57.0	185.7 ± 80.0	-33.4 ± 24.6

The AEBSF-based approach refined the shotgun findings by isolating serine proteases in their active forms, thereby offering insights into proteolytic activity specific to disease pathology. This targeted method highlighted a significant increase in active serine proteases within nephrotic samples, particularly those associated with coagulation and complement systems. By identifying proteases that covalently bound to AEBSF (a serine protease inhibitor), this method confirmed that many serine proteases present in nephrotic urine were not only abundant but functionally active, suggesting a direct role in pathological tissue damage. The AEBSF approach thus allowed for the selective enrichment of proteases driving active disease processes, providing a focused lens on enzymes with potential pathogenic roles in nephrotic syndrome.

3.2.2.2 Aprotinin approach

In nephrotic samples, a significantly higher level of aprotinin-sensitive protease activity was detected using the universal substrate, indicating increased proteolytic activity. To further investigate this, aprotinin was also used as a binding inhibitor on beads in the way like AEBSF, tagged by hemagglutinin as HA-aprotinin, to selectively capture all aprotinin-sensitive proteases from the urine samples for mass spectrometry analysis. With this approach, all specific proteases bound to aprotinin were identified, particularly those known to be involved in the pathogenesis of nephrotic syndrome. The findings were then compared to the results obtained from a previous shotgun proteomics approach, allowing for a more targeted investigation of proteases specifically relevant to the disease process.

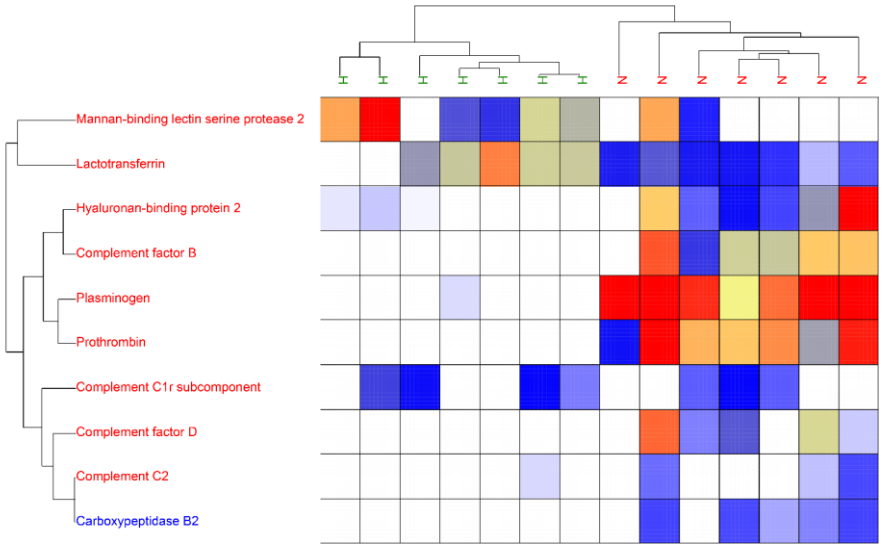

Figure 38: Hierarchical Clustering of human urine (n=7 each), HA-aprotinin approach

Serine proteases are highlighted in red and metalloproteases in blue

H = healthy samples, N = nephrotic samples; intensity values in the legend are shown as log2(LFQ units)

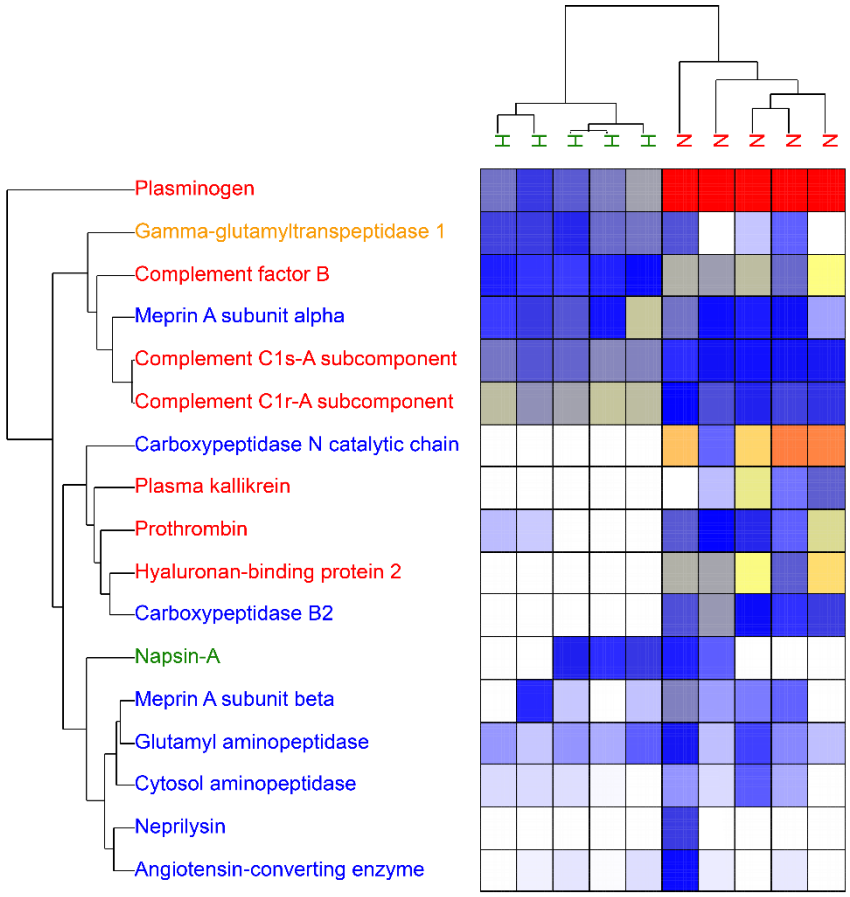

Figure 39: Hierarchical Clustering of mouse urine (n=5 each), HA-aprotinin approach

Serine proteases are highlighted in red, metalloproteases in blue, aspartate proteases in green and threonine proteases in orange. Nephrotic samples were characterized by a cluster of high molecular proteases from the coagulation and complement cascade (upper right cluster). In contrast, healthy samples were characterized by proteases with a low molecular weight that are locally expressed (lower left cluster).

H = healthy samples, N = nephrotic samples; intensity values in the legend are shown as log2(LFQ units)

This selective aprotinin binding approach enriches for proteases that are not only present but also highly active and potentially pathogenic in the context of nephrotic syndrome.

In the shotgun proteomics analysis, several unique proteins were identified that were absent in the aprotinin-binding list, indicating their presence in nephrotic urine samples

but a lack of specific affinity for aprotinin. These included Gamma-glutamyl hydrolase, Coagulation factor XI, Hepatocyte Growth Factor Activator, Aminopeptidase N, Carboxypeptidase M, and Urokinase-type plasminogen activator. The presence of these proteases suggests roles in broader proteolytic and regulatory processes rather than direct aprotinin-sensitive activity. For instance, Gamma-glutamyl hydrolase and Carboxypeptidase M are involved in amino acid metabolism and peptide processing, while Urokinase-type plasminogen activator has a well-known role in fibrinolysis. The detection of these proteases highlights additional pathways of protein degradation and regulation in nephrotic syndrome, which might contribute to disease pathology independently of the aprotinin-sensitive proteolytic activity.

Some proteins, including Plasminogen, Complement factor D, Hyaluronan-binding protein 2, and Mannan-binding lectin serine protease 2, were identified in both datasets, indicating their dual presence in general proteomic landscapes and among those selectively bound by aprotinin. This overlap underscores the potential central role of these proteases in both baseline and disease-specific proteolytic activity, making them of particular interest for further research into their roles in glomerular permeability and inflammation.

Among the identified proteins, Complement C1r subcomponent was unique to the aprotinin-captured set, emphasizing its potential role as an aprotinin-sensitive protease. It highlights the increased activation of the complement pathway as a central feature in nephrotic pathology.

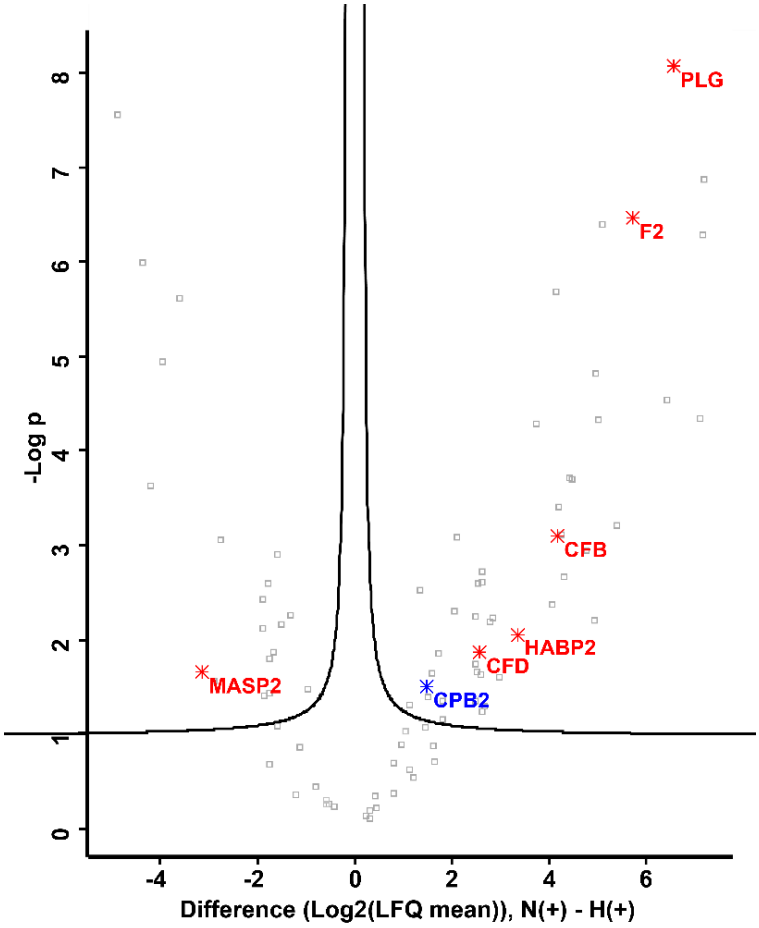

Figure 40: Volcano plots of proteases differentially excreted in human urine samples, HA-Aprotinin approach

from healthy persons and nephrotic patients (n=7 each)

Metalloproteases (blue): CPB2 = Carboxypeptidase B2**; Serine proteases (red):** CFB = Complement factor B, CFD = Complement factor D, F2 = Prothrombin, HABP2 = Hyaluronan-binding protein 2, MASP2 = Mannan-binding lectin serine protease 2, PLG = Plasminogen

H(+) = healthy samples, with HA (hemagglutinin)-tagged aprotinin on beads; N(+) = nephrotic samples, with HA (hemagglutinin)-tagged aprotinin on beads.

In human samples (Figure 40), several proteases were significantly higher excreted in nephrotic urine compared to healthy controls. Key upregulated proteases include plasminogen, Complement Factor B, and Mannan-binding lectin serine protease 2, which play important roles in the complement and coagulation pathways. These proteases are not only more abundant in nephrotic urine but also likely contribute to the pathological mechanisms underlying nephrotic syndrome. Plasminogen, for instance, is known for its role in fibrinolysis, and its increased levels in nephrotic urine suggest a heightened state

of proteolytic activity that could be damaging to kidney tissue. Additionally, proteases like Hyaluronan-binding protein 2, which is involved in extracellular matrix remodeling, are also elevated, indicating that tissue remodeling processes may be exacerbated in nephrotic conditions.

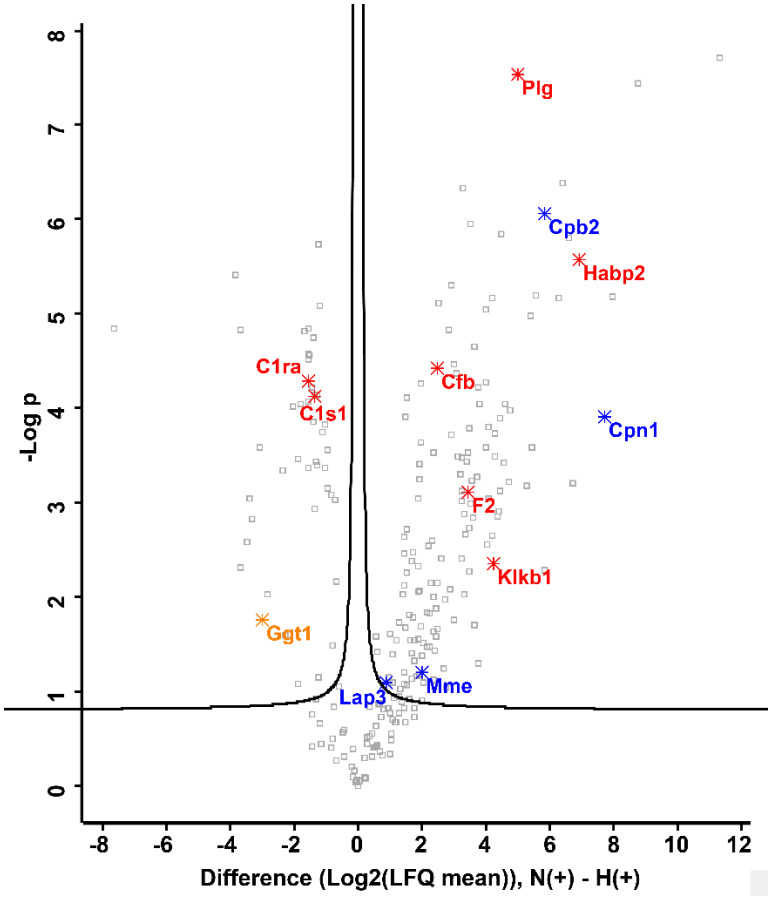

Figure 41: Volcano plots of proteases differentially excreted in mouse urine samples, HA-Aprotinin approach

from healthy and nephrotic mice (n=5 each)

Metalloproteases (blue): Cpb2 = Carboxypeptidase B2, Cpn1 = Carboxypeptidase N catalytic chain, Mme = Neprilysin, Lap3 = Cytosol aminopeptidase, **Threonine proteases (orange):** Ggt1 = Glutathione hydrolase 1 proenzyme, **Serine proteases (red):** C1ra = Complement C1r-A subcomponent, C1s1 = Complement C1s-1 subcomponent, Cfb = Complement factor B, F2 = Prothrombin, Habp2 = Hyaluronan-binding protein 2, Klkb1 = Plasma kallikrein, Plg = Plasminogen

H(+) = healthy samples, with HA (hemagglutinin)-tagged aprotinin on beads; N(+) = nephrotic samples, with HA (hemagglutinin)-tagged aprotinin on beads.

Mouse urine samples (Figure 41) showed similar trends, with significant upregulation of aprotinin-sensitive proteases in nephrotic samples. Complement components and coagulation-related proteases were prominent again, with their role in inflammatory and immune responses associated in nephrotic syndrome. The parallels between human and mouse samples in these aprotinin-sensitive protease profiles underscore the potential use of these proteases as biomarkers for nephrotic syndrome and as potential future targets for therapeutic intervention.

3.2.3 Sensitivity analyses with LFQ values without normalization and XIC values

Sensitivity analyses of the data sets from the shotgun and AEBSF approaches presented in Figure 36 and Figure 37 were carried out using raw intensity XIC (eXtracted Ion Current) values from the same MaxQuant runs that produced the LFQ values, as well as LFQ values from separate MaxQuant runs without normalization procedure. The results were arranged as volcano plots in the Figure 42-Figure 45.

The obtained results confirmed many of the proteases which were already identified using the LFQ-based analysis. But additionally, some further low abundant proteases were detected as significant enrichment in both humans and mice under healthy and nephrotic conditions.

In nephrotic urine, key coagulation proteases such as Factor IX (F9), Factor X (F10), and Factor XII (F12) were newly detected. Additionally, complement Factor I (CFI), plasma kallikrein (KLKB1), prothrombin (F2), and Hyaluronan-binding protein 2 (HABP2) were significantly elevated. Healthy urine exhibited higher levels of regulatory proteases, including prostasin (PRSS8), tissue kallikrein (KLK1), and transmembrane serine protease 2 (TMPRSS2).

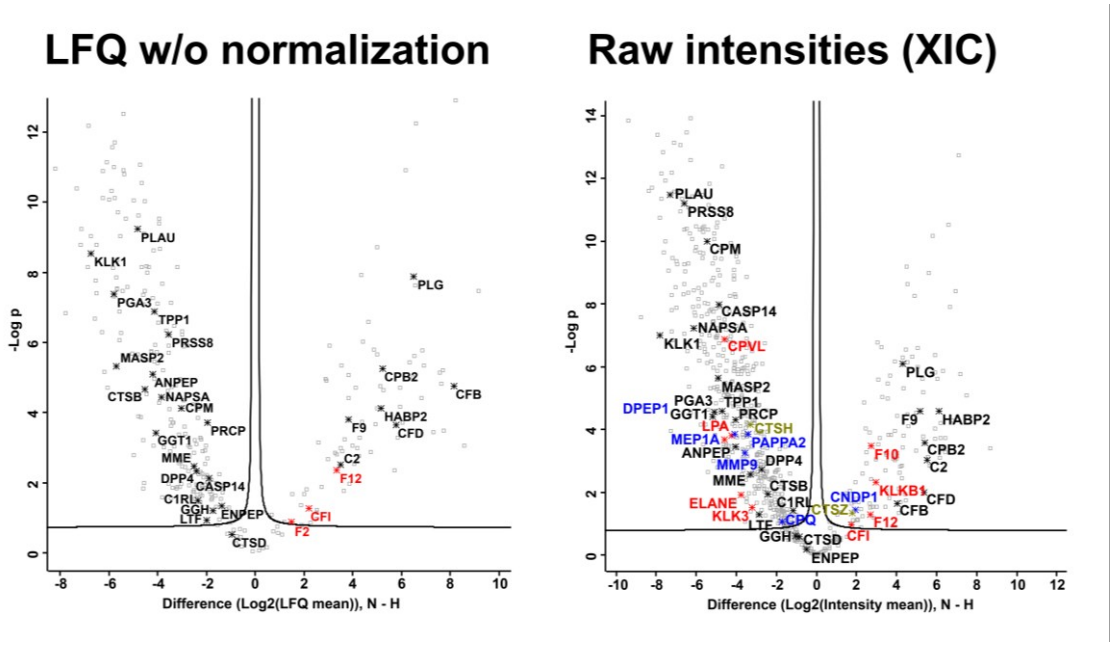

Figure 42: LFQ w/o normalization and XIC values, compared to normalized LFQ values from human samples, shotgun approach.

adopted from first-authorship publication [68]

Comparison of the volcano plots obtained with normalized LFQ values (shown in Figure 36A) with LFQ values without normalization and raw intensity values as extracted ion current (XIC). All newly and significantly arising proteases are shown in color of the protease class, as described below.

Gene name abbreviations, written out as full protein names (sorted by alphabet, first the classes, then the gene names):

Aspartic proteases (green): CTSD = Cathepsin D, NAPSA = Napsin-A, PGA3 = Pepsin A-3 + Pepsin A-4 + Pepsin A-5; **Cysteine proteases (olive green):** CASP14 = Caspase-14, CTSB = Cathepsin B, CTSH = Pro-cathepsin H, CTSZ = Cathepsin Z; **Metalloproteases (blue):** ANPEP = Aminopeptidase N, CNPD1 = Beta-Ala-His dipeptidase, CPB2 = Carboxypeptidase B2, CPM = Carboxypeptidase M, CPQ = Carboxypeptidase Q, DPEP1 = Dipeptidase 1, ENPEP = Glutamyl aminopeptidase, GGH = Gamma-glutamyl hydrolase, MEP1A = Meprin A subunit alpha, MME = Neprilysin, MMP9 = Matrix metalloproteinase-9, PAPPA2 = Pappalysin-2; **Threonine proteases (orange):** GGT1 = Glutathione hydrolase 1 proenzyme + Putative glutathione hydrolase 3 proenzyme; **Serine proteases (red):** C1RL = Complement C1r subcomponent-like protein, C2 = Complement C2, CFB = Complement factor B, CFD = Complement factor D, CFI = Complement factor I, CPVL = Probable serine carboxypeptidase CPVL, DPP4 = Dipeptidyl peptidase 4, ELANE = Neutrophil elastase, F2 = Prothrombin, F9 = Coagulation factor IX, F10 = Coagulation factor X, F12 = Coagulation factor XII, HABP2 = Hyaluronan-binding protein 2, KLK1 = Kallikrein-1, KLK3 = Prostate-specific antigen, KLKB1 = Plasma kallikrein, LPA = Apolipoprotein(a), LTF = Lactotransferrin, MASP2 = Mannan-binding lectin serine protease 2, PLAU = Urokinase-type

plasminogen activator, PLG = Plasminogen, PRCP = Lysosomal Pro-X carboxypeptidase, PRSS8 = Prostasin, TPP1 = Tripeptidyl-peptidase 1; H = healthy samples, N = nephrotic samples.

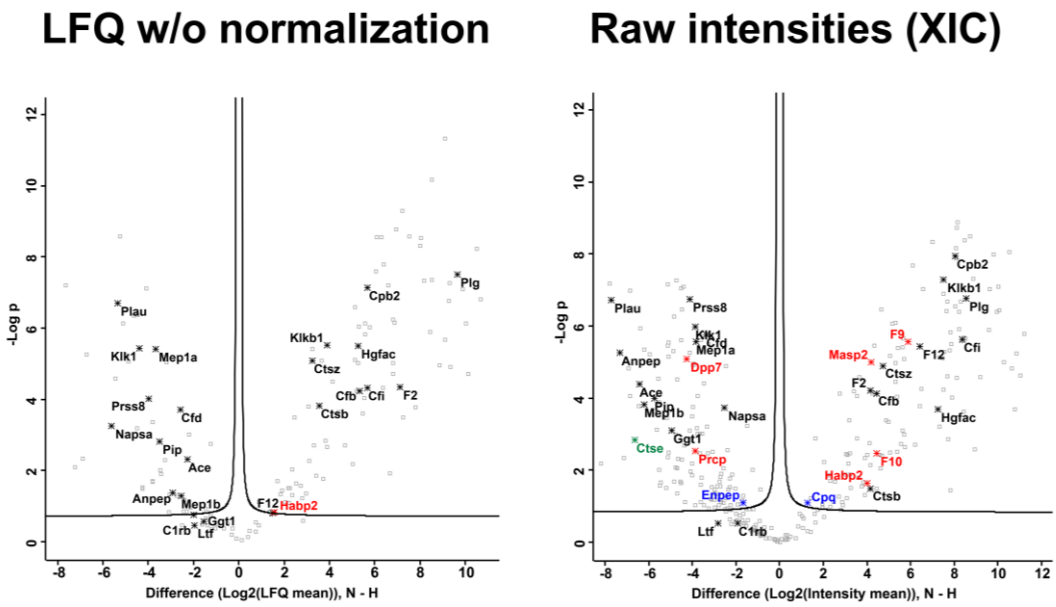

Figure 43: LFQ w/o normalization and XIC values, compared to normalized LFQ values from mouse samples, shotgun approach.

adopted from first-authorship publication [68]

Comparison of the volcano plots obtained with normalized LFQ values (shown in Figure 36B) with LFQ values without normalization and raw intensity values as extracted ion current (XIC). All newly and significantly arising proteases are shown in color of the protease class, as described below.

Gene name abbreviations, written out as full protein names (sorted by alphabet, first the classes, then the gene names):

Aspartic proteases (green): Ctse = Cathepsin E, Napsa = Napsin-A, Pip = Prolactin-inducible protein homolog; **Cysteine proteases (olive green):,** Ctsb = Cathepsin B, Ctsz = Cathepsin Z; **Metalloproteases (blue):** Ace = Angiotensin-converting enzyme, Anpep = Aminopeptidase N, Cpb2 = Carboxypeptidase B2, Cpq = Carboxypeptidase Q, Mep1a = Meprin A subunit alpha, Mep1b = Meprin A subunit beta; **Threonine proteases (orange):** Ggt1 = Glutathione hydrolase 1 proenzyme, **Serine proteases (red):** C1ra = Complement C1r-A subcomponent, C1rb = Complement C1r-B subcomponent, Cfb = Complement factor B, Cfd = Complement factor D, Cfi = Complement factor I, Enpep = Glutamyl aminopeptidase, Dpp7 = Dipeptidyl peptidase 2, F2 = Prothrombin, F9 = Coagulation factor IX, F10 = Coagulation factor X, F12 = Coagulation factor XII, Habp2 = Hyaluronan-binding protein 2, Hgfac = Hepatocyte growth factor activator, Klk1 = Kallikrein-1, Klkb1 = Plasma kallikrein, Ltf = Lactotransferrin, Masp2 = Mannan-binding lectin serine protease 2, Plau = Urokinase-type plasminogen activator, Plg = Plasminogen, Prcp = Lysosomal Pro-X carboxypeptidase, Prss8 = Prostasin; H = healthy samples, N = nephrotic samples.

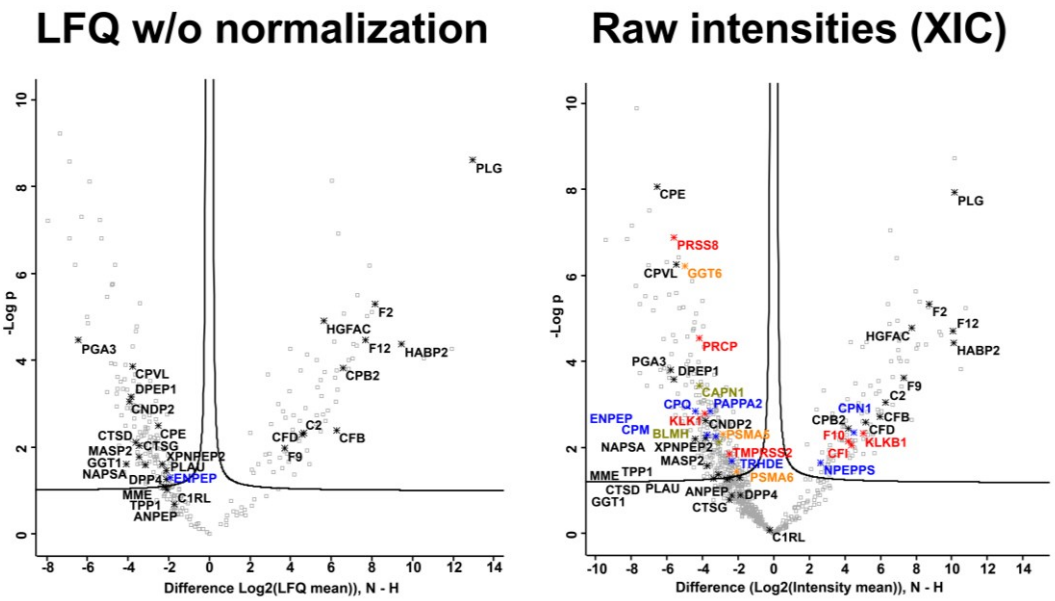

Figure 44: LFQ w/o normalization and XIC values, compared to normalized LFQ values from human samples, AEBSF approach.

adopted from first-authorship publication [68]

Comparison of the volcano plots obtained with normalized LFQ values (shown in Figure 37A) with LFQ values without normalization and raw intensity values as extracted ion current (XIC). All newly and significantly arising proteases are shown in color of the protease class, as described below.

Gene name abbreviations, written out as full protein names (sorted by alphabet, first the classes, then the gene names):

Aspartic proteases (green): CTSD = Cathepsin D, NAPSA = Napsin-A, PGA3 = Pepsin A-3; **Cysteine proteases (olive green):** BLMH = Bleomycin hydrolase, CAPN1 = Calpain-1 catalytic subunit; **Metalloproteases (blue):** ANPEP = Aminopeptidase N, CNDP2 = Cytosolic non-specific dipeptidase, CPB2 = Carboxypeptidase B2**,** CPE = Carboxypeptidase E, CPM = Carboxypeptidase M, CPN1 = Carboxypeptidase N catalytic chain, CPQ = Carboxypeptidase Q, DPEP1 = Dipeptidase 1, ENPEP = Glutamyl aminopeptidase, MME = Neprilysin, NPEPPS = Puromycin-sensitive aminopeptidase, PAPPA2 = Pappalysin-2, TRHDE = Thyrotropin-releasing hormone-degrading ectoenzyme, XPNPEP2 = Xaa-Pro aminopeptidase 2; **Threonine proteases (orange):** GGT1 = Glutathione hydrolase 1 proenzyme + GGT3P = Putative glutathione hydrolase 3 proenzyme, GGT6 = Gamma-glutamyltransferase 6, PSMA5 = Proteasome subunit alpha type-5, PSMA6 = Proteasome subunit alpha type-6; **Serine proteases (red):** C1RL = Complement C1r subcomponent-like protein, C2 = Complement C2, CFB = Complement factor B, CFD = Complement factor D, CFI = Complement factor I, CPVL = Probable serine carboxypeptidase CPVL, CTSG = Cathepsin G, DPP4 = Dipeptidyl peptidase 4, F2 = Prothrombin, F9 = Coagulation factor IX, F10 = Coagulation factor 10, F12 = Coagulation factor XII, HABP2 = Hyaluronan-binding protein 2,

HGFAC = Hepatocyte growth factor activator, KLK1 = Kallikrein-1, KLKB1 = Plasma kallikrein, MASP2 = Mannan-binding lectin serine protease 2, PLAU = Urokinase-type plasminogen activator, PLG = Plasminogen, PRCP = Lysosomal Pro-X carboxypeptidase, PRSS8 = Prostasin, TMPRSS2 = Transmembrane protease serine 2, TPP1 = Tripeptidyl-peptidase 1; H = healthy samples, N = nephrotic samples.

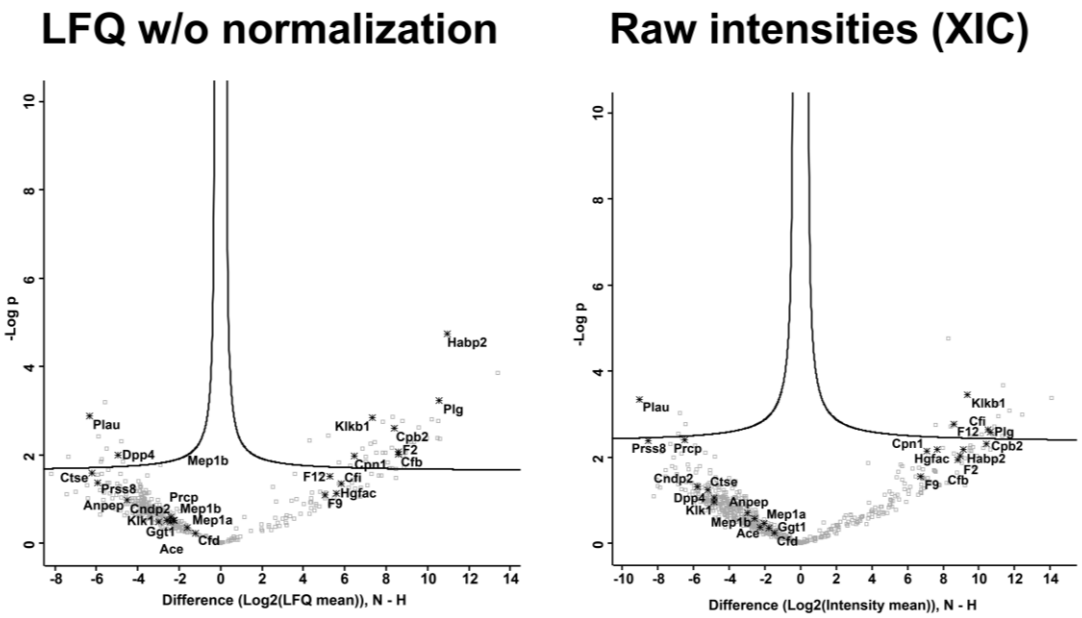

Figure 45: LFQ w/o normalization and XIC values, compared to normalized LFQ values from mouse samples, AEBSF approach.

adopted from first-authorship publication [68]

Comparison of the volcano plots obtained with normalized LFQ values (shown in Figure 37B) with LFQ values without normalization and raw intensity values as extracted ion current (XIC). All newly and significantly arising proteases are shown in color of the protease class, as described below.

Gene name abbreviations, written out as full protein names (sorted by alphabet, first the classes, then the gene names):

Aspartic proteases (green): Ctse = Cathepsin E; **Metalloproteases (blue):** Ace = Angiotensin-converting enzyme, Anpep = Aminopeptidase N, Cndp2 = Cytosolic non-specific dipeptidase, Cpb2 = Carboxypeptidase B2, Cpn1 = Carboxypeptidase N catalytic chain, Mep1a = Meprin A subunit alpha, Mep1b = Meprin A subunit beta; **Threonine proteases (orange):** Ggt1 = Glutathione hydrolase 1 proenzyme; **Serine proteases (red):** Cfb = Complement factor B, Cfd = Complement factor D, Cfi = Complement factor I, Dpp4 = Dipeptidyl peptidase 4, F2 = Prothrombin, F9 = Coagulation factor IX, F12 = Coagulation factor XII, Habp2 = Hyaluronan-binding protein 2, Hgfac = Hepatocyte growth factor

activator, Klk1 = Kallikrein-1, Klkb1 = Plasma kallikrein, Plau = Urokinase-type plasminogen activator, Plg = Plasminogen, Prcp = Lysosomal Pro-X carboxypeptidase, Prss8 = Prostasin
H = healthy samples, N = nephrotic samples.

3.3 Western Blots of plasma/urinary proteases showing expression and activity patterns

The expression of many of the identified proteases was validated on the protein level by performing Western blot analysis.

3.3.1 Plasma proteases from coagulation cascade

3.3.1.1 Plasminogen in human plasma/urine samples

Plasminogen as most abundant protease in nephrotic urine samples – does it arise there in the active state as plasmin?

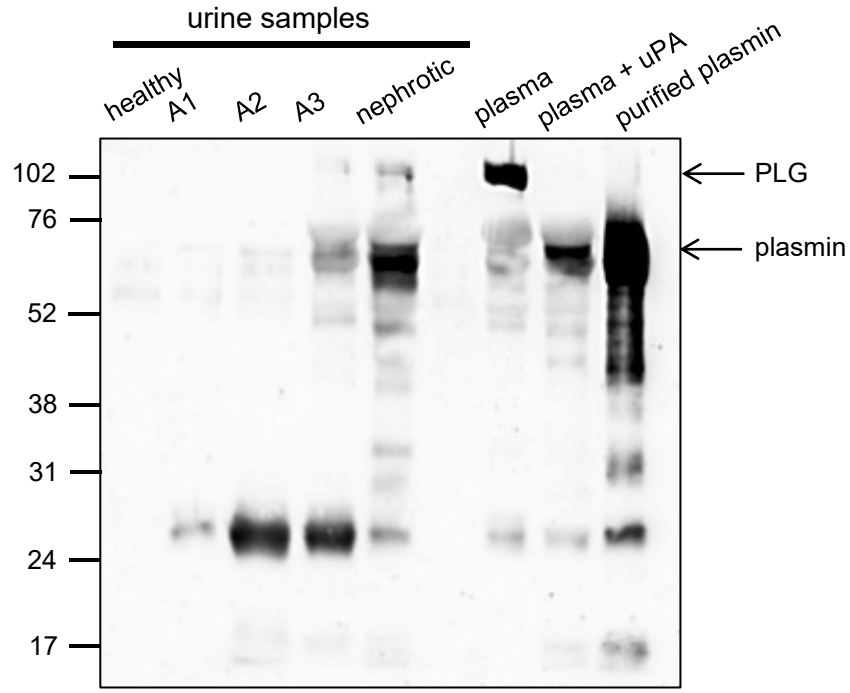

Figure 46: Western blot against plasminogen in mouse urine and plasma samples + control

The western blot showed that the urine contained plasmin and several smaller cleavage products. Their abundance increased with higher stages of albuminuria and reached the highest levels in patients with nephrotic-range proteinuria. In contrast, plasminogen was marginally detectable in the urine, unlike in plasma. This suggests that most of the filtered plasminogen was converted into plasmin and subsequently into smaller fragments.

The Western blot of representative urine samples and plasma shows demonstrated the presence of plasminogen (91 kDa) and and its active, cleaved form plasmin (72 kDa), together with additional low-molecular-weight bands. Across the stages of increasing albuminuria, the blot also showed a clear increase in plasmin, and nephrotic urine contained markedly higher levels of plasminogen and plasmin compared to healthy control urine. As expected under healthy physiological conditions in plasma, active plasmin was not detected there. But when urokinase-type plasminogen activator (uPA) was added to plasma, a distinct plasmin band appeared, confirming that plasminogen could be activated to plasmin by urokinase. A lane containing purified plasmin served as positive control and validated the detection of the active protease in the other lanes like in the nephrotic urine sample. Overall, the blot illustrates that nephrotic urine contained active plasmin, most likely because plasminogen passed the damaged glomerular filter. After that it is converted into plasmin within the urinary space due to new activation factors, such as possible urokinase which served here as a control activator. This contrasts with healthy urine, where little to no plasminogen or plasmin was detected, indicating intact glomerular filtration. The progressive increase in plasmin correlated with the severity of albuminuria stages, suggesting its potential role in the pathophysiology of nephrotic syndrome.

3.3.1.2 Plasminogen in mouse plasma/urine samples (uPA-WT, heterozygous/homozygous KO

How is the influence of urokinase to plasminogen activation?

This western blot shows the impact of urokinase (uPA) on plasminogen activation by analyzing urinary excretion of plasminogen in nephrotic mice with varying levels of uPA expression: wild-type (uPA+/+), heterozygous knockout (uPA+/−), and homozygous

knockout (uPA−/−). The Western blot presented here demonstrates the relationship between uPA activity and the extent of plasminogen cleavage, focusing on the appearance of the plasminogen heavy chain (around 78 kDa), which indicated plasminogen activation.

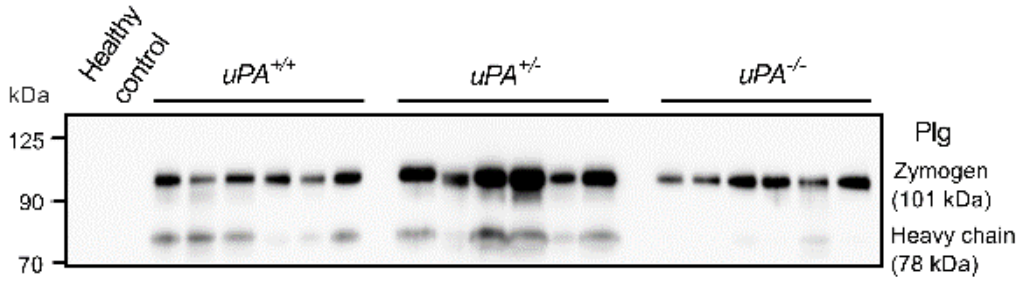

Figure 47: Western blot against plasminogen in nephrotic mouse urine samples of uPA genotypes

In wild-type (uPA+/+) nephrotic mice, the Western blot shows strong detection of the plasminogen zymogen (~101 kDa) as well as the heavy chain (~78 kDa), indicating robust plasminogen activation into plasmin. This suggests that in wild-type mice, the urokinase pathway was fully functional, resulting in significant cleavage of plasminogen.

In contrast, heterozygous uPA+/− mice exhibited a noticeable reduction in the intensity of the plasminogen heavy chain band, though it was still detectable. This indicates that the reduction in uPA expression limited, but did not entirely abolish plasminogen cleavage and subsequent plasmin formation.

In homozygous knockout (uPA−/−) mice, the plasminogen heavy chain was nearly absent, as reflected by a very faint or undetectable band at 78 kDa. This result strongly suggests that in the absence of uPA, urinary plasminogen activation was significantly impaired, and the pathway responsible for plasmin generation was effectively non-functional in these mice. The lack of uPA-mediated cleavage indicated that plasminogen remained largely in its inactive zymogen form.

3.3.1.3 Plasminogen in nephrotic urine of klkb1+/+ and klkb1-/- mice

Has plasma kallikrein an influence to plasmiogen activation?

This western blot demonstrates that mice excreted both plasminogen and plasmin detected as bands around 105 kDa (zymogen) and a band at about 75 kDa (heavy chain of plasmin) after the cleavage and dissociation from the light chain under reducing conditions. Each lane represents a urine sample from an individual mouse from day 8 of the experiment. The appearance of double bands suggests that there were cleavage products, which might indicate partial processing of plasminogen.

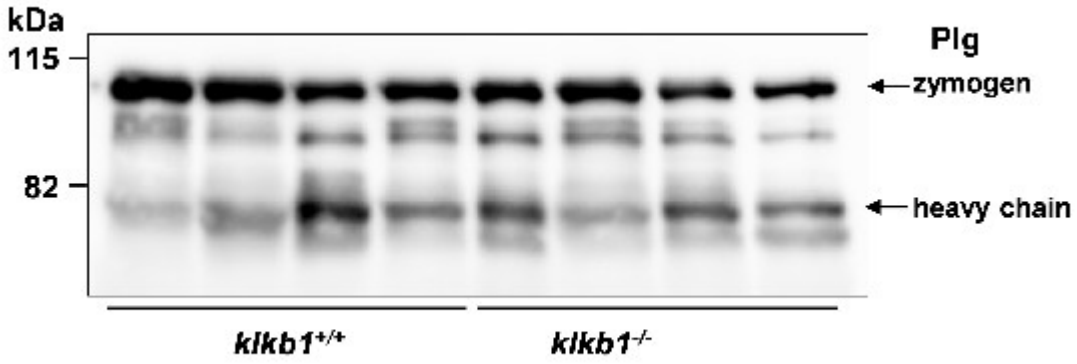

Figure 48: Western blot against plasminogen in nephrotic urine samples from klkb1+/+ and klkb1-/- mice.

In this analysis, urine samples from both klkb1+/+ (wild-type) and klkb1-/- (knockout) mice were compared to investigate whether plasma kallikrein (KLKB1) influences plasminogen activation in nephrotic conditions. Despite the expectation that plasma kallikrein could enhance plasminogen cleavage, no significant difference was observed between the wild-type and knockout groups. Both genotypes showed similar levels of plasminogen zymogen and heavy chain, suggesting that plasma kallikrein does not play a major role in the activation of plasminogen in vivo under these conditions.

3.3.1.4 Plasminogen in nephrotic urine of vehicle- and amiloride-treated nephrotic mice

Does amiloride influence the plasminogen cleavage by uPA?

Amiloride is known to counteract sodium retention, like it could be shown in rats with experimental nephrotic syndrome, by directly blocking ENaC [43]. Amiloride also suppresses uPA with a Ki value of 7 µM [96], which lies below the urinary concentrations measured in the treated animals [97]. Because of this secondary effect, amiloride likely influences two pathways simultaneously: On the one hand, it directly inhibits ENaC activity and on the other hand, it prevents plasminogen activation within the tubular lumen by urokinase. Previous experiments with amiloride treatment in nephrotic rats support this interpretation as it has been reported to reduce urinary plasmin generation by urokinase, thereby it could indirectly reduce proteolytic ENaC activation.

A comparable pattern was observed in nephrotic mice urine samples. Four hours after amiloride treatement, urinary plasmin activity was almost completely suppressed in samples collected 4 hours after injection but it returned to baseline when it was measured after 24 hours (Figure 49). The western blot revealed that mice treated with only empty vehicle solution excreted both the 105 kDa plasminogen precursor and its 75 kDa heavy chain fragment, indicating the activation cleavage at the R561/V562 site (Figure 49A). The light chain with the size of 22 kDa and contained catalytic domain of plasmin couldn't be detected because the used antibody is specific only for the heavy chain. In accordance with the functional findings on uPA and plasmin activity, the high amiloride concentration 4 hours after injection was associated with a complete absence of full-length plasminogen in urine samples which indicates efficient inhibition of urokinase-mediated plasminogen cleavage. This cleavage reappeared toward the end of the dosing interval, when amiloride was almost completely excreted from urine.

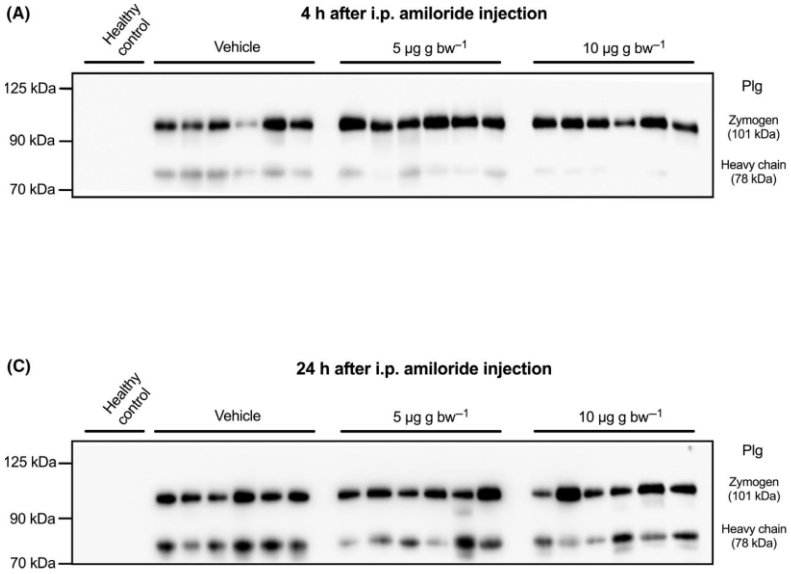

Figure 49: Western blot against plasminogen and its heavy chain in urine samples of vehicle- and amiloride-treated nephrotic mice.

3.3.1.5 Expression of plasma kallikrein in human urine samples

Figure 50 depicts the results from representative samples of different diseased patients including urine of a healthy control person, chronic kidney diseases (CKD) patients with albuminuria spanning the stages A1 (<30 mg/g creatinine), A2 (30-300 mg/g creatinine), A3 (>300 mg/g creatinine) and nephrotic syndrome (NS). Only in the patient with distinctive nephrotic syndrome plasma kallikrein was detectable as zymogen at 82 kDa (marked by *) and as light chain at 36 kDa (marked by **). In plasma, only the zymogen was detectable, whereas in active plasma kallikrein only light chains at 32 and 36 kDa were strongly visible. For optimal contrast range of the signal, WB membranes containing urine, plasma samples and positive control were developed separately. The antibody also cross-reacted a little bit with human albumin.

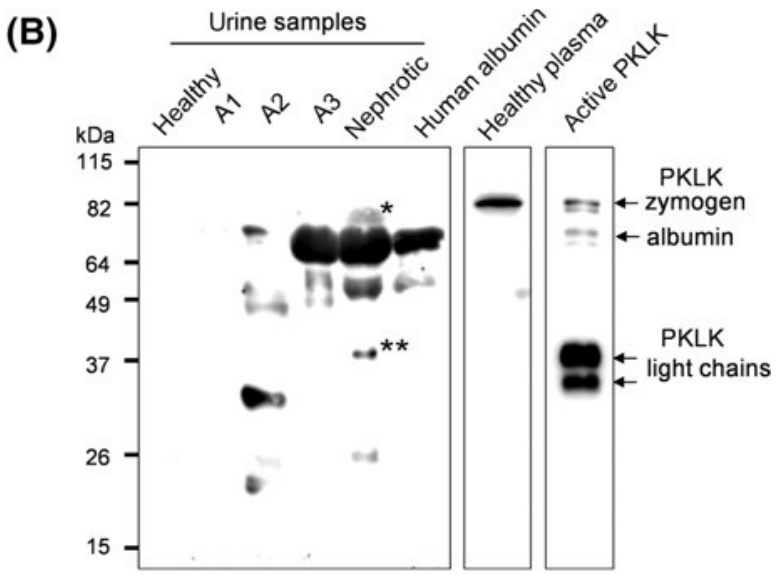

Figure 50: Western blot against plasma kallikrein in urine samples of patients with different stages of albuminuria and nephrotic syndrome + controls with healthy urine and plasma

The latter band corresponds to the light chain of plasma kallikrein indicating plasma kallikrein cleavage and dissociation from the heavy chain under reducing conditions.

3.3.1.6 Plasma Kallikrein in mouse plasma/urine samples

These western blot results show in Figure 51 the plasma kallikrein expression in plasma and urine from wild-type (klkb1+/+) mice compared with samples from mice lacking plasma kallikrein (klkb1-/-). In healthy klkb1+/+ mice, the plasma kallikrein zymogen was mainly visible as an 82 kDa band in both plasma and urine. When these mice were getting nephrotic, the intensity of this zymogen band was clearly reduced in the plasma sample, most likely due to loss through the damaged glomerular filter into the urine. Furthermore, several lower–molecular-weight fragments of plasma kallikrein were detected, indicating intensive proteolytic processing. Samples of mice with plasma kallikrein knockout (klkb1-/-) showed some unspecific band signal in plasma and to a smaller degree in urine. The prominent band at 69 kDa most likely corresponds to unspecific binding to the most abundant plasma protein albumin.

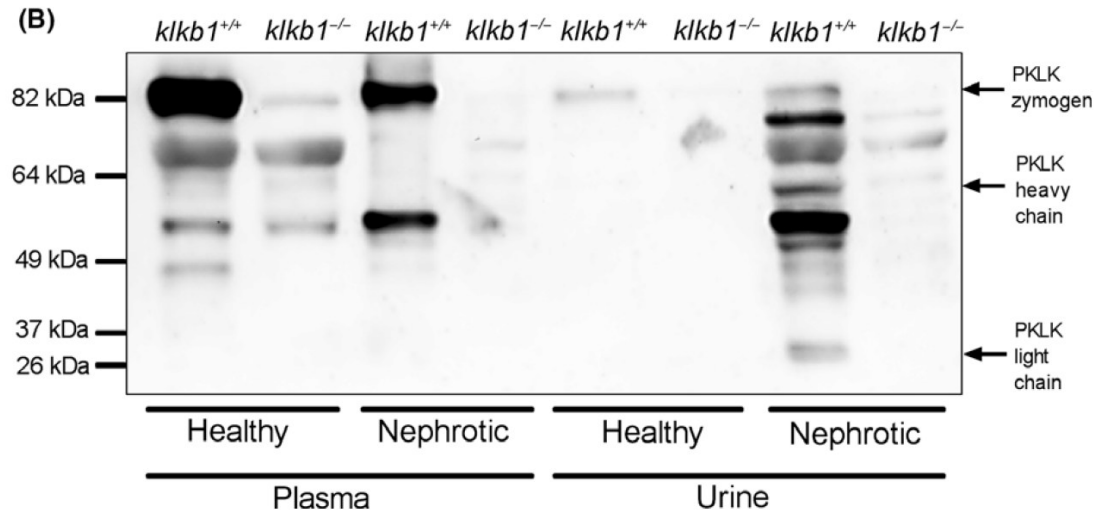

Figure 51: Western Blot against plasma kallikrein in plasma and urine samples of healthy and nephrotic klkb1+/+ and klkb1-/- mice

In urine samples from healthy klkb1+/+ mice, the plasma kallikrein zymogen appeared only as a very weak band at approximately 88 kDa. In contrast, nephrotic klkb1+/+ mice excreted a range of plasma kallikrein-derived fragments between 30 and 88 kDa. The bands at about 30 and 52 kDa are consistent with the light and heavy chain of plasma kallikrein after their connecting disulfide bond was dissociated under reducing conditions. In healthy plasma from klkb1+/+ mice, plasma kallikrein was detected predominantly at 88 kDa whereas this band was entirely absent in klkb1-/- mice as expected.

3.3.1.7 Expression of Factor VII-activating protease (FSAP) in human urine samples

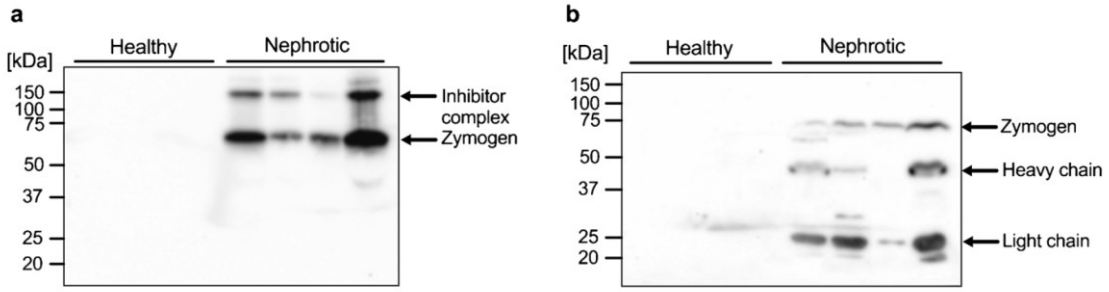

Figure 52: Factor VII-activating protease (FSAP) in human urine samples

(n = 4 healthy, n = 4 nephrotic) under reducing and non-reducing conditions

In the first blot in panel a), FSAP was detected in the nephrotic group at 64 kDa as the inactive zymogen and at 150 kDa as a high–molecular-weight inhibitor complex. Western blot of the same samples (n = 4 healthy, n = 4 nephrotic) under reducing conditions also showed the FSAP zymogen as single chain (64 kDa), but also the light (27 kDa) and heavy chain (50 kDa) which indicates a previous activation cleavage at the bond on arginine R311. After that, both chains could dissociate under reducing conditions.

3.3.2 Plasma proteases from complement system

3.3.2.1 Expression of Complement Factor B in human urine samples

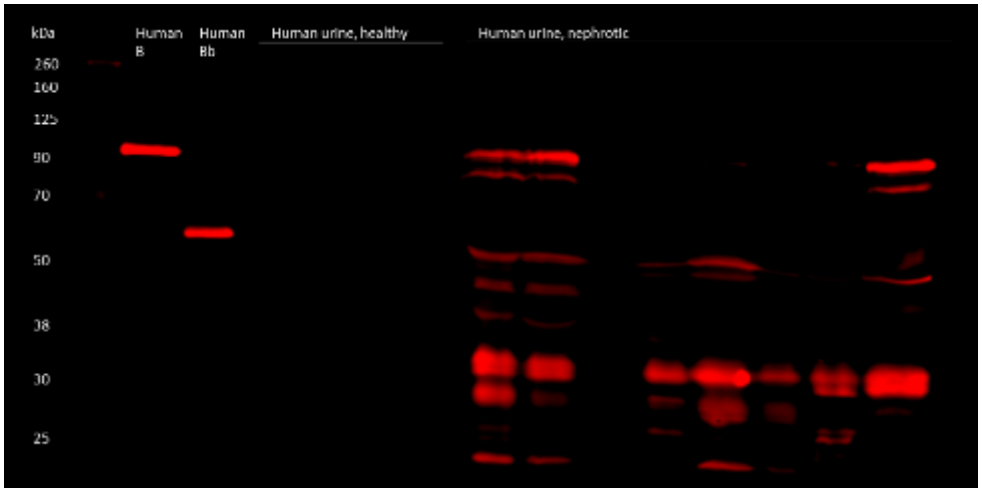

Figure 53: Complement Factor B in human urine samples

The Western blot shown investigated the presence of Complement Factor B in human urine samples, with the first two lanes representing controls and the remaining lanes showing urine samples from healthy and nephrotic individuals.

The nephrotic urine lanes displayed multiple strong bands. The ~100 kDa zymogen form of Factor B is prominently detected, along with several additional bands below 70 kDa, which likely represented cleavage products of activated Factor B (including the Bb fragment at ~55 kDa). The presence of these bands indicated that Factor B was not only excreted in higher amounts in nephrotic urine but was also activated in the disease state.

The blot clearly demonstrates that both the zymogen form and the cleavage products of activated Complement Factor B were detected in nephrotic urine, indicating increased

complement system activity and activation in nephrotic syndrome. This contrasts with healthy urine, where no Factor B bands were visible.

3.3.2.2 Expression of Complement Factor B in mouse urine samples

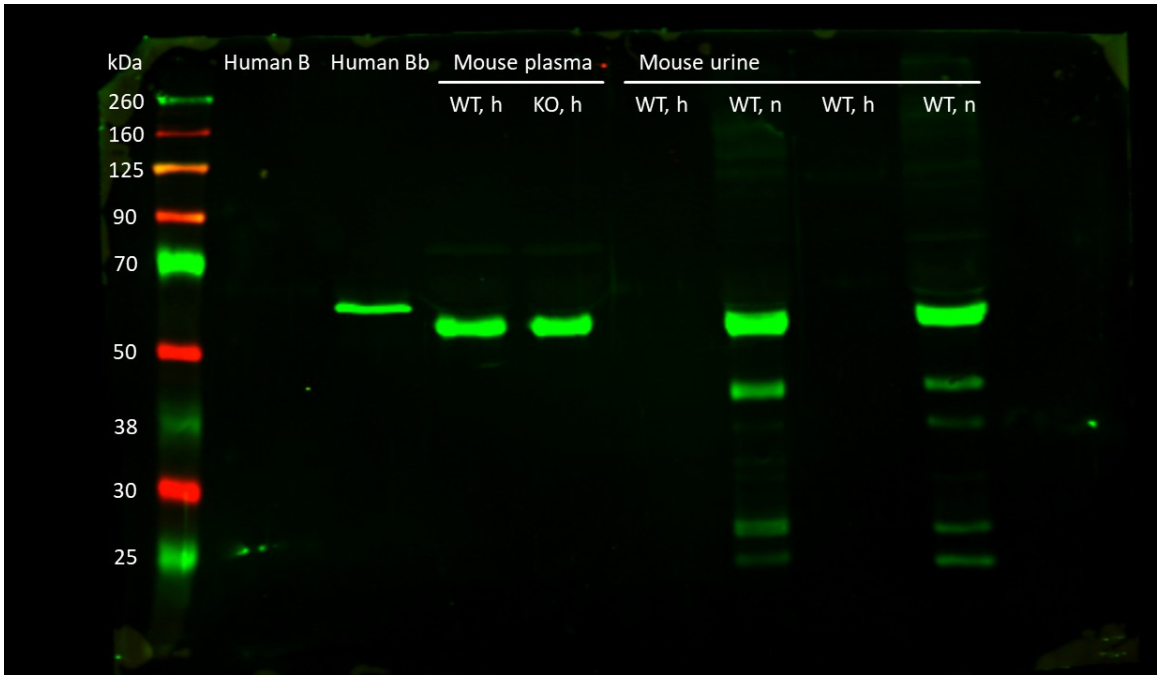

Figure 54: Complement Factor B in mouse urine samples

Factor B was arising in its zymogen form and also in cleaved variants in nephrotic mouse urine samples. In the nephrotic wild-type mouse urine samples, both the zymogen form (~100 kDa) of Factor B and the cleaved Bb fragment (~55 kDa) were prominently visible. The presence of these bands indicated that Factor B is not only present but also actively undergoing cleavage in nephrotic conditions. Additionally, several smaller bands appeared, corresponding to further cleavage products, which suggest that Factor B is undergoing extensive processing and activation in nephrotic urine.

The increase in cleavage products in nephrotic urine suggests enhanced complement activation in nephrotic conditions.

3.3.2.3 Complement Factor B in healthy mouse plasma + in healthy and nephrotic mouse urine (WT, Plg-KO, Cfb-Ko; Aprotinin-treated)

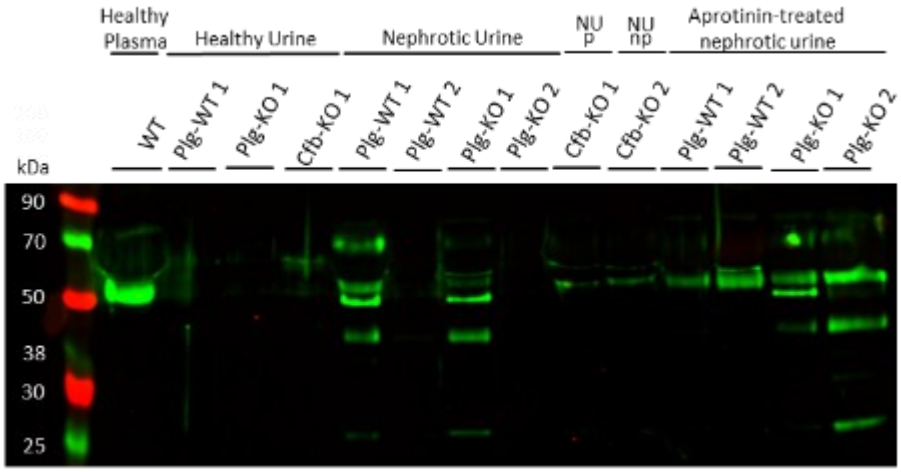

Figure 55: Complement Factor B in healthy mouse plasma + in healthy and nephrotic mouse urine (WT, Plg-KO, Cfb-Ko; Aprotinin-treated)

This Western blot investigated the presence and cleavage patterns of Complement Factor B in mouse plasma and urine samples under various conditions, including wild-type (WT), plasminogen knockout (Plg-KO), and complement factor B knockout (Cfb-KO) mice. Additionally, urine samples treated with aprotinin, a serine protease inhibitor, were included to assess the effect of inhibiting protease activity.

Healthy plasma served as a control and showed a strong band around ~50 kDa, which corresponds to the zymogen form of Complement Factor B. This band is expected in plasma, where Factor B circulates in its inactive form.

The Western blot demonstrated that Factor B was present in its zymogen form in both healthy and nephrotic urine, with enhanced cleavage products in nephrotic samples, indicating increased complement activation. The Cfb-KO samples lacked Factor B, as expected, while Plg-KO mice showed similar activation patterns to WT, suggesting plasminogen did not significantly influence Factor B cleavage. However, aprotinin treatment reduced the appearance of cleavage products, confirming that serine protease activity contributes to Factor B activation in nephrotic urine.

3.3.2.4 Expression of Complement Factor D in mouse urine samples

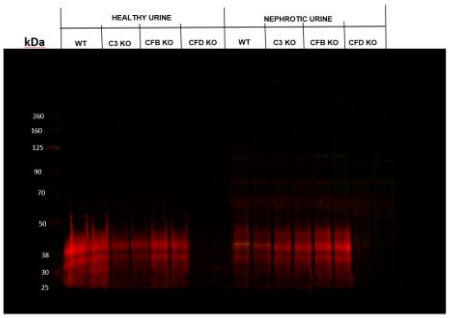

Figure 56: Complement Factor D in mouse urine samples

The Western blot revealed that Complement Factor D is consistently expressed in mouse urine, both in healthy and nephrotic conditions. The presence of Factor D in healthy urine samples was corroborated by mass spectrometry (MS) data, indicating that Factor D is not only present in pathological conditions but is also a component of the baseline urinary proteome. Factor D's presence in nephrotic urine supports its role in complement system activation, potentially contributing to the progression of kidney damage in nephrotic syndrome.

3.3.2.5 Expression of Complement C2 in human urine samples

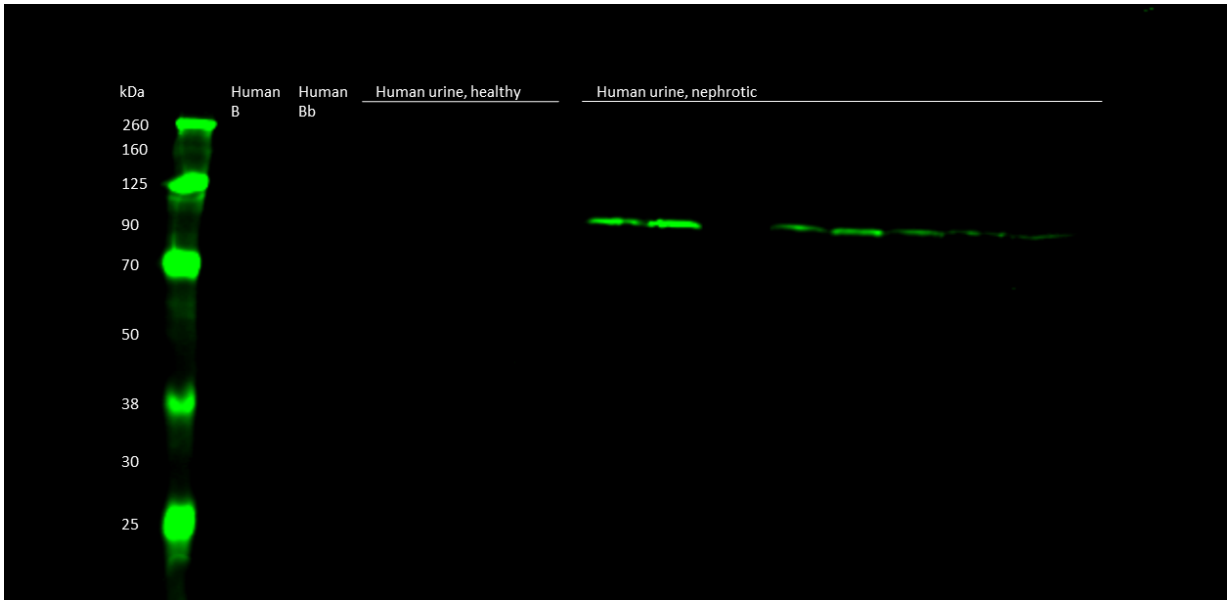

Figure 57: Complement C2 in human urine samples

In healthy urine samples, no visible bands corresponding to Complement C2 were detected. This suggests that C2 was not present or is present at levels below the detection

limit in the urine of healthy individuals, consistent with normal kidney function, which prevents significant complement protein leakage.

In nephrotic urine samples, a clear band was detected at around ~100 kDa, representing the zymogen form of Complement C2. These bands were indicative of the new appearance of Complement C2 in nephrotic urine. The findings suggest that C2 plays a role in complement activation and kidney inflammation during nephrotic conditions.

3.3.3 Urinary proteases

3.3.3.1 Expression of urokinase in human plasma/urine samples

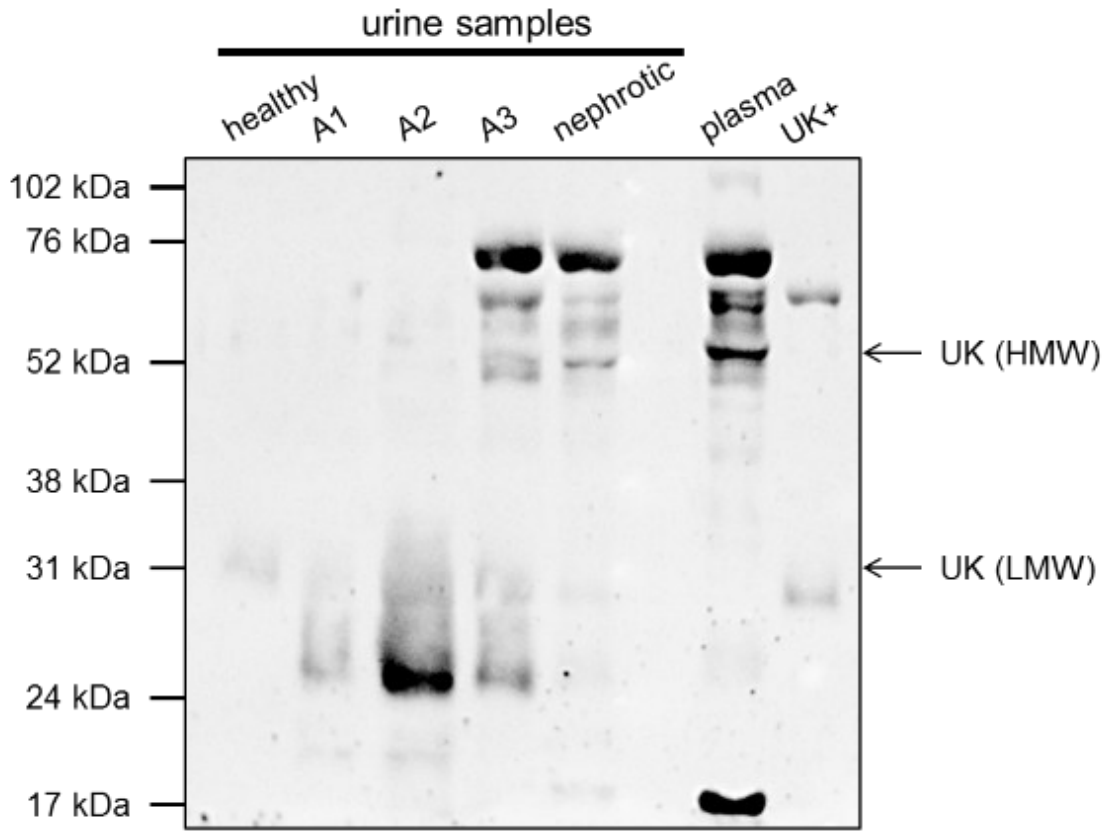

Figure 58: Urokinase in human plasma/urine samples

In the Western blot shown in Figure 58, distinct differences in urokinase-type plasminogen activator (uPA) expression could be observed between healthy urine, urine from patients with progressive albuminuria stages (A1–A3), and nephrotic urine, as well as in comparison to plasma.

In healthy urine and low albuminuria A1, only faint or undetectable bands were visible, reflecting the low physiological excretion of uPA under intact glomerular filtration and

limited local tubular release. With increasing albuminuria, a gradual rise in uPA signal intensity was seen, with the appearance of distinct bands corresponding to both the high molecular weight (HMW) uPA form (~54 kDa) and the low molecular weight (LMW) form (~33 kDa). These findings indicate a progressive urinary appearance and partial cleavage of uPA, consistent with enhanced filtration and intratubular activation during glomerular injury.

Physiologically, HMW-uPA is the proenzyme secreted mainly by renal epithelial and endothelial cells, while LMW-uPA arises after cleavage at Lys158–Ile159, generating the active two-chain enzyme responsible for plasminogen activation to plasmin. Thus, the strong LMW band in high albuminuria- and nephrotic urine, especially in the A2 state, reflected an increased conversion to the active enzyme, in line with the elevated plasmin activity and enhanced proteolytic potential observed in nephrotic states.

3.3.3.2 Prostasin in mouse kidney lysates

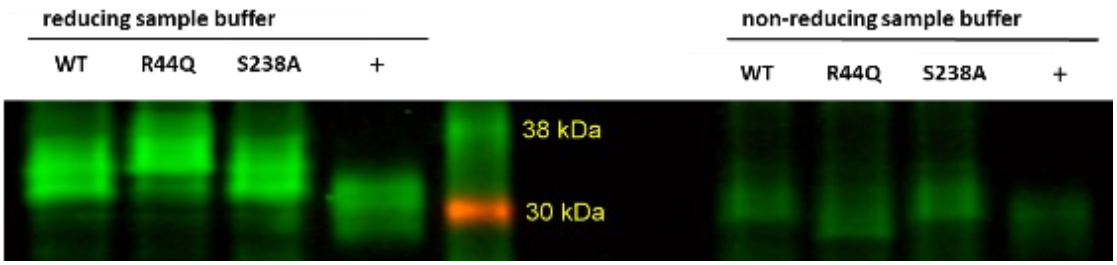

Figure 59: Prostasin in mouse kidney lysates

In the non-reducing buffer, the detected Prostasin (PRSS8) signal appeared with lower band intensity compared to the reducing conditions, and the proteins migrated faster, displaying an apparently lower molecular weight. This migration shift reflected the absence of disulfide bond cleavage, causing the active, two-chain form of Prostasin to remain partially associated. Under reducing conditions, however, disulfide bonds were cleaved, leading to the dissociation of the light and heavy chains of Prostasin, thereby confirming the presence of its activated form.

Notably, the R44Q mutant—which lacked the canonical cleavage site within the activation peptide—migrated even faster than wild-type (WT) and catalytically inactive S238A variants, indicating a conformational alteration and incomplete zymogen activation. The migration pattern of WT and S238A under reducing conditions

demonstrated that these variants undergo proper processing at the activation bond between Arg44 and Ile45, resulting in a cleaved and thus activated Prostasin.
The prostasin scaffold function for recruiting another serine protease was disrupted in the zymogen-locked variant, in which arginine was mutated to glutamine at the cleavage site position 44 (Prss8-R44Q). This loss of function is most plausibly explained by an altered protein conformation of the uncleaved single-chain prostasin. This different conformation was confirmed by different band size compared to S238A and WT, even under non-reducing conditions.

3.4 Proteolytic activity against the distal polybasic tract of γ-ENaC in urine from nephrotic humans and mice

The results in this section are based on the first-author publication "Proteolytic Activity against the Distal Polybasic Tract of the Gamma Subunit of the Epithelial Sodium Channel ENaC in Nephrotic Urine" [90]

3.4.1 HPLC separation and fluorescene detection of cleaved γ-ENaC fragments by AMCA substrate

To evaluate if nephrotic urine from nephrotic people and mice have proteolytic activity against the distal polybasic tract of γ-ENaC (186RKRK in mice), a synthetic peptide substrate spanning the amino acid sequence 180-194 of murine γ-ENaC was generated. On the N-terminal side, it was labelled with the 7-amino-4-methylcoumarin-3-acetic acid (AMCA) fluorophore (sequence: AMCA-FTGRKRKISGKIIHK, short name: AMCA substrate, with coupled γ-ENaC180-194). When analyzed by HPLC, this substrate consistently eluted at a retention time of 18.29±0.20 min (Figure 60).

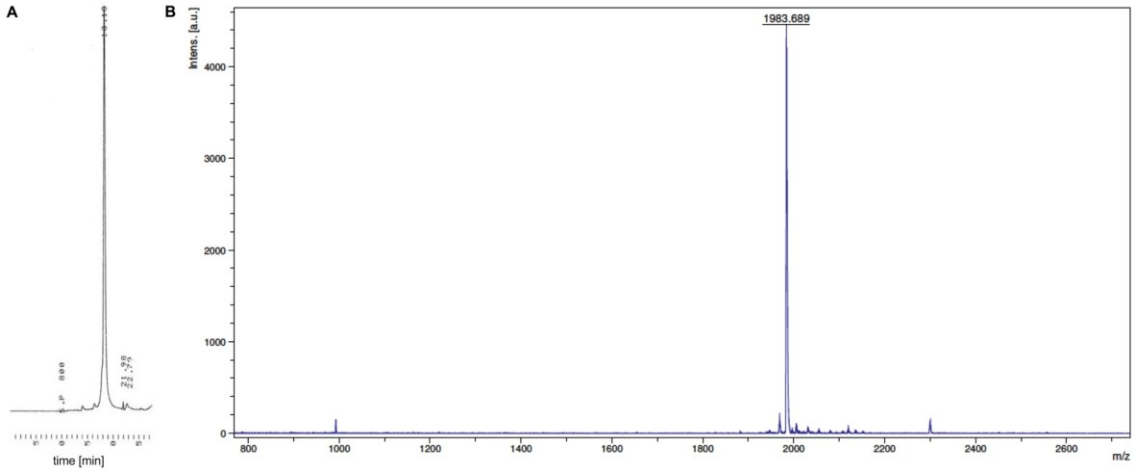

Figure 60: Chromatogram of the intact AMCA-coupled γ-ENaC$^{180-194}$ peptide substrate adopted from first-authorship publication [90]

A Representative chromatogram showing a single peak with a retention time of 18.10 min after injection of stock solution to the circuit
B Confirmation of the intact sequence of AMCA-coupled γ-ENaC$^{180-194}$ peptide substrate (1987 Da measured, 1983 Da expected) in a MALDI spectrum (designated with ° in Figure 2&3)

The human urine samples were also incubated with the same mouse-sequence substrate due to very similar sequence around the polybasic tract, only differing in most times the same or similar amino acid positions of the sequence FTGRKRKVGGSIIHK, with underlined differences and one possible arginine cleavage site less at 185VGGS instead of mouse substrate with the correlating sequence 190ISGK.

Human samples showed hardly any degradation in the healthy state. In contrast to the healthy subjects, a dominant degradation product with a prolonged retention time of 0.9 min compared to the initial substrate could be detected in the urine of 3 of 4 patients with acute nephrotic syndrome. After collection of the eluate solution in the MALDI-TOF instrument, this yielded the mass of the AMCA-FTGRKR fragment. AMCA-FTGRK and AMCA-FTGR could be reliably detected as further degradation products in the subsequent later peaks.

In both healthy and nephrotic wild-type mice, the degradation product AMCA-FTGRKR was also found in the urine samples; furthermore, several degradation products with a prolonged retention time (>4 min) were found in the nephrotic urine. In the urine samples from nephrotic plasminogen KO mice, mostly only the AMCA-FTGRKR fragment appeared. After aprotinin addition, the formation of this fragment was almost completely inhibited.

When the peptide substrate was incubated with urine from healthy individuals (n=8) chromatographic analysis consistently showed a single peak at 18.98±0.11 min (Figure 61A). The addition of the serine protease inhibitor aprotinin to these samples had no effect on the elution profile (Figure 61B). In contrast to this, incubation of the substrate with urine samples from nephrotic patients (n=8) yielded to a new, additional peak. This indicates a cleavage product, and it eluted approximately 0.95±0.05 min later than the intact substrate (Figure 61C). Next to this main cleavage product, minor products were also detected, with retention time shifts of Δ+0.45±0.02 min, Δ+1.88±0.08 min and Δ+3.09±0.07 min. When aprotinin was included in the sample mixture, the cleavage of the substrate formation of these fragments was largely suppressed (Figure 61D). All retention time of the intact substrate and its fragments are listed in Table 5, together with the mouse values directly listed below, with the significances between healthy and nephrotic groups (unpaired test) as well as between with or without aprotinin coincubation (paired test), for a compact overview and direct comparison of the values between the species in tabular form.

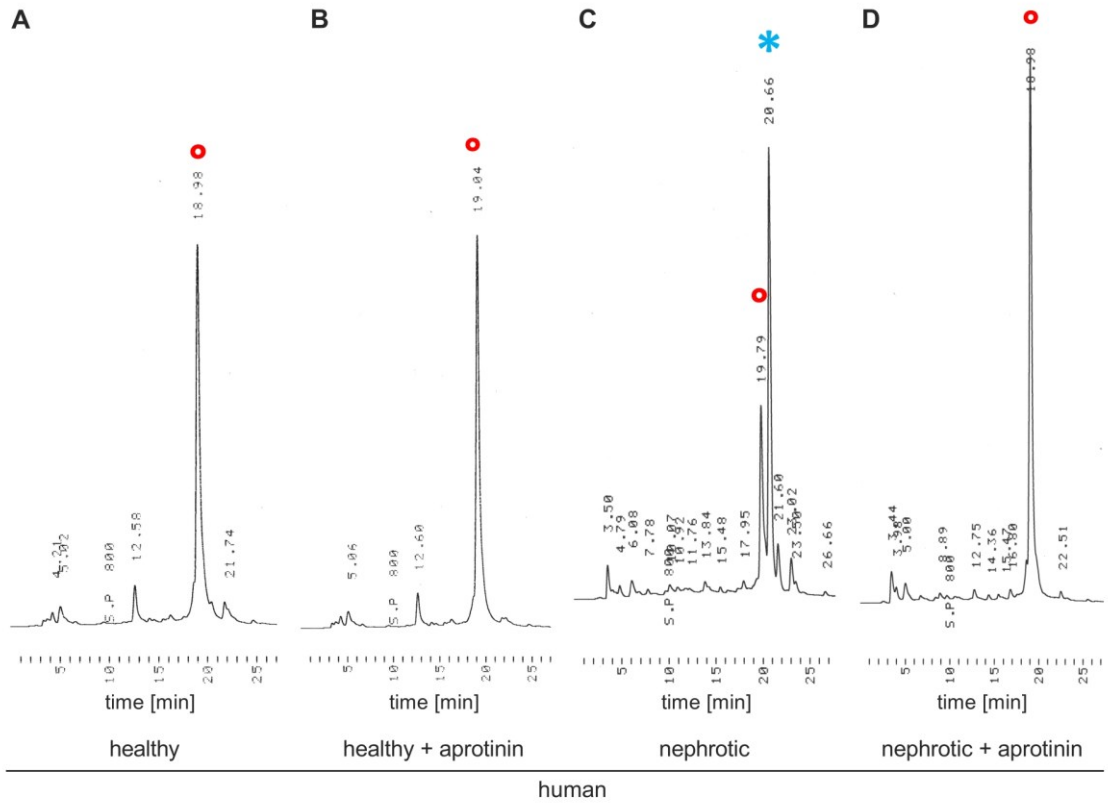

Figure 61: Cleavage of the AMCA-coupled γ-ENaC$^{180-194}$ peptide substrate in human urine

from a healthy person and a patient with nephrotic syndrome

adopted from first-authorship publication [90]

A Representative chromatogram for overnight incubation of the AMCA substrate with urine from a healthy person, showing the dominant peak of the intact substrate at 18.98 min (marked with °) and a minor peak at 21.74 min
B Representative chromatogram of the same healthy sample like in A, but with co-incubation of aprotinin, showing only the dominant intact substrate peak, here at 19.04 min (marked with °)
C Representative chromatogram for overnight incubation of the AMCA substrate with urine from a nephrotic patient, showing another stronger fragment peak arising at 20.66 min (marked with *)
D Representative chromatogram of the same nephrotic sample like in C, showing the recovery of the intact substrate peak at 18.98 min (marked with °) and complete disappearance of all other peaks corresponding to the degradation products.

The AMCA-coupled γ-ENaC180-194-substrate was also incubated with urine samples from mice. The yielded cleavage pattern closely matched those observed in the previous experiments with human urine samples. Urine samples obtained from healthy 129S1/SvImJ mice showed only minimal activity against the substrate, but this activity was already sensitive to inhibition by aprotinin (Figure 62A/B). Similar to nephrotic patients, the urine from doxorubicin-injected nephrotic 129S1/SvImJ mice (n=4) also cleaved the substrate to a large extent to a dominant cleavage product, Δ+1.01±0.09 min in relation to the intact substrate. Additional, less abundant fragment peaks were detected at Δ+2.24±0.01 min and Δ+2.75±0.01 min (Figure 62C). As seen in human nephrotic samples, co-incubation with aprotinin largely suppressed the proteolytic activity of nephrotic urine and thus prevented the cleavage of the substrate (Figure 62D). A comparable fragmentation profile was observed in urine samples from nephrotic B6-Nphs2Δipod mice. In this mouse model, a major peak appeared at +Δ1.78±0.02 min accompanied by additional fragments at a range of Δ+3.71 to 6.72 min (n=4, (Figure 62E)). Again, the presence of aprotinin during incubation completely suppressed detectable proteolytic activity, so that only the peak of the intact substrate was measured (Figure 62F).

Plasminogen is the dominant serine protease in nephrotic urine of humans and mice, both in terms of quantity and activity, and accounts for almost >90% of the proteolytic activity [68]. To evaluate its contribution to the overall proteolytic activity against the AMCA substrate, urine samples from nephrotic B6-Nphs2$^{\Delta ipod}$ mice lacking plasminogen (Plg$^{-/-}$) were studied. As shown in Figure 62G, the plasminogen-free nephrotic urine from these B6-Nphs2$^{\Delta ipod}$ * Plg$^{-/-}$ mice still produced a cleavage product with a retention time shift of Δ+0.85±0.01 min. This residual activity was almost entirely eliminated again by the

co-incubation with aprotinin (Figure 62H), which indicates an aprotinin-sensitive activity against this AMCA substrate even without the high plasminogen activity.

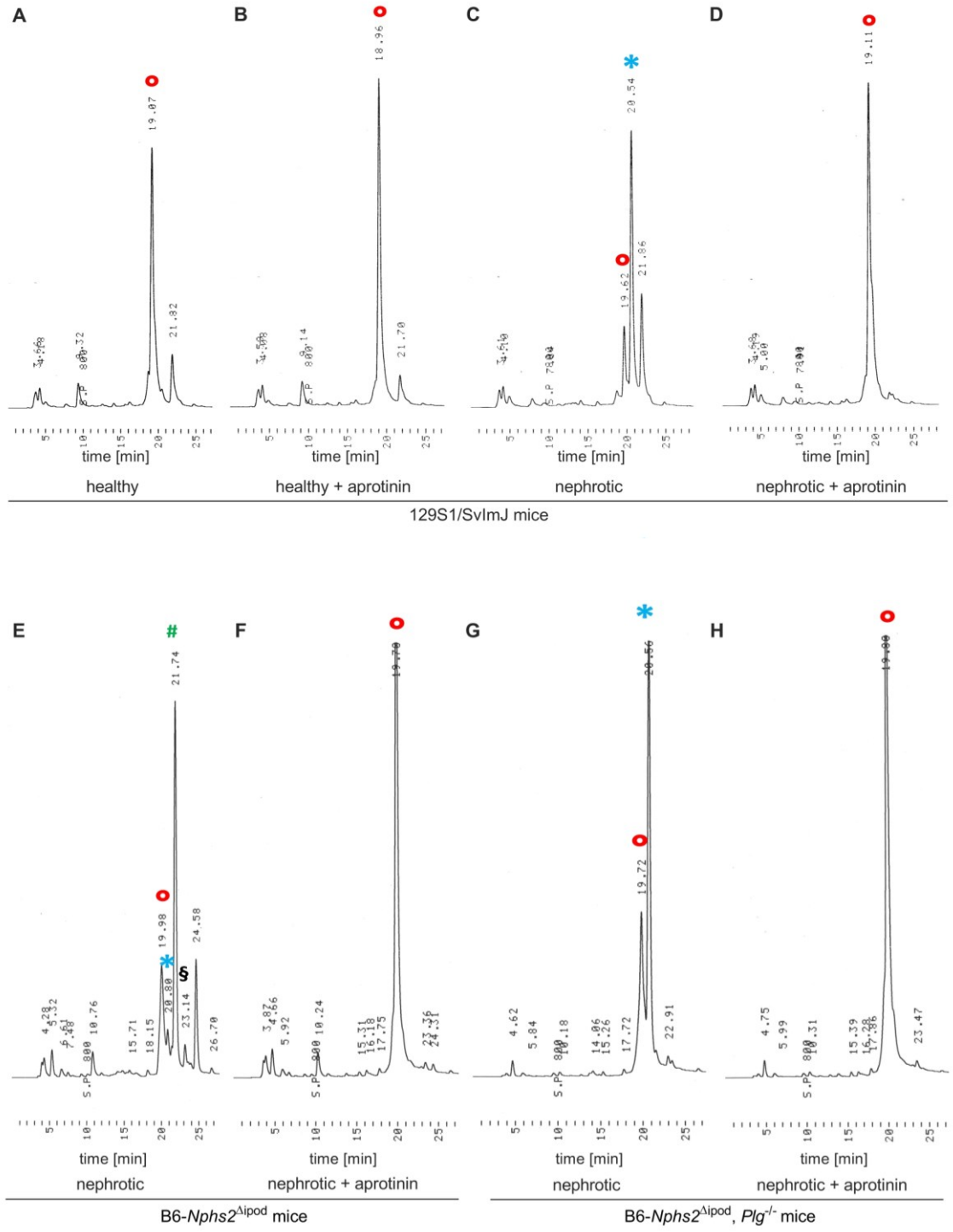

Figure 62: Cleavage of the AMCA-coupled γ-ENaC$^{180-194}$ peptide substrate in mice with experimental nephrotic syndrome

adopted from first-authorship publication [90]

A Representative chromatogram for overnight incubation of the AMCA substrate with urine from a healthy mouse, showing the dominant peak of the intact substrate at 19.07 min (marked with °) and a minor peak at 21.82 min
B Representative chromatogram of the same healthy mouse sample as in A, but with co-incubation of aprotinin, showing the dominant peak at 18.96 min (marked with °) and the still visible, but here smaller minor peak at 21.70 min compared to A
C Representative chromatogram for overnight incubation of the AMCA substrate with urine from a doxorubicin-injected nephrotic 129S1/SvImJ mouse, showing a newly arising AMCA fragment peak at 20.54 min (marked with *)
D Representative chromatogram of the same nephrotic sample as in C, but with co-incubation of aprotinin, showing the recovery of the intact substrate peak at 19.11 min (marked with °) and complete disappearance of the fragment peak at 20.54 min, as detected in C (marked with *)
E Representative chromatogram for overnight incubation of the AMCA substrate with urine from a nephrotic B6-*Nphs2*$^{\Delta ipod}$ mouse, showing the intact substrate peaks at 19.98 min (marked with *) and two AMCA fragment peaks 20.80 and 21.74 min (marked with # and §)
F Representative chromatogram of the same nephrotic sample as in E, but with co-incubation of aprotinin, showing only the intact substrate peak peak at 19.70 min (marked with °) and complete disappearance of the fragment peaks at 20.80 and 21.74 min, as detected in E (marked with # and §)
G Representative chromatogram for overnight incubation of the AMCA substrate with urine from a nephrotic B6-*Nphs2*$^{\Delta ipod}$**Plg*$^{-/-}$ mouse, showing the intact substrate peak at 19.72 min (marked with °) and a fragment peak at 20.56 min (marked with *)
H Representative chromatogram of the same nephrotic sample as in G, but with co-incubation of aprotinin, showing only the intact substrate peak at 19.80 min (marked with °) and complete disappearance of the fragment peak at 20.56 min, as detected in G (marked with *)

To assign the detected chromatographic peaks to the specific proteolytic AMCA fragments, very exact mass determination of these fragments was applied by MALDI-TOF mass spectrometry (MALDI-TOF-MS) of HPLC eluates. These eluates were collected from the HPLC separations, in which the previous chromatograms were also generated, after incubating the AMCA substrate with healthy or nephrotic urine samples from B6-Nphs2$^{\Delta ipod}$ mice. As shown in Figure 63A, the peak with a retention time of 18.98±0.11 min after incubation with healthy urine displayed a molecular mass of 1987 Da, which closely matched and therefore corresponded to the expected mass of 1983 Da for the intact substrate. Incubation with nephrotic urine samples resulted in a prominent additional peak, arising at Δ+0.95 ± 0.05 min after the intact substrate peak which clearly corresponded to AMCA-FTGRKR with measured 1107 Da, which is also exactly the calculated mass (Figure 63B). Further, less intense cleavage fragments at Δ+0.45±0.02 min, Δ+1.88±0.08 min and Δ+3.09±0.07 min corresponded to AMCA-FTGRKRK, AMCA-FTGRK and AMCA-FTGR, respectively (Figure 63C-F). The stepwise prolongation of retention time was indicative of a progressive increase in hydrophobic character of the fragments , most likely caused by the sequential removal of positively charged amino acid residues.

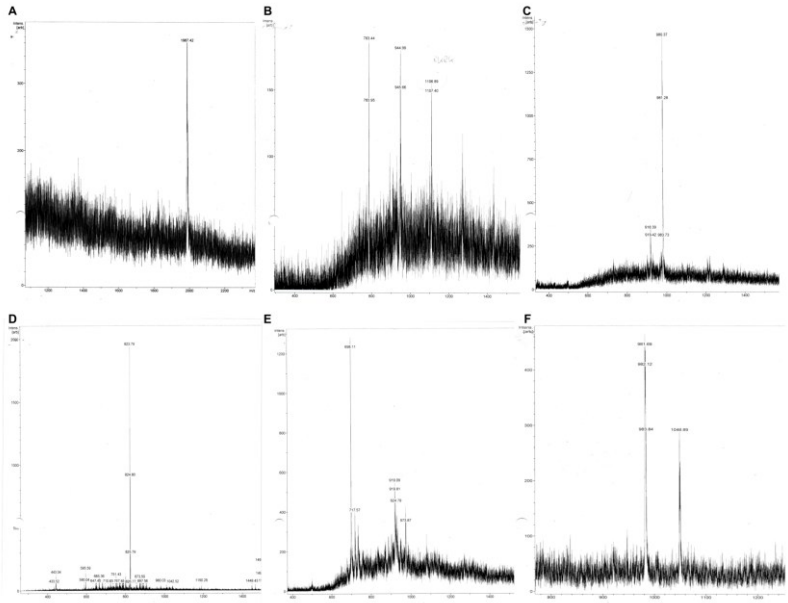

Figure 63: Identification of the intact AMCA-coupled γ-EnaC$^{180-194}$ peptide substrate and its cleavage products

adopted from first-authorship publication [90]

from time-dependent eluates after incubation with urine samples from healthy or nephrotic B6-*Nphs2*$^{\Delta ipod}$ mice (A-E) and from a nephrotic patient (F)

A Identification of the intact sequence of AMCA-coupled γ-EnaC$^{180-194}$ peptide substrate (1987 Da measured, 1983 Da expected) in a MALDI spectrum (designated with ° in Figure 2&3)

B Identification of the cleavage product AMCA-FTGRKRK (1107 Da measured, 1107 Da expected) in a MALDI spectrum

C Identification of the cleavage product AMCA-FTGRKR (980 Da measured, 979 Da expected) in a MALDI spectrum (designated with * in Figure 2&3)

D Identification of the cleavage product AMCA-FTGRK (824 Da measured, 823 Da expected) in a MALDI spectrum (designated with # in Figure 2&3)

E Identification of the cleavage product AMCA-FTGR (698 Da measured, 694 Da expected) in a MALDI spectrum (designated with § in Figure 2&3)

F Identification of the cleavage product AMCA-FTGRKR (980 Da measured, 979 Da expected) in a MALDI spectrum of a nephrotic urine of a patient

Quantitative comparisons of the peak intensities confirmed the dominance of the cleavage product AMCA-FTGRKR. For example, it accounts for 44% of the total fluorescent signal in nephrotic urine of humans, which is followed by AMCA-FTGRK with 15% (Figure 64A). Taken together, these fragments, resulted from cleavages within the polybasic tract, contributed for 75% of the total signal. Upon addition of aprotinin, this proportion decreased markedly to 23%, indicating that the remaining activity should originate largely from proteases other than serine proteases.

In healthy urine of 129S1/SvImJ mice, there was already a slight aprotinin-sensitive activity (Figure 64B). After induction of nephrotic syndrome, the cleavage product AMCA-FTGRKR emerged as the major fragment accounting for 58% of the total signal, while AMCA-FTGRK contributed 21%. Altogether, cleavage products of the polybasic tract also showed a high proportion here with 81% of the total signal, similar to human samples. In the presence of aprotinin, this proportion was also similar reduced to 25%.
In nephrotic B6-Nphs2$^{\Delta ipod}$ mice, one difference from previous groups was that the proportion of FTGRK was more abundant than FTGRKR, however, a high proportion (50%) originated from cleavage products that could not be assigned to defined fragment masses. All these fragments decreased markedly upon coincubation with aprotinin (Figure 64C). In nephrotic B6-Nphs2$^{\Delta ipod}$*$Plg^{-/-}$ mice lacking plasminogen, FTGRKR still was still the most dominant cleavage product with 37%. The plasminogen-independent activity against this fragment was completely suppressed when the urine-substrate mixture was incubated together with aprotinin (Figure 64D).

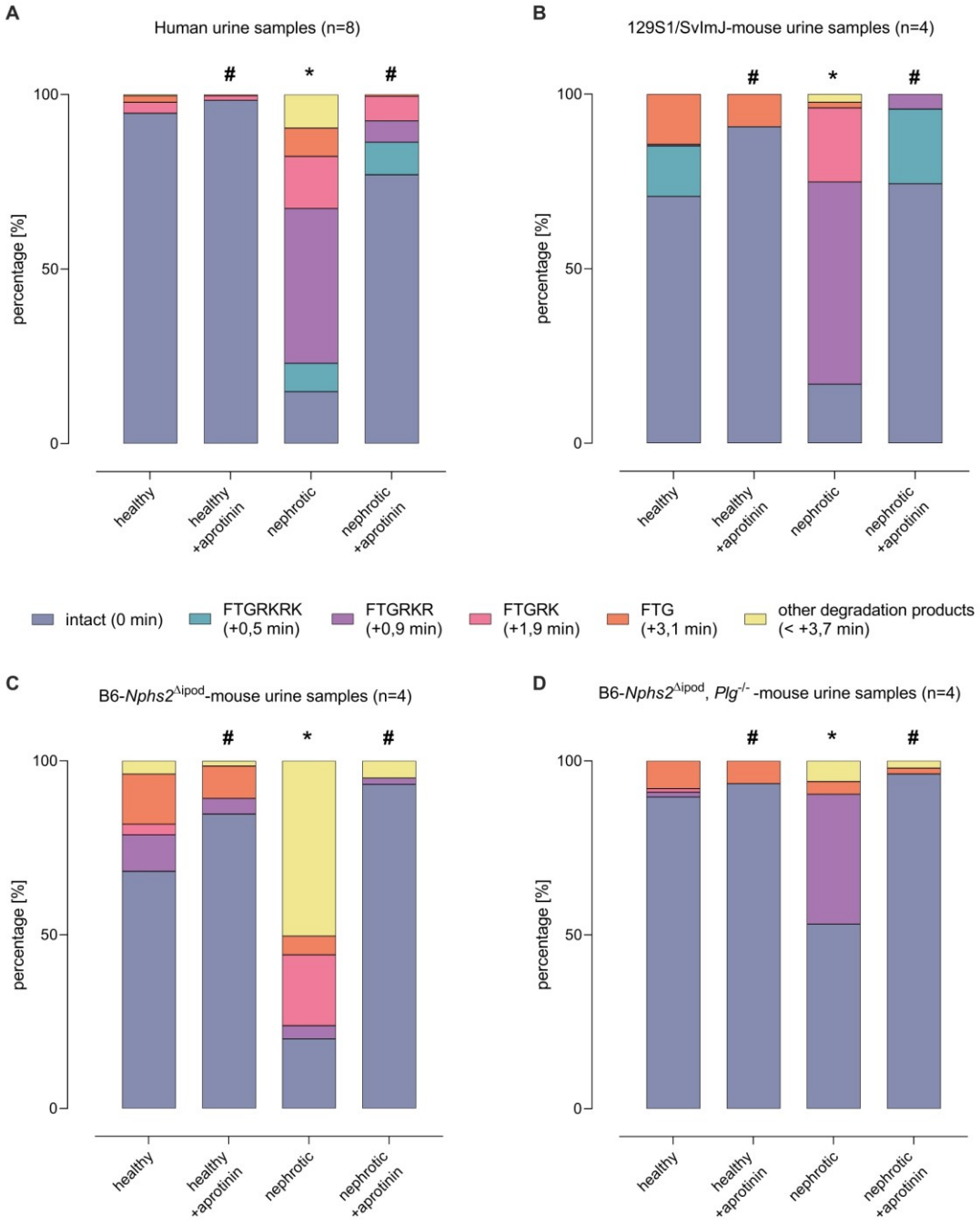

Figure 64: Relative composition of the intact substrate and the cleavage products of the AMCA substrate

representing the distal polybasic tract of γ-ENaC$^{183-186}$, after incubation with urine samples from healthy and nephrotic humans (A) and mice (B-D)

adopted from first-authorship publication [90]

Stacked bar graph representing the mean proportion of each fluorescent AMCA cleavage product, calculated from the single chromatograms (n=8 for human samples, n=4 for mouse samples each). Arithmetic means ± SEM are given in Table 5.
significant difference of the distribution between samples with and without aprotinin co-incubation, * significant difference of the distribution between healthy and nephrotic samples

Table 5: Relative abundance of the AMCA substrate cleavage products,

within the distal polybasic tract of γ-ENaC$^{180-194}$, after incubation with urine samples from healthy and nephrotic humans and mice

adopted from first-authorship publication [90]

Arithmetic means ± SEM, expressed in percentage of the relative fluorescent signal, as determined from the chromatograms (n=8 for human samples, n=4 for mice samples). Each line sums up to 100%. APR, aprotinin, n.d. not detectable.

§ day 6 - 8 after doxorubicin injection, §§ day 6 - 8 after end of doxycycline induction

significant difference between with or without aprotinin coincubation (paired test), * significant difference between healthy and nephrotic (unpaired test)

	AMCA-coupled full length substr.	AMCA-FTGRKRK	AMCA-FTGRKR	AMCA-FTGRK	AMCA-FTGR	other cleavage products (range)
human						
retention time, min	18.98 ± 0.11	Δ+0.45 ± 0.02	Δ+0.95 ± 0.05	Δ+1.88 ± 0.08	Δ+3.09 ± 0.07	Δ+3.75 – 6.86
healthy	95 ± 2 %	n.d.	n.d.	3 ± 2 %	2 ± 1 %	0.3 ± 0.3 %
+ APR	98 ± 1 %#	n.d.	n.d.	1 ± 1 %	0.4 ± 0.4 %	n.d.
nephrotic	15 ± 4 % *	8 ± 7 %	44 ± 12 %	15 ± 5 % *	8 ± 2 % *	10 ± 7 %
+ APR	77 ± 10 % #	9 ± 9 %	6 ± 4 % #	7 ± 5 %#	1 ± 1 %#	n.d.
129S1/SvImJ mice						
retention time, min	19.44 ± 0.08	Δ+0.49 ± 0.01	Δ+1.01 ± 0.09	Δ+2.24 ± 0.01	Δ+2.75 ± 0.01	Δ+3.33
healthy	71 ± 10 %	14 ± 8 %	0.4 ± 0.4 %	n.d.	14 ± 2 %	n.d.
+ APR	91 ± 1 %	n.d.	n.d.	n.d.	9 ± 1 %	n.d.
nephrotic§	17 ± 5 % *	n.d.	58 ± 5 % *	21 ± 2 %	2 ± 2 %*	2 ± 1 %
+ APR	74 ± 10 % #	21 ± 12 %	4 ± 4 % #	n.d.	n.d.	n.d.
B6-*Nphs2$^{\Delta ipod}$*						
retention time, min	19.51 ± 0.06	n.d.	Δ+0.89 ± 0.02	Δ+1.78 ± 0.02	Δ+3.19 ± 0.02	Δ+3.71 – 6.72
healthy	68 ± 6 %	n.d.	11 ± 6 %	3 ± 2 %	14 ± 1 %	4 ± 3 %
+ APR	85 ± 3 % #	n.d.	5 ± 5 %	n.d.	9 ± 2 %#	1 ± 1 %
nephrotic§§	20 ± 9 % *	n.d.	4 ± 2 %	20 ± 13 %	5 ± 4 %	50 ± 25 %
+ APR	93 ± 4 %#	n.d.	2 ± 1 %	n.d.	n.d.	5 ± 3 %
B6-*Nphs2$^{\Delta ipod}$* * *Plg$^{-/-}$*						
retention time, min	19.48 ± 0.05	n.d.	Δ+0.85 ± 0.01	Δ+1.73 ± 0.07	Δ+3.21 ± 0.01	Δ+4.70 – 6.79
healthy	90 ± 3 %	n.d.	1 ± 1 %	1 ± 1 %	8 ± 2 %	n.d.
+ APR	93 ± 2 %	n.d.	n.d.	n.d.	7 ± 2 %#	n.d.
nephrotic§§	53 ± 11 % *	n.d.	37 ± 12 % *	n.d.	4 ± 3 %	6 ± 6 %
+ APR	96 ± 4 %#	n.d.	n.d.	n.d.	2 ± 2 %	2 ± 2 %

3.4.2 Quantitation of urinary proteolytic activity against the polybasic tract of γ-ENaC by AMC substrates

To enable a more precise quantification of specific cleavage events within the polybasic tract, a series of fluorogenic peptides fluorogenic substrates was synthesized. These substrates consisted of the sequences FTGR, FTGRK, FTGRKR and FTGRKRK, each linked at the C-terminus to 7-amino-4-methylcoumarin (AMC). Incubation of these peptide substrates with the same urine sample set as with the AMCA-coupled γ-ENaC$^{180-194}$ substrate similarly reproduced the intensities of the cleavage pattern observed there.
Likewise, urine samples from healthy humans did not exhibit any measurable aprotinin-sensitive activity against any of the four AMC-coupled substrates. . In contrast, urine samples from nephrotic patients displayed high aprotinin-inhibitable proteolytic activity, with a strong preference for FTGRKR-AMC (Figure 65A), which also confirmed the results obtained with the AMCA substrate and the sequence γ-ENaC$^{180-194}$.
Urine samples from healthy mice also showed no aprotinin-sensitive proteolytic activity against the AMC substrates (Figure 65B). Conversely, in urine samples from nephrotic doxorubicin-injected 129S1/SvImJ or podocin-deficient B6-*Nphs2*$^{\Delta ipod}$ mice, there were strong activities against AMC-coupled FTGRKRK, FTGRKR and FTGRK in similar intensities, but interestingly not against FTGR (Figure 65C). In nephrotic B6-*Nphs2*$^{\Delta ipod}$ * *Plg*$^{-/-}$ mice without expressed plasminogen, the proteolytic activity was markedly reduced for all substrates, however, there was still some activity against FTGRK- and FTGRKR-AMC, as they were significantly different to values that would only fluctuate around zero (Figure 65D).

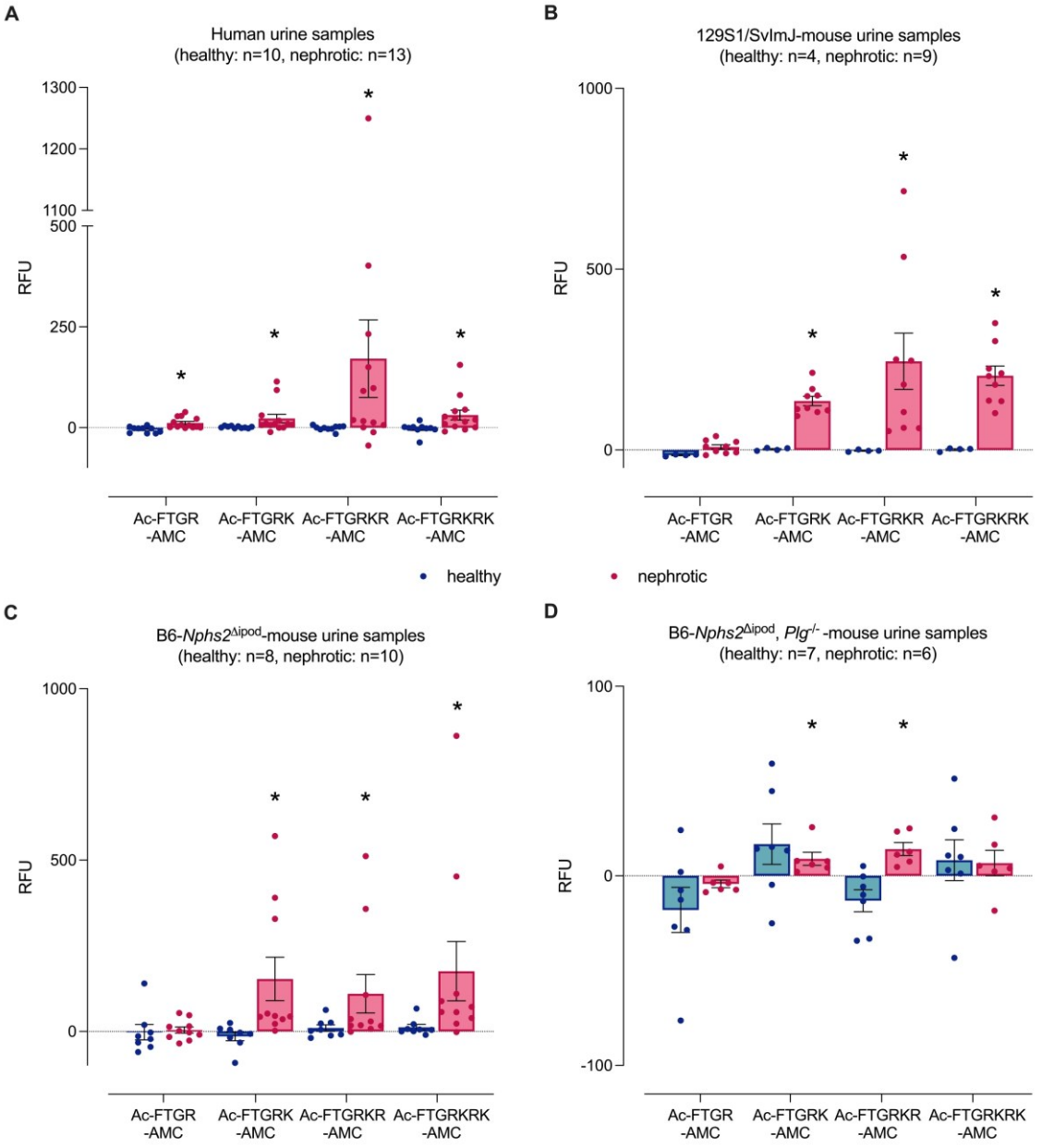

Figure 65: Quantification of the cleavage events within the polybasic tract of γ-ENaC$^{183-186}$ adopted from first-authorship publication [90]

Fluorescence signal after incubation of each AMC substrate with urine samples from healthy and nephrotic humans (A) and mice (B-D) as aprotinin-sensitive activity, after subtraction of samples without aprotinin with the same samples after co-incubation with aprotinin. In plasminogen-deficient nephrotic B6-*Nphs2*$^{\Delta ipod}$ * *Plg*$^{-/-}$ mice, the aprotinin-sensitive serine protease activity is markedly lower (D).
RFU Relative fluorescent unit, normalized to urinary creatinine.
* significant difference from 0

4 Discussion

4.1 Identification of active proteases in nephrotic urine, by universal peptide substrate, mass spectrometry and western blots

4.1.1 Increased protease activity and high abundance of AEBSF- and aprotinin-sensitive serine proteases in nephrotic urine

Using the universal peptide substrate library, the activity of urinary protease could be quantified and it was found that urine samples already show low protease activity when they are collected in the healthy state. Proteases that are produced in the kidney and then eliminated through the urine are the primary enzymes responsible for this activity. Nephrotic syndrome patients and mice were found to have significantly higher levels of urinary protease activity than the healthy population. This occurred as a result of aberrantly filtered plasma proteases, due to damaged the glomerular filters. In spite of the fact that plasma proteases are found to circulate in the plasma as inactive zymogens, it was discovered that they are highly active in the urine of nephrotic mice and humans.

In nephrotic states, the urinary proteolytic activity shifted significantly toward aprotinin-sensitive serine proteases. While AEBSF inhibited a similar fraction of the total activity in both healthy and nephrotic urine – indicating a high basal presence of AEBSF-sensitive serine proteases under physiological conditions with low total protease activity – the proportion of aprotinin-sensitive activity rose sharply in nephrotic urine, exceeding 80% of the total protease activity compared to only about 25% in healthy samples. The strong response to aprotinin inhibition demonstrated that the predominant urinary proteolytic activity arises from newly filtered serine proteases from the plasma compartment. As this was measured in both humans and mice compared to the healthy state, this could indicate similar pathological mechanisms across species. Furthermore, the specificity of protease inhibitors such as aprotinin and AEBSF in suppressing proteolytic activity show potential targeted therapeutic interventions. For example, treatment of nephrotic mice with aprotinin strongly reduced urinary serine protease activity against ENaC. These resulted in protection from typical symptoms of nephrotic syndrome like sodium retention and edema formation [38].

4.1.2 Proteomic identification of (active) plasma proteases filtered into urine

The proteomic findings were firstly supported by bioinformatic analyses with gene ontology, using the GO and KEGG databases with the GO terms and their FDR values. They identified "acute inflammatory response" and "protein activation cascade" as key pathways in nephrotic urine. Specifically, the "acute inflammatory response" category was enriched with proteins related to complement activation and cytokine signaling, indicating a robust immune response in nephrotic conditions. The "protein activation cascade" pathway highlighted the roles of coagulation factors and protease inhibitors, reflecting their involvement in both pathological and compensatory processes. These pathways were consistent across both human and murine samples, suggesting shared mechanisms of disease. Additionally, extracellular matrix proteins and components of vesicle-mediated transport were also prominent, underscoring their significance in the extracellular dynamics of nephrotic syndrome.

The tandem mass spectrometry results revealed that many of the active proteases were trypsin-like serine proteases of the S1 family within the PA(S) clan and that they were integral components of the complement and coagulation cascades. This was particularly evident in the enrichment of proteins such as plasminogen, factor VII activating protease (FSAP), prothrombin, plasma kallikrein and complement factor B + D in nephrotic samples. These proteases might not only be byproducts of glomerular damage but active determinants in disease progression. Their presence is indicative of systemic inflammatory and coagulative responses that likely exacerbate renal injury disease progression [98, 99]. Their high molecular weight typically prevents their passage through an intact glomerular filtration barrier, underscoring the pathological nature of their appearance in nephrotic urine.

The fact that the plasma serine protease were often strongly active in the tubular space suggests that they do so either as a consequence of physiological activators or as a result of their interaction with one another. Plasminogen, for instance, can be activated by tubular uPA [60], or it can be activated by abnormally filtered plasma kallikrein [100]. Both of these activation mechanisms are possible. Further examples include the activation of Factor XII into XIIa and the subsequent activation of prekallikrein to kallikrein, which can amplify proteolytic cascades [101]. Prothrombin may be cleaved to thrombin in

nephrotic urine, while Factor IX and Factor X can also become activated as components of the coagulation cascade. In addition, complement proteases such as Complement Factor B, Factor D and Factor I have been detected in their active or partially activated forms, indicating complement activation within the urinary space. Hyaluronan-binding protein 2 (HABP2) and hepatocyte growth factor activator (HGFA) likewise appear in nephrotic urine as active serine proteases, consistent with mass spectrometry data from nephrotic human and mouse samples. These findings demonstrate that multiple plasma-derived protease systems - coagulation, fibrinolysis, and complement - are aberrantly activated in nephrotic urine.

This also suggests that the excretion of proteins which function as plasma protease inhibitors in the nephrotic syndrome plasma compartment is insufficient to suppress newly urinary protease activity. In particular, major plasma inhibitors such as α2-antiplasmin, α1-antitrypsin, antithrombin III, and C1 esterase inhibitor, which normally neutralize plasmin, thrombin, and complement proteases, are themselves lost through the damaged filtration barrier. Under physiological conditions, these inhibitors are essential in the plasma compartment for maintaining hemostatic balance and preventing uncontrolled proteolysis [102]. α2-antiplasmin ensures that fibrinolysis remains localized by rapidly binding to free plasmin, while antithrombin III limits coagulation by neutralizing thrombin and factor Xa. α1-antitrypsin protects tissues from excessive proteolytic damage by inhibiting elastase and trypsin-like enzymes, and C1 esterase inhibitor regulates complement and kallikrein-kinin activation [103]. Their reduced concentrations impair the capacity to inhibit serine proteases like plasmin, kallikrein, and thrombin. The depletion of α2-antiplasmin allows enhanced plasmin activation, while the loss of antithrombin III facilitates thrombin and factor Xa activity. Furthermore, insufficient C1 inhibitor and α2-macroglobulin contribute to excessive complement and protease activation within the tubular lumen.

4.1.3 Strengths and limitations of the mass spectrometry methodology

The current tandem mass spectrometry extended previous proteomic work by providing a broader and more detailed overview of urinary proteases in healthy and nephrotic humans and mice. Earlier studies in idiopathic nephrotic syndrome, membranous nephropathy, and podocin-deficient mice had already identified several key enzymes such

as plasminogen, prothrombin, and urokinase, yet missed others that this thesis now identified, including complement factors B and D, factor VII activating protease (FSAP), hepatocyte growth factor activator and coagulation factors IX and XII [64, 104-106]. Such discrepancies likely result from methodological and cohort differences but also indicate disease-specific protease profiles across nephrotic subtypes. This suggests that distinct protease profiles may characterize different nephrotic conditions, underscoring potential diagnostic and mechanistic variations. Overall, while overlapping with prior work, the present study expands the known urinary "proteasome" spectrum and reveals a broader spectrum of proteases associated with nephrotic syndrome. The mass spectrometry methodology has several strengths to find all newly arising, active serine proteases in nephrotic urine of humans and mice:

First, AEBSF- and aprotinin-coupled beads were used in a pull-down method, next to the standard shotgun method with precipitation of all proteins. The bead methodology directly targeted serine proteases at their exposed active site and allowed in the case of AEBSF beads in comparison with uncoupled beads to calculate and analyze each individual activity state of the detected proteases and whether they are more or less active in the urinary space and might be involved in pathogenic processes that could be investigated further using mouse models, such as knock out strains.

Additionally, the analyses of the enriched or decreased appearance of urinary proteases were based on label-free quantification (LFQ) values. This approach provides relative abundance information for each detected protein across all samples without the need for labeling, enabling accurate comparison between nephrotic and healthy urine. The LFQ values were statistically evaluated to identify significantly altered proteases, and their distribution visualized using volcano plots, which combine fold-change with significance testing. This allows a robust and quantitative identification of proteases that are selectively enriched or depleted in nephrotic samples.

Furthermore, human and murine samples were analyzed side by side and revealed high common overlap in protein abundance and activities which argues against relevant interspecies differences, particularly in nephrotic syndrome. This close similarity can likely be explained by fact that plasma proteases translocating to the urine in nephrotic syndrome are almost identical in both species. Consequently, results from rodent models of nephrotic syndrome are often likely to be transferable to humans.

One important limitation of the proteomics results is that the possibility of incomplete protease detection so that the urinary proteases may not have been captured completely. Proteases present with low abundance may have remained undetected and thus could be underrepresented in the dataset. This issue is especially relevant in nephrotic urine, where highly abundant plasma-derived proteins such as albumin and immunoglobulins, which were filtered through the damaged glomeruli and which may mask signals from low abundant proteases. Among all detected proteases, plasminogen clearly dominated in nephrotic urine with a concentration of around 1 mg/ml. This predominance can be explained by the highest plasma concentration among the proteases of the coagulation and complement system (100-300 mg/L[58]). The strongly altered composition of urinary proteins in nephrotic syndrome could also explain why proteases, which are found in the healthy urine, were barely detectable in nephrotic urine. But also a decrease in expression of these renal proteases that are expressed in healthy kidney tubules could be a further conceivable mechanism during nephrotic syndrome.

Summarized, a systematic and quantitative overview of the urine protease landscape could be provided by the different mass spectrometry approaches, with the focus on the proteolytic abundance and activity. These results can establish a good basis for further studies to investigate how urinary proteolysis contributes to renal function, with particular focus on the protease-dependent regulation of ENaC.

4.1.4 Western blot validation of active plasma proteases

The Western blot analyses confirmed as a further, independent methodology the active excretion of activated several coagulation and complement proteases on the protein level, demonstrating a markedly enhanced activation of these cascades in nephrotic urine compared to their tightly regulated state in plasma.

Active plasmin appeared as a 72 kDa band with smaller degradation fragments, derived from plasminogen, indicating extensive conversion by activators like urokinase (uPA), which itself was detected in both its pro-form (54 kDa) and active low-molecular-weight form (33 kDa). Plasma kallikrein was present as zymogen (82–88 kDa) and as active protease, cleaved into heavy (52 kDa) and light (30 kDa) chains, just like FSAP as a 64 kDa zymogen and dissociated into 50 kDa and 27 kDa subunits.

Complement factors B, D, and C2 likewise showed zymogen bands (100, 30 and 100 kDa) together with characteristic fragments such as the Bb band (55 kDa), indicating the activation of the alternative complement pathway.

In kidney lysates, prostasin was detected in single- and two-chain forms under reducing conditions, verifying its cleavage at the canonical R44–I45 site and confirming its role as a physiological ENaC activator [51].

These findings indicate a concerted activation of especially the coagulation and alternative complement pathways within the tubular system. The simultaneous presence of zymogen and active fragments highlights intratubular proteolytic processing rather than simple filtration. Collectively, these results support that nephrotic proteasuria represents a pathologically active process, reflecting local activation of plasma protease systems in urine.

4.1.5 Single-Protease-KO mouse models of candidate proteases from proteomic results are not protected against sodium retention and edema formation

The findings of the present results indicate that sodium retention in nephrotic syndrome is likely influenced by the activity of several, functional redundant serine protease. However, the identity of the serine proteases that are indispensable for acting and mediating proteolytic ENaC overactivation is still unclear. One major reason for this uncertainty is that many single knockouts of highly abundant and active proteases were already tested by our research group of Prof. Ferruh Artunc over the course of the past few years in many mouse models. So far, it could be demonstrated that mice lacking urokinase-plasminogen activator (uPA) [60] or plasma kallikrein [59] were not protected and even not reduced from very high sodium retention in experimental nephrotic syndrome. Further examples include prostasin [107], transmembrane serine protease 2 (Tmprss2, [108]) and factor VII activating protease (FSAP, [109]). Notably, this was also reproduced for plasminogen/plasmin as most abundant serine protease in nephrotic urine of both humans and mice [69]. Some of these results have already been published, as can be seen in the following Table 6, while others are still in progress or planned. But until now, all of the candidates for the coagulation and complement cascade provided no protection against the overactivation of ENaC and edema formation yet.

Table 6: Serine proteases investigated to date in relation to ENaC activation and edema development *in vivo*. The selection was based on the proteomic data of AEBSF bound active serine proteases in Figure 37

Serin protease (gen name)	Locali-zation	Molecular weight, kDa	Inhibition by Aprotinin	ENaC activation *in vitro*	Edema formation in KO mouse model	Publication
Urokinase (*Plau*)	Tubule / Urine	49	yes	yes	no protection	[60]
Prostasin (*Prss8*)	Tubule / Urine	38	yes	yes	no protection	[107]
Transmembrane serine protease 2 (*Tmprss2*)	Tubule	60	yes	yes	no protection	[108]
Plasminogen (*Plg*)	Plasma	91	yes	yes	no protection	[69]
Plasma Kallikrein (*Klkb1*)	Plasma	71	yes	yes	no protection	[59]
Faktor VII activating protease (*Habp2*)	Plasma	64	yes	yes	no protection	[109]
Coagulation factor XI (*F11*)	Plasma	160	yes	no data	no protection	Preliminary
Coagulation Factor XII (*F12*)	Plasma	68	yes	no data	no protection	Preliminary
Complement factor B (*Cfb*)	Plasma	80	unclear	no data	no protection	In preparation
Complement factor D (*Cfd*)	Plasma / Urine	30	unclear	no data	no protection	In preparation
Cfb x Cfd	Plasma	80 / 30	unclear	no data	no protection	In preparation

It is therefore conceivable that the proteolytic activation of ENaC can be mediated by several alternative serine proteases with overlapping substrate specificities. When one candidate protease is genetically deleted, others may compensate by activating the same cleavage sites on the γ-ENaC subunit or by participating in interconnected proteolytic cascades. This redundancy would explain why none of the individual knockouts provided protection *in vivo*, even though many of them are capable of ENaC activation *in vitro* [52]. Consequently, while a robust correlation exists between the presence of plasma-derived, aprotinin-sensitive proteases and increased ENaC activity, which is also strengthened by protection of mice treated with aprotinin after induced experimental kidney damage [38], a really clear causal relationship on a clear protease subset hasn't yet been demonstrated. So, the currently available evidence supports a model in which a

network of redundant serine proteases collectively drives ENaC activation and sodium retention in nephrotic syndrome, rather than a single indispensable enzyme. Future combinatorial knockout of several proteases for example by RNA-interference approaches will be required to unravel which subsets of these proteases act cooperatively and which are merely bystanders within the broader proteolytic milieu of the nephrotic kidney.

4.2 Proteolytic activity against the second cleavage site of γ-ENaC

4.2.1 Detection of dominant γ-ENaC cleavage fragment FTGRKR by AMCA- and AMC-labelled peptide substrates

The cleavage products of the AMCA substrate have shown that urine samples from nephrotic patients and corresponding mouse models contain a significantly increased proteolytic activity against the distal polybasic tract of γ-ENaC where the second cleavage for full activation is located (γ-ENaC$^{180\text{-}194}$). This finding confirmed that nephrotic urine contains soluble active proteases, termed as proteasuria [36, 38]. Interestingly, the proteolytic activity was quite specifically directed against the bonds within the polybasic RKRK motif among the potential 14 amid bonds within the γ-ENaC$^{180\text{-}194}$ substrate. And also there, the highest specificity was directed against the second arginine resulting in the dominant FTGRKR fragment in both nephrotic humans and mice. The preferential cleavage at arginine- and lysine-containing positions and the sensitivity to aprotinin strongly indicates the involvement of trypsin-like serine proteases belonging to the S1 peptidase family, such as proteases from the coagulation or complement system, like they was identified and confirmed by the mass spectrometry measurements ([68], all S1 members are listed in the MEROPS database [110]). The positively charged RKRK sequence therefore seems to represent a favored recognition and cleavage site for these serine proteases.

Based on these results, proteolysis of the distal polybasic tract could be a biochemical correlate the proteolytic ENaC overactivation in the kidney. However, cleavage of this sequence has not a very high specificity as many trypsin-like serine proteases are capable of cleaving this motif in a relatively promiscuous manner, particularly during longer incubation time with a soluble peptide in a reaction tube. Consequently, proteolytic

activity of the urine measured *ex vivo* does not necessarily mirror the situation *in vivo* present on ENaC expressing principal cells of the distal nephron. Here, the serine protease bind to ENaC in the natural three-dimensional conformation, together with many adjacent and presumably binding-enhancing factor like other membrane proteins, as it is for example known for prostasin. Nevertheless, *in vitro* experiments performed in ENaC-expressing heterologous systems like in oocyte-based electrophysiological models for electrophysiology studies [52, 111, 112] also have validated that several trypsin-like serine proteases were capable to cleave the γ-subunit of ENaC for complete activation.
Consistent with mass spectrometry data of the shotgun and AEBSF approach which had showed the high activity and abundance of plasminogen in nephrotic urine, plasmin also had a very high proportion to the overall proteolytic activity against the four AMC substrates which represented different cleavage sites within the polybasic tract of γ-ENaC. This was especially observed between the high protease in nephrotic urine samples from wild-type mice, compared to the much lower activity of samples from plasminogen-deficient nephrotic mice. But remarkably, there was still aprotinin-sensitive activity in this plasminogen-deficient nephrotic urine which also led to cleavage of the polybasic tract, yielding the AMCA fragments FTGRKR and FTGRK. This observation fits with previous mouse studies in which plasminogen-deficient mice still developed proteolytic ENaC overactivation and high sodium retention after induction of experimental nephrotic syndrome [69]. In these mice as well, sodium retention could be prevented by treatment with aprotinin that is excreted with the urine *in vivo* [113]. Thus, the residual activity in plasminogen-lacking nephrotic urine may comprise all (further) critical serine protease(s) responsible for ENaC-dependent sodium retention. But to date, the exact composition and identities of the essential serine proteases which drives proteolytic ENaC overactivation in experimental nephrotic syndrome is still unresolved. To get an idea, which protease could be more likely involved in this process than another, their natural specificity was compared with the cleavage site after the second arginine of the polybasic tract.

4.2.2 Evaluated *in silico* protease specifities against the dominant FTGRKR cleavage fragment

As found out in nephrotic human as well as in WT and Plg-KO mice, the cleavage was predominantly observed at AMCA-FTGRKR↓KISGKIIHK and Ac-FTGRKR-AMC,

representing the second γ-ENaC cleavage site. With the known protease specificities for the recognition sequence of their cleavage sites, these specificities were analyzed against FTGRKR↓KISGKIIHK in detail. Therefore, several proteases were compared which were detected in the MS experiments or are naturally cleaving γ-ENaC, like furin at the maturation of the first γ-ENaC cleavage and prostasin for physiologically full activation, in order to identify potential enzymes responsible for this proteolytic event. According to the Schechter and Berger nomenclature, residues P4–P1 are located N-terminally of the cleavage site and P1′–P4′ C-terminally, resulting here in P4–P1 = G–R–K–R and P1′–P4′ = K–I–S–G. The commonly known specificities were extracted from the *MEROPS* database on the website https://www.ebi.ac.uk/merops/, and the matching sites were highlighted light green, when it were the same amino acids, or dark green, when the amino acids are chemically similar.

Table 7: Protease specificities for the dominant AMCA-/AMC-FTGRKR fragment in nephrotic human and PLG-KO-urine samples

	P4	P3	P2	P1	P1'	P2'	P3'	P4'
Reference sequence (PLG-KO fragment)_AMCA-FT…	**Gly**	**Arg**	**Lys**	**Arg**	**Lys**	**Ile**	**Ser**	**Gly**
Protease								
Coagulation Faktor XII	Thr, Pro > Iso, Ser	Ser, Met > Lys, Gln	Broad: Thr>**Lys,** Pro, Gly…	Arg	Ile, Val, Leu	Val, Thr	Gly, Leu	Gly
FSAP	Apolar AA	Apolar AA > Arg	Lys > Gln, Cys	Arg > Lys	Tyr, Arg, Ser	Gly, Val	Gly	Gly>, Leu, Phe
Plasminogen	Lys > Broad	Broad	Aromatic>Broad	Lys > Arg	Broad	Broad	Broad	Broad
Prostasin (γ-ENaC)	Arg	Lys	Arg	Lys	Ile	Ser	Gly	Lys
Complement Factor B	Gln, Gly	Leu	Gly, Ala, Lys	Arg	Leu, Ser	Asn, His	Leu, Met	Lys, Asp
Plasma Kallikein	Ser	Broad	Lys > Phe, Thr	Arg > Lys	Tyr, Arg, Ser	Gly, Val	Gly	Gly
Complement Factor D	Gln	Gln	Lys	Arg	Lys	Ile	Val	Leu
Thrombin	Ala	Broad	Pro>Ala, Gly, Leu	Arg	Ser>Ala, Gly	Broad	Broad	Broad
Furin	Arg	Lys	Arg	Arg	Glu	Ala	Gly	Ser

The comparison revealed that several serine proteases – particularly Complement Factor D, complement factor B, plasma kallikrein, and factor VII activating protease (FSAP) – show substrate preferences that fit well_with this polybasic motif. These enzymes typically favor a basic residue at P1 (Arg or Lys) and often also at P2 and/or P1′, which precisely matches the experimentally observed R–K–R↓K core sequence.

Among them, complement factor D shows the closest recognition sequence around the catalytic center (P2 Lys / P1 Arg / P1′ Lys / P2′ Ile). Moreover, its physiological substrate, complement Factor B, is cleaved by CFD at a similar basic motif, further supporting the structural plausibility of CFD as a possible active protease toward the studied ENaC cleavage site. Factor B, plasma kallikrein, and FSAP also display strong similarity at the central positions while tolerating chemically related residues in the flanking regions. All four enzymes are abundant plasma serine proteases and have been detected in nephrotic samples, which strengthens their relevance in this context.

In contrast, thrombin, furin and prostasin show a less compatible pattern, as thrombin prefer more non-polar or slightly negatively charged residues at P1′ and P2, furin strongly negatively charged glutamate acid P1’ and prostasin non-polar isoleucine at P1’, conflicting with the positively charged, basic Lys residue after the scissile bond. For furin and prostasin, that’s a possible reason that they don’t cleave or only slightly cleave this second γ-ENaC cleavage site in ENaC maturation and under physiological conditions. Coagulation factor XII shows a moderate fit, as it prefers Arg at P1 but nonpolar residues on the prime side (Ile/Val/Leu) that differs from the observed Lys at P1′. Plasminogen typically favors Lys at P1 and tolerates Arg, so that it moderately matches for the scissile site, though its preference for smaller or uncharged residues at P1′ weakens the fit.

In summary, this supports the active binding and cleavage of a trypsin-like serine protease with polybasic substrate preference in performing the characteristic R↓K cleavage within the ENaC γ-subunit. Among the tested candidates, complement factor D represents the most fitting match to this observed cleavage site, followed by factor B, plasma kallikrein, and FSAP, which together is the most plausible group of proteases potentially responsible for the pathophysiologically relevant cleavage observed in nephrotic urine.

4.2.3 Cross-species comparison of proteolytic activity against the γ-ENaC peptides, with validities and limitations

With investigation of urine samples from healthy and nephrotic humans and from three distinct mouse models, which were all analyzed with the same samples, consistent and reproducible results across species were obtained. Across all four analyzed urine sets – from healthy and nephrotic humans, as well as from nephrotic 129S1/SvImJ, B6-*Nphs2*$^{\Delta ipod}$, and plasminogen-deficient *and* B6-*Nphs2*$^{\Delta ipod}$ * *Plg*$^{-/-}$ mice – the results reveal a remarkably consistent proteolytic pattern against the γ-ENaC polybasic tract, characterized by the dominant formation of the fragment FTGRKR, followed by lower amounts of FTGRK and FTGR. The addition of aprotinin consistently inhibited the appearance of these fragments in all nephrotic samples, confirming that the proteolytic activity was mediated by serine proteases. The similarity between the human and murine cleavage spectra emphasizes a conserved pathogenic mechanism of urinary serine protease activity in nephrotic syndrome. This is confirmed by the translocation of similar serine proteases from the plasma into the urinary space, which was shown by the detailed proteomic analyses [68]. This translocation may reflect shared pathways of disease progression and potentially offers insights into conserved therapeutic targets.

Nevertheless, while the findings suggest similarities, there may also be subtle but decisive differences in the composition and behavior of active serine proteases between humans and mice. These variations could be attributed to the specific underlying causes of nephrotic syndrome in humans or to differences in the genetic and experimental models of the condition in mice. Such differences may influence the exact filtering of these large molecular weight proteases through the glomerular filtration barrier, potentially resulting in unique profiles of proteasuria depending on the disease context or experimental conditions. Consequently, variations in the extent or type of protease translocation could impact both the qualitative and quantitative nature of proteinuria observed in different settings.

A limitation of these peptide substrates for assessing of urinary proteolytic activity against the γ-ENaC$^{180\text{-}194}$ peptide, is that it serve as valuable, but only indirect surrogate marker of nephrotic proteasuria. It does not provide direct proof of proteolytic activation of ENaC in the kidney itself. While the observed activity strongly suggests the presence of proteases capable of modulating ENaC function, additional studies are required to

confirm whether these proteases directly activate ENaC channels *in vivo* within the renal epithelial cells. Such confirmation would require complementary approaches, such as localized assessments of proteolytic activity in the kidney using advanced imaging techniques or enzyme activity assays to identify specific regions of protease action. Additionally, functional studies employing ENaC-specific inhibitors could involve *in vivo* experiments with pharmacological or genetic inhibition of ENaC channels in cell culture to directly observe their role under nephrotic conditions. These approaches could be supplemented with *ex vivo* analyses of isolated renal tissue to evaluate protease-ENaC interactions under controlled conditions, thereby establishing a more definitive link between proteasuria and ENaC activation in nephrotic syndrome. The methods for that purposes are discussed in the next section as outlooks.

4.3 Outlook with further, even more comprehensive experimental approaches

In order to identify all key serine proteases, cofactors and inhibitors involved in the complex nephrotic process of pathologic ENaC overactivation in nephrotic syndrome, further experiments should combine even more advanced proteomic and functional approaches.

New mass spectrometry experiments are planned in our research group where nephrotic urine samples are combined with post-nephrotic ones from the same mice, after observed recovery processes, and related plasma samples which could reveal how protease activity changes during disease progression from plasma to urine and after normalized ENaC activity and sodium retention, when the pathological processes with the involved proteases are stopping or are strongly reduced again [44]. Also parallel comparisons with non-nephrotic control samples would help distinguish proteases specifically activated under pathological conditions from those that are constitutively present and which are not alone sufficient for ENaC overactivation. In these datasets, the focus should also include inhibitory and cofactor proteins that may regulate protease activation, such as α_2-antiplasmin and further serpins. Together with enhanced proteomic workflows using advances such as data-independent acquisition (DIA), and artificial intelligence (AI)-assisted data evaluation combined with neural-network based analysis tools (e.g., DIA-NN or Proteoscape), this allows an even more comprehensive and reproducible detection

of proteases, cofactors, and inhibitors even in such complex urine or plasma matrices. Increasing the sample number (n≈20 per group) will further improve statistical power, enabling detection of subtle but biologically relevant differences between nephrotic, post-nephrotic and non-nephrotic states

For investigation of many different possible conditions for the ENaC expressing cells, it will also be important to establish reliable *in vitro* systems that mimic distal tubular ENaC expression and regulation. For this purpose, well-characterized renal epithelial cell lines, such as mpkCCDcl4 cells derived from mouse cortical collecting duct principal cells [114], can serve as an effective model for ENaC function. These cultures expressing ENaC could directly test the functional effects of these proteases. By adding nephrotic urine, isolated proteases, or more specific serine protease inhibitors like different serpins, like α_2-antiplasmin, antithrombin III and protein C inhibitor, one could measure changes in ENaC cleavage and sodium transport. Techniques such as patch-clamp recordings or western blotting would allow linking biochemical proteolysis to direct ion channel activity or indirect analysis of the activated γ-ENaC protein bands. Cross-linking and co-immunoprecipitation experiments could further uncover which proteases directly bind or interact with ENaC at the cell surface. For example, biotin-based or photoactivatable cross-linkers can stabilize transient protease–ENaC complexes, which can then be identified by mass spectrometry or western blotting. Co-immunoprecipitation using ENaC antibodies would allow the detection of associated serine proteases and further co-binding protein compleses, such as plasmin, prostasin, or plasma kallikrein, revealing their direct molecular interactions. These complementary approaches can therefore clarify which proteases physically associate with ENaC in nephrotic conditions and help to define the mechanisms underlying its proteolytic activation.

To identify the proteases that are directly bound to ENaC *in vivo*, a further advanced technique is the laser microdissection, where distal tubular segments from nephrotic mouse kidneys showing positive γ-ENaC immunostaining can be precisely cut out and subjected to proteomic mass spectrometry. This allows a highly specific analysis of proteases physically interacting with ENaC-expressing principal cells. In addition, co-expression analyses through immunofluorescence microscopy can visualize spatial co-localization of candidate serine proteases with ENaC within tubular structures, providing morphological evidence of direct interaction. Finally, the proximity ligation assay (PLA)

offers a powerful method to confirm such interactions at the molecular level, detecting proteins located within 40 nm of each other in tissue sections [115]. Combining these histological and proteomic approaches will make it possible to pinpoint which serine proteases are directly associated with ENaC activation in nephrotic kidneys.

In a final step, the most relevant serine proteases identified in these studies could be validated *in vivo* knockout or knockdown mouse models again. Using a combination of genetic and RNA-interference approaches, it will be possible to examine whether the absence of more than only one selected protease and related proteins significantly reduces ENaC activation and sodium retention in the nephrotic mouse models. A combined constitutive knockout and AAV8-mediated knockdown approach could be employed to suppress several candidate proteases simultaneously. By crossbreeding existing knockout lines to for example double knockouts, like complement factor B and D together, and/or introducing AAV8 (adeno-associated virus) vectors expressing small hairpin RNA (shRNA) sequences under the liver-specific TBG promoter, the expression of individual or multiple serine proteases can be effectively reduced [116]. This allows for the investigation of redundant protease activation pathways and for determining whether their combined deficiency attenuates ENaC activation and sodium retention in nephrotic mouse models.

Combining these proteomic, cellular, and genetic mouse model strategies in a complementary manner could provide a comprehensive understanding of how proteases and their activation and inhibition contribute to nephrotic sodium dysregulation with focus on ENaC regulation and may ultimately guide to protease-targeted therapeutic interventions. Such integrative approaches will help to understand which pathways are obligatory, compensatory or redundant and reveal the specific protease networks responsible for ENaC activation *in vivo*, both in the physiological and nephrotic context. By linking molecular mechanisms with functional and phenotypic outcomes, these studies may bridge the gap between experimental nephrology and translational application. In the long term, identifying and selectively inhibiting the key serine proteases involved in pathological ENaC overactivation could be finally a new base for the translational development of more precise and safer therapies to prevent edema formation in patients with nephrotic syndrome.

Summary of the dissertation

In this thesis, the mechanisms of sodium retention in nephrotic syndrome (NS) were investigated, focusing on the proteolytic overactivation of the epithelial sodium channel (ENaC) in the distal tubule of kidney by aberrantly filtered plasma serine proteases due to a damaged glomerular filter system. This is known as overfill theory, complementary to the classical aldosterone dependent ENaC activation as classical underfill theory.

Urine samples from healthy and nephrotic humans and mice were analyzed and compared by the protease activity against a universal substrate peptide mixture and peptides representing the distal cleavage region of γ-ENaC, for full activation of the channel. Inhibitors were added to determine protease class specificities, like AEBSF for all serine proteases. The corresponding active proteases were identified by mass spectrometry (MS) and western blot (WB) experiments.

Nephrotic urine samples showed a strong, significant increase in aprotinin-sensitive serine protease activity. Proteomic analysis of this activity revealed a strong enrichment of plasma proteases from the coagulation and complement cascades, including plasminogen, plasma kallikrein, Factor XII, FSAP, and Complement Factors B and D. The active state was confirmed by additional MS preparation with AEBSF and aprotinin coupled beads and WB experiments for detection of active cleavage and degradation products.

Substrate assays with peptides representing the distal cleavage site of γ-ENaC and coupled to the fluorophors AMCA and AMC identified a dominant cleavage fragment (FTGRKR↓KISGK) that highly matches with the substrate specificities of several candidate proteases, especially Complement Factor D, Complement Factor B, plasma kallikrein, and FSAP, for both human and different mouse models.

The results give a very detailed, comprehensive insight into the overfill theory with proteolytic ENaC overactivation. The nephrotic protease activity presumably involved in this process, called proteasuria, arises from redundant and complex cascades of very active coagulation and complement proteases. The further search, analysis and understanding of key components or regulatory cofactors of these protease networks could be a new basis of more effective therapeutic strategies for preventing and treating nephrotic syndrome in patients.

Zusammenfassung der Dissertation

In dieser Arbeit wurden die Mechanismen der Natriumretention beim nephrotischen Syndrom im Menschen und in Maus-Modellen untersucht, mit Fokus auf der proteolytischen Überaktivierung des epithelialen Natriumkanals (ENaC) im distalen Tubulus der Niere, mutmaßlich ausgelöst durch aberrant filtrierte Plasma-Serinproteasen infolge des geschädigten glomerulären Filters. Dies wird als Overfill-Theorie bezeichnet und ergänzt die klassische Aldosteron-abhängige ENaC-Aktivierung als klassische Underfill-Theorie.

Urinproben von gesunden und nephrotischen Menschen und Mäusen wurden auf ihre Protease-Aktivität gegenüber einem universellen Peptid-Substrat-Mix sowie repräsentativen Substraten der distalen γ-ENaC-Spaltstelle (zur vollständigen Aktivierung des Kanals) analysiert und verglichen. Hierbei kamen Inhibitoren zur Bestimmung der Protease-Klassen zum Einsatz, wie AEBSF für alle Serinproteasen. Die entsprechenden Proteasen wurden mittels Massenspektrometrie (MS) und Western Blot (WB) identifiziert.

Die nephrotischen Urinproben zeigten einen deutlichen, signifikanten Anstieg v.a. der Aprotinin-sensitiven Serinproteasen. Die proteomische Analyse ergab eine starke Anreicherung von Plasma-Serinproteasen aus der Gerinnungs- und Komplementkaskade, einschließlich Plasminogen, Plasma-Kallikrein, Faktor XII, FSAP sowie der Komplementfaktoren B und D. Der aktive Zustand wurde durch MS-Experimente mit AEBSF- und Aprotinin-gekoppelten Beads sowie durch WB-Analysen aktiver Spalt- und Abbauprodukte bestätigt.

In Peptid-Assays zur distalen γ-ENaC-Spaltstelle (mit AMCA oder AMCgekoppelt) wurde ein dominantes Spaltfragment (FTGRKR↓KISGK) detektiert, welches stark mit den Substrat-Spezifitäten mehrerer aktiver Proteasen übereinstimmt, insbesondere Komplementfaktor D und B, Plasma-Kallikrein und FSAP, sowohl beim Menschen als auch in den Maus-Modellen.

Die Ergebnisse geben einen sehr detaillierten, umfassenden Einblick in die Overfill-Theorie mit proteolytischer ENaC-Überaktivierung. Die deutlich erhöhte Proteaseaktivität, als Proteasurie bezeichnet, stammt von redundanten und komplexen Protease-Kaskaden v.a. aus den Gerinnungs- und Komplement-Systemen. Ein tiefergehendes Verständnis dieser Protease-Netzwerke mit gezielter Beeinflussung von

gemeinsamen Schlüsselkomponenten oder regulatorischen Kofaktoren statt bisher für den Krankheitsverlauf noch folgenloser Inaktivierung einzelner Proteasen könnte die Grundlage für eine effektivere Therapiestrategie zur Prävention und Behandlung des nephrotischen Syndroms bei Patienten bilden.

References

[1] M.W. Taal, G.M. Chertow, P.A. Marsden, K. Skorecki, S. Alan, B.M. Brenner, Brenner and Rector's The Kidney E-Book, Elsevier Health Sciences2011.

[2] R. Kettritz, J. Loffing, Potassium homeostasis - Physiology and pharmacology in a clinical context, Pharmacol Ther 249 (2023) 108489.

[3] P.A. Welling, Y.P. Chang, E. Delpire, J.B. Wade, Multigene kinase network, kidney transport, and salt in essential hypertension, Kidney Int 77(12) (2010) 1063-9.

[4] B.M. Koeppen, The kidney and acid-base regulation, Adv Physiol Educ 33(4) (2009) 275-81.

[5] J.W. Fisher, Erythropoietin: physiology and pharmacology update, Exp Biol Med (Maywood) 228(1) (2003) 1-14.

[6] J.F. Bertram, R.N. Douglas-Denton, B. Diouf, M.D. Hughson, W.E. Hoy, Human nephron number: implications for health and disease, Pediatr Nephrol 26(9) (2011) 1529-33.

[7] M.R. Pollak, S.E. Quaggin, M.P. Hoenig, L.D. Dworkin, The glomerulus: the sphere of influence, Clin J Am Soc Nephrol 9(8) (2014) 1461-9.

[8] R.P. Scott, S.E. Quaggin, Review series: The cell biology of renal filtration, J Cell Biol 209(2) (2015) 199-210.

[9] A. Tojo, S. Kinugasa, Mechanisms of glomerular albumin filtration and tubular reabsorption, Int J Nephrol 2012 (2012) 481520.

[10] J.E. Hall, M.E. Hall, Guyton and Hall textbook of medical physiology e-Book, Elsevier Health Sciences2011.

[11] B. Haraldsson, J. Nystrom, W.M. Deen, Properties of the glomerular barrier and mechanisms of proteinuria, Physiol Rev 88(2) (2008) 451-87.

[12] J.H. Miner, The glomerular basement membrane, Exp Cell Res 318(9) (2012) 973-8.

[13] Y.S. Kanwar, A. Linker, M.G. Farquhar, Increased permeability of the glomerular basement membrane to ferritin after removal of glycosaminoglycans (heparan sulfate) by enzyme digestion, J Cell Biol 86(2) (1980) 688-93.

[14] H. Pavenstadt, W. Kriz, M. Kretzler, Cell biology of the glomerular podocyte, Physiol Rev 83(1) (2003) 253-307.

[15] R. Brandes, F. Lang, R.F. Schmidt, Physiologie des Menschen, Springer2019.

[16] B.A. Julian, H. Suzuki, Y. Suzuki, Y. Tomino, G. Spasovski, J. Novak, Sources of Urinary Proteins and their Analysis by Urinary Proteomics for the Detection of Biomarkers of Disease, Proteomics Clin Appl 3(9) (2009) 1029-1043.

References

[17] P.C. Heinrich, M. Müller, L. Graeve, Löffler/Petrides Biochemie und Pathobiochemie, Springer-Verlag2014.

[18] A.L. Rops, J. van der Vlag, J.F. Lensen, T.J. Wijnhoven, L.P. van den Heuvel, T.H. van Kuppevelt, J.H. Berden, Heparan sulfate proteoglycans in glomerular inflammation, Kidney Int 65(3) (2004) 768-85.

[19] B.M. Brenner, T.H. Hostetter, H.D. Humes, Molecular basis of proteinuria of glomerular origin, N Engl J Med 298(15) (1978) 826-33.

[20] J.H. Suh, J.H. Miner, The glomerular basement membrane as a barrier to albumin, Nat Rev Nephrol 9(8) (2013) 470-7.

[21] M. Chrysopoulou, M.M. Rinschen, Metabolic Rewiring and Communication: An Integrative View of Kidney Proximal Tubule Function, Annu Rev Physiol 86 (2024) 405-427.

[22] L.A. Urry, M.L. Cain, S.A. Wasserman, P.V. Minorsky, R.B. Orr, N.A. Campbell, Campbell biology, Twelfth edition. ed., Pearson, New York, NY, 2021.

[23] S.M. Nwia, X.C. Li, A.P.O. Leite, R. Hassan, J.L. Zhuo, The Na(+)/H(+) Exchanger 3 in the Intestines and the Proximal Tubule of the Kidney: Localization, Physiological Function, and Key Roles in Angiotensin II-Induced Hypertension, Front Physiol 13 (2022) 861659.

[24] C.N. Englisch, F. Paulsen, T. Tschernig, TRPC Channels in the Physiology and Pathophysiology of the Renal Tubular System: What Do We Know?, Int J Mol Sci 24(1) (2022).

[25] C. Tapia, K. Bashir, Nephrotic Syndrome, StatPearls, Treasure Island (FL), 2020.

[26] M. Vivarelli, L. Massella, B. Ruggiero, F. Emma, Minimal Change Disease, Clin J Am Soc Nephrol 12(2) (2017) 332-345.

[27] K.D. Guruswamy Sangameswaran, M.F. Hashmi, K.M. Baradhi, Focal Segmental Glomerulosclerosis, StatPearls, Treasure Island (FL), 2024.

[28] M. Shah, A. DeLaat, C. Cavanaugh, Treatment of membranous nephropathy: Perspectives on current and future therapies, Front Nephrol 3 (2023) 1110355.

[29] A.O. Phillips, K. Baboolal, S. Riley, H. Grone, U. Janssen, R. Steadman, J. Williams, J. Floege, Association of prolonged hyperglycemia with glomerular hypertrophy and renal basement membrane thickening in the Goto Kakizaki model of non-insulin-dependent diabetes mellitus, Am J Kidney Dis 37(2) (2001) 400-10.

[30] C.H. Siegel, L.R. Sammaritano, Systemic Lupus Erythematosus: A Review, JAMA 331(17) (2024) 1480-1491.

[31] G.A. Kaysen, J. Gambertoglio, I. Jimenez, H. Jones, F.N. Hutchison, Effect of dietary protein intake on albumin homeostasis in nephrotic patients, Kidney Int 29(2) (1986) 572-7.

[32] J.B. Kopp, H.J. Anders, K. Susztak, M.A. Podesta, G. Remuzzi, F. Hildebrandt, P. Romagnani, Podocytopathies, Nat Rev Dis Primers 6(1) (2020) 68.

[33] S. Agrawal, J.J. Zaritsky, A. Fornoni, W.E. Smoyer, Dyslipidaemia in nephrotic syndrome: mechanisms and treatment, Nat Rev Nephrol 14(1) (2018) 57-70.

[34] A.A. Epstein, Concerning the causation of edema in chronic parenchymatous nephritis; method for its alleviation, Am J Med 13(5) (1952) 556-61.

[35] H. Triebel, H. Castrop, The renin angiotensin aldosterone system, Pflugers Arch 476(5) (2024) 705-713.

[36] F. Artunc, M. Worn, A. Schork, B.N. Bohnert, Proteasuria-The impact of active urinary proteases on sodium retention in nephrotic syndrome, Acta Physiol (Oxf) 225(4) (2019) e13249.

[37] M. Nagase, Recent topics on podocytes and aldosterone, J Ren Nutr 25(2) (2015) 201-4.

[38] B.N. Bohnert, M. Menacher, A. Janessa, M. Worn, A. Schork, S. Daiminger, H. Kalbacher, H.U. Haring, C. Daniel, K. Amann, F. Sure, M. Bertog, S. Haerteis, C. Korbmacher, F. Artunc, Aprotinin prevents proteolytic epithelial sodium channel (ENaC) activation and volume retention in nephrotic syndrome, Kidney Int 93(1) (2018) 159-172.

[39] F. Artunc, O. Nasir, K. Amann, K.M. Boini, H.U. Haring, T. Risler, F. Lang, Serum- and glucocorticoid-inducible kinase 1 in doxorubicin-induced nephrotic syndrome, Am J Physiol Renal Physiol 295(6) (2008) F1624-34.

[40] J.I. Meltzer, H.J. Keim, J.H. Laragh, J.E. Sealey, K.M. Jan, S. Chien, Nephrotic syndrome: vasoconstriction and hypervolemic types indicated by renin-sodium profiling, Ann Intern Med 91(5) (1979) 688-96.

[41] B.C. Rossier, M.J. Stutts, Activation of the epithelial sodium channel (ENaC) by serine proteases, Annu Rev Physiol 71 (2009) 361-79.

[42] I. Ichikawa, H.G. Rennke, J.R. Hoyer, K.F. Badr, N. Schor, J.L. Troy, C.P. Lechene, B.M. Brenner, Role for Intrarenal Mechanisms in the Impaired Salt Excretion of Experimental Nephrotic Syndrome, J Clin Invest 71(1) (1983) 91-103.

[43] G. Deschenes, M. Wittner, A. Di Stefano, S. Jounier, A. Doucet, Collecting duct is a site of sodium retention in PAN nephrosis: A rationale for amiloride therapy, Journal of the American Society of Nephrology 12(3) (2001) 598-601.

[44] B.N. Bohnert, D. Essigke, A. Janessa, J.C. Schneider, M. Worn, M.Z. Kalo, M. Xiao, L. Kong, K. Omage, J. Hennenlotter, B. Amend, A.L. Birkenfeld, F. Artunc, Experimental nephrotic syndrome leads to proteolytic activation of the epithelial Na(+) channel in the mouse kidney, Am J Physiol Renal Physiol 321(4) (2021) F480-F493.

[45] B.N. Bohnert, F. Artunc, Induction of Nephrotic Syndrome in Mice by Retrobulbar Injection of Doxorubicin and Prevention of Volume Retention by Sustained Release Aprotinin, J Vis Exp (135) (2018).

[46] L.G. Palmer, Ion selectivity of epithelial Na channels, J Membr Biol 96(2) (1987) 97-106.

[47] V. Bhalla, K.R. Hallows, Mechanisms of ENaC regulation and clinical implications, J Am Soc Nephrol 19(10) (2008) 1845-54.

[48] M.D. Carattino, G.M. Mueller, L.G. Palmer, G. Frindt, A.C. Rued, R.P. Hughey, T.R. Kleyman, Prostasin interacts with the epithelial Na+ channel and facilitates cleavage of the gamma-subunit by a second protease, Am. J. Physiol.-Renal Physiol. 307(9) (2014) F1080-F1087.

[49] A. Diakov, K. Bera, M. Mokrushina, B. Krueger, C. Korbmacher, Cleavage in the gamma-subunit of the epithelial sodium channel (ENaC) plays an important role in the proteolytic activation of near-silent channels, J. Physiol.-London 586(19) (2008) 4587-4608.

[50] O.B. Kashlan, B.M. Blobner, Z. Zuzek, M.D. Carattino, T.R. Kleyman, Inhibitory tract traps the epithelial Na+ channel in a low activity conformation, J Biol Chem 287(24) (2012) 20720-6.

[51] J.B. Bruns, M.D. Carattino, S. Sheng, A.B. Maarouf, O.A. Weisz, J.M. Pilewski, R.P. Hughey, T.R. Kleyman, Epithelial Na+ channels are fully activated by furin- and prostasin-dependent release of an inhibitory peptide from the gamma-subunit, J Biol Chem 282(9) (2007) 6153-60.

[52] S. Haerteis, M. Krappitz, A. Diakov, A. Krappitz, R. Rauh, C. Korbmacher, Plasmin and chymotrypsin have distinct preferences for channel activating cleavage sites in the gamma subunit of the human epithelial sodium channel, J Gen Physiol 140(4) (2012) 375-89.

[53] R.P. Hughey, J.B. Bruns, C.L. Kinlough, K.L. Harkleroad, Q.S. Tong, M.D. Carattino, J.P. Johnson, J.C. Stockand, T.R. Kleyman, Epithelial sodium channels are activated by furin-dependent proteolysis, J. Biol. Chem. 279(18) (2004) 18111-18114.

[54] T.R. Kleyman, M.D. Carattino, R.P. Hughey, ENaC at the cutting edge: regulation of epithelial sodium channels by proteases, J Biol Chem 284(31) (2009) 20447-51.

[55] N.D. Rawlings, A.J. Barrett, P.D. Thomas, X. Huang, A. Bateman, R.D. Finn, The MEROPS database of proteolytic enzymes, their substrates and inhibitors in 2017 and a comparison with peptidases in the PANTHER database, Nucleic Acids Research 46(D1) (2018) D624-D632.

[56] C. López-Otín, J.S. Bond, Proteases: multifunctional enzymes in life and disease, The Journal of biological chemistry 283(45) (2008) 30433-30437.

[57] J.S. Bond, Proteases: History, discovery, and roles in health and disease, Journal of Biological Chemistry 294(5) (2019) 1643-1651.

[58] A. Schork, M. Woern, H. Kalbacher, W. Voelter, R. Nacken, M. Bertog, S. Haerteis, C. Korbmacher, N. Heyne, A. Peter, H.U. Haring, F. Artunc, Association of Plasminuria with Overhydration in Patients with CKD, Clin. J. Am. Soc. Nephrol. 11(5) (2016) 761-769.

[59] S. Haerteis, A. Schork, T. Dörffel, B.N. Bohnert, R. Nacken, M. Wörn, M. Xiao, D. Essigke, A. Janessa, A.H. Schmaier, E.P. Feener, H.U. Haring, M. Bertog, C. Korbmacher, F. Artunc, Plasma kallikrein activates the epithelial sodium channel (ENaC) in vitro but is not essential for volume retention in nephrotic mice, Acta Physiol (Oxf) 224(1) (2018) e13060.

[60] B.N. Bohnert, S. Daiminger, M. Worn, F. Sure, T. Staudner, A.V. Ilyaskin, F. Batbouta, A. Janessa, J.C. Schneider, D. Essigke, S. Kanse, S. Haerteis, C. Korbmacher, F. Artunc, Urokinase-type plasminogen activator (uPA) is not essential for epithelial sodium channel (ENaC)-mediated sodium retention in experimental nephrotic syndrome, Acta Physiol (Oxf) 227(4) (2019) e13286.

[61] D.A. Bachovchin, B.F. Cravatt, The pharmacological landscape and therapeutic potential of serine hydrolases, Nat Rev Drug Discov 11(1) (2012) 52-68.

[62] S. Serim, The development of activity-based probes for serine proteases, 2014.

[63] N. Sturm, Enzyme Mechanisms: Serine Proteases, 2015.

[64] L. Pang, Q. Li, Y. Li, Y. Liu, N. Duan, H. Li, Urine proteomics of primary membranous nephropathy using nanoscale liquid chromatography tandem mass spectrometry analysis, Clinical Proteomics 15(1) (2018) 5.

[65] P. Svenningsen, U.G. Friis, J.B. Versland, K.B. Buhl, B. Moller Frederiksen, H. Andersen, R.M. Zachar, C. Bistrup, O. Skott, J.S. Jorgensen, R.F. Andersen, B.L. Jensen, Mechanisms of renal NaCl retention in proteinuric disease, Acta Physiol (Oxf) 207(3) (2013) 536-45.

[66] P. Svenningsen, C. Bistrup, U.G. Friis, M. Bertog, S. Haerteis, B. Krueger, J. Stubbe, O.N. Jensen, H.C. Thiesson, T.R. Uhrenholt, B. Jespersen, B.L. Jensen, C. Korbmacher, O. Skøtt, Plasmin in nephrotic urine activates the epithelial sodium channel, J Am Soc Nephrol 20(2) (2009) 299-310.

[67] F. Artunc, Proteolytic Activation of the Epithelial Sodium Channel in Nephrotic Syndrome by Proteasuria: Concept and Therapeutic Potential, Turk J Nephrol 29(1) (2020) 59-65.

[68] M. Worn, B.N. Bohnert, F. Alenazi, K. Boldt, F. Klose, K. Junger, M. Ueffing, A.L. Birkenfeld, H. Kalbacher, F. Artunc, Proteasuria in nephrotic syndrome-quantification and proteomic profiling, J Proteomics 230 (2021) 103981.

[69] M. Xiao, B.N. Bohnert, H. Aypek, O. Kretz, F. Grahammer, U. Aukschun, M. Worn, A. Janessa, D. Essigke, C. Daniel, K. Amann, T.B. Huber, E.F. Plow, A.L. Birkenfeld, F. Artunc, Plasminogen deficiency does not prevent sodium retention in a genetic mouse model of experimental nephrotic syndrome, Acta Physiol (Oxf) (2020) e13512.

[70] M. Kakoki, O. Smithies, The kallikrein-kinin system in health and in diseases of the kidney, Kidney Int 75(10) (2009) 1019-30.

[71] A. Shamanaev, M. Litvak, D. Gailani, Recent advances in factor XII structure and function, Curr Opin Hematol 29(5) (2022) 233-243.

[72] J.X. Yu, L. Chao, J. Chao, Prostasin is a novel human serine proteinase from seminal fluid. Purification, tissue distribution, and localization in prostate gland, J Biol Chem 269(29) (1994) 18843-8.

[73] P. Svenningsen, T.R. Uhrenholt, Y. Palarasah, K. Skjodt, B.L. Jensen, O. Skott, Prostasin-dependent activation of epithelial Na+ channels by low plasmin concentrations, Am J Physiol Regul Integr Comp Physiol 297(6) (2009) R1733-41.

[74] D.E. Peters, R. Szabo, S. Friis, N.A. Shylo, K. Uzzun Sales, K. Holmbeck, T.H. Bugge, The membrane-anchored serine protease prostasin (CAP1/PRSS8) supports epidermal development and postnatal homeostasis independent of its enzymatic activity, J Biol Chem 289(21) (2014) 14740-9.

[75] D. Essigke, A.V. Ilyaskin, M. Worn, B.N. Bohnert, M. Xiao, C. Daniel, K. Amann, A.L. Birkenfeld, R. Szabo, T.H. Bugge, C. Korbmacher, F. Artunc, Zymogen-locked mutant prostasin (Prss8) leads to incomplete proteolytic activation of the epithelial sodium channel (ENaC) and severely compromises triamterene tolerance in mice, Acta Physiol (Oxf) (2021) e13640.

[76] Aprotinin, in: J.K. Aronson (Ed.), Meyler's Side Effects of Drugs (Sixteenth Edition), Elsevier, Oxford, 2016, pp. 660-667.

[77] A. Narayanan, L.H. Jones, Sulfonyl fluorides as privileged warheads in chemical biology, Chem Sci 6(5) (2015) 2650-2659.

[78] K. Matsumoto, K. Mizoue, K. Kitamura, W.C. Tse, C.P. Huber, T. Ishida, Structural basis of inhibition of cysteine proteases by E-64 and its derivatives, Biopolymers 51(1) (1999) 99-107.

[79] K.C. Pandey, R. Dixit, Structure-function of falcipains: malarial cysteine proteases, J Trop Med 2012 (2012) 345195.

[80] J. Dostal, J. Brynda, L. Vankova, S.R. Zia, I. Pichova, O. Heidingsfeld, M. Lepsik, Structural determinants for subnanomolar inhibition of the secreted aspartic protease Sapp1p from Candida parapsilosis, J Enzyme Inhib Med Chem 36(1) (2021) 914-921.

[81] S. Eckert, E.J. Mascarenhas, R. Mitzner, R.M. Jay, A. Pietzsch, M. Fondell, V. Vaz da Cruz, A. Fohlisch, From the Free Ligand to the Transition Metal Complex: FeEDTA(-) Formation Seen at Ligand K-Edges, Inorg Chem 61(27) (2022) 10321-10328.

[82] U.M. Moissl, P. Wabel, P.W. Chamney, I. Bosaeus, N.W. Levin, A. Bosy-Westphal, O. Korth, M.J. Muller, L. Ellegard, V. Malmros, C. Kaitwatcharachai, M.K. Kuhlmann, F. Zhu, N.J. Fuller, Body fluid volume determination via body composition spectroscopy in health and disease, Physiol Meas 27(9) (2006) 921-33.

[83] B.N. Bohnert, T. Dorffel, S. Daiminger, C. Calaminus, S. Aidone, A. Falkenau, A. Semrau, M.J. Le, F. Iglauer, F. Artunc, Retrobulbar Sinus Injection of Doxorubicin is More Efficient Than Lateral Tail Vein Injection at Inducing Experimental Nephrotic Syndrome in Mice: A Pilot Study, Lab Anim 53(6) (2019) 564-576.

[84] A.S. Levey, J. Coresh, T. Greene, J. Marsh, L.A. Stevens, J.W. Kusek, F. Van Lente, Expressing the Modification of Diet in Renal Disease Study equation for estimating

glomerular filtration rate with standardized serum creatinine values, Clinical chemistry 53(4) (2007) 766-72.

[85] H.P. Kapprell, A. Maurer, F. Kramer, B. Heinrich, C. Buenning, A. Narvaez, H. Kalbacher, T. Flad, Development of a fluorescence resonance energy transfer peptide library technology for detection of protease contaminants in protein-based raw materials used in diagnostic assays, Assay Drug Dev Technol 9(5) (2011) 549-53.

[86] Shotgun proteomics-label-free quantification workflow. https://www.mpi-marburg.mpg.de/519542/Proteomics.

[87] Pierce™ NHS-aktivierte Magnetic Beads. https://www.thermofisher.com/order/catalog/product/de/de/88826.

[88] B. Turriziani, A. Garcia-Munoz, R. Pilkington, C. Raso, W. Kolch, A. von Kriegsheim, On-beads digestion in conjunction with data-dependent mass spectrometry: a shortcut to quantitative and dynamic interaction proteomics, Biology (Basel) 3(2) (2014) 320-32.

[89] J.V. Olsen, L.M. de Godoy, G. Li, B. Macek, P. Mortensen, R. Pesch, A. Makarov, O. Lange, S. Horning, M. Mann, Parts per million mass accuracy on an Orbitrap mass spectrometer via lock mass injection into a C-trap, Molecular & cellular proteomics : MCP 4(12) (2005) 2010-21.

[90] M. Worn, H. Kalbacher, F. Artunc, Proteolytic Activity against the Distal Polybasic Tract of the Gamma Subunit of the Epithelial Sodium Channel ENaC in Nephrotic Urine, Curr Med Chem 29(42) (2022) 6433-6445.

[91] M. Althaus, R.Y. Lawong, Proteolytic ENaC activation in health and disease-a complicated puzzle, Pflugers Arch (2021).

[92] D. Baechle, A. Cansier, R. Fischer, J. Brandenburg, T. Burster, C. Driessen, H. Kalbacher, Biotinylated fluorescent peptide substrates for the sensitive and specific determination of cathepsin D activity, J Pept Sci 11(3) (2005) 166-74.

[93] T. Jores, A. Klinger, L.E. Groß, S. Kawano, N. Flinner, E. Duchardt-Ferner, J. Wöhnert, H. Kalbacher, T. Endo, E. Schleiff, D. Rapaport, Characterization of the targeting signal in mitochondrial β-barrel proteins, Nat Commun 7 (2016) 12036.

[94] N. Zaidi, T. Herrmann, D. Baechle, S. Schleicher, J. Gogel, C. Driessen, W. Voelter, H. Kalbacher, A new approach for distinguishing cathepsin E and D activity in antigen-processing organelles, Febs j 274(12) (2007) 3138-49.

[95] A. Croxatto, G. Prod'hom, G. Greub, Applications of MALDI-TOF mass spectrometry in clinical diagnostic microbiology, FEMS Microbiol Rev 36(2) (2012) 380-407.

[96] J.D. Vassalli, D. Belin, Amiloride selectively inhibits the urokinase-type plasminogen activator, FEBS Lett 214(1) (1987) 187-91.

[97] M. Staehr, K.B. Buhl, R.F. Andersen, P. Svenningsen, F. Nielsen, G.R. Hinrichs, C. Bistrup, B.L. Jensen, Aberrant glomerular filtration of urokinase-type plasminogen activator in nephrotic syndrome leads to amiloride-sensitive plasminogen activation in urine, Am. J. Physiol.-Renal Physiol. 309(3) (2015) F235-F241.

[98] B.N. Bohnert, I. Gonzalez-Menendez, T. Dorffel, J.C. Schneider, M. Xiao, A. Janessa, M.Z. Kalo, B. Fehrenbacher, M. Schaller, N. Casadei, K. Amann, C. Daniel, A.L. Birkenfeld, F. Grahammer, L. Izem, E.F. Plow, L. Quintanilla-Martinez, F. Artunc, Essential role of DNA-PKcs and plasminogen for the development of doxorubicin-induced glomerular injury in mice, Dis Model Mech 14(9) (2021).

[99] H.I. Kenawy, I. Boral, A. Bevington, Complement-Coagulation Cross-Talk: A Potential Mediator of the Physiological Activation of Complement by Low pH, Front Immunol 6 (2015) 215.

[100] L.A. Miles, J.S. Greengard, J.H. Griffin, A comparison of the abilities of plasma kallikrein, beta-Factor XIIa, Factor XIa and urokinase to activate plasminogen, Thromb Res 29(4) (1983) 407-17.

[101] L.A. Miles, J.S. Greengard, J.H. Griffin, A Comparison of the Abilities of Plasma Kallikrein, Beta-Factor-Xiia, Factor-Xia and Urokinase to Activate Plasminogen, Thromb. Res. 29(4) (1983) 407-417.

[102] R.N. Pike, A.M. Buckle, B.F. le Bonniec, F.C. Church, Control of the coagulation system by serpins. Getting by with a little help from glycosaminoglycans, FEBS J 272(19) (2005) 4842-51.

[103] G.A. Silverman, P.I. Bird, R.W. Carrell, F.C. Church, P.B. Coughlin, P.G. Gettins, J.A. Irving, D.A. Lomas, C.J. Luke, R.W. Moyer, P.A. Pemberton, E. Remold-O'Donnell, G.S. Salvesen, J. Travis, J.C. Whisstock, The serpins are an expanding superfamily of structurally similar but functionally diverse proteins. Evolution, mechanism of inhibition, novel functions, and a revised nomenclature, J Biol Chem 276(36) (2001) 33293-6.

[104] R.F. Andersen, J. Palmfeldt, B. Jespersen, N. Gregersen, S. Rittig, Plasma and urine proteomic profiles in childhood idiopathic nephrotic syndrome, Proteomics Clin Appl 6(7-8) (2012) 382-93.

[105] Y.W. Choi, Y.G. Kim, M.Y. Song, J.Y. Moon, K.H. Jeong, T.W. Lee, C.G. Ihm, K.S. Park, S.H. Lee, Potential urine proteomics biomarkers for primary nephrotic syndrome, Clin Proteomics 14 (2017) 18.

[106] A. Larionov, E. Dahlke, M. Kunke, L. Zanon Rodriguez, I.M. Schiessl, J.L. Magnin, U. Kern, A.A. Alli, G. Mollet, O. Schilling, H. Castrop, F. Theilig, Cathepsin B increases ENaC activity leading to hypertension early in nephrotic syndrome, J Cell Mol Med 23(10) (2019) 6543-6553.

[107] D. Essigke, B.N. Bohnert, A. Janessa, M. Worn, K. Omage, H. Kalbacher, A.L. Birkenfeld, T.H. Bugge, R. Szabo, F. Artunc, Sodium retention in nephrotic syndrome is independent of the activation of the membrane-anchored serine protease prostasin (CAP1/PRSS8) and its enzymatic activity, Pflugers Arch 474(6) (2022) 613-624.

[108] F. Sure, S. Afonso, D. Essigke, P. Schmidt, M.Z. Kalo, V. Nesterov, A. Kissler, M. Bertog, R. Rinke, S. Wittmann, K.A.E. Broeker, T. Gramberg, F. Artunc, C. Korbmacher, A.V. Ilyaskin, Transmembrane Serine Protease 2 and Proteolytic Activation of the Epithelial Sodium Channel in Mouse Kidney, J Am Soc Nephrol 36(3) (2025) 420-434.

[109] F. Artunc, B.N. Bohnert, J.C. Schneider, T. Staudner, F. Sure, A.V. Ilyaskin, M. Wörn, D. Essigke, A. Janessa, N.V. Nielsen, A.L. Birkenfeld, M. Etscheid, S. Haerteis,

References

C. Korbmacher, S.M. Kanse, Proteolytic activation of the epithelial sodium channel (ENaC) by factor VII activating protease (FSAP) and its relevance for sodium retention in nephrotic mice, Pflugers Arch (2021).

[110] MEROPS, Peptidase S1 family, 2021. https://www.ebi.ac.uk/merops/cgi-bin/famsum?family=S1.

[111] M. Adachi, K. Kitamura, T. Miyoshi, T. Narikiyo, K. Iwashita, N. Shiraishi, H. Nonoguchi, K. Tomita, Activation of epithelial sodium channels by prostasin in Xenopus oocytes, J Am Soc Nephrol 12(6) (2001) 1114-1121.

[112] C.J. Passero, G.M. Mueller, H. Rondon-Berrios, S.P. Tofovic, R.P. Hughey, T.R. Kleyman, Plasmin Activates Epithelial Na+ Channels by Cleaving the gamma Subunit, J. Biol. Chem. 283(52) (2008) 36586-36591.

[113] S. Worner, B.N. Bohnert, M. Worn, M. Xiao, A. Janessa, A.L. Birkenfeld, K. Amann, C. Daniel, F. Artunc, Renal effects of the serine protease inhibitor aprotinin in healthy conscious mice, Acta Pharmacol Sin (2021).

[114] M. Bens, V. Vallet, F. Cluzeaud, L. Pascual-Letallec, A. Kahn, M.E. Rafestin-Oblin, B.C. Rossier, A. Vandewalle, Corticosteroid-dependent sodium transport in a novel immortalized mouse collecting duct principal cell line, J Am Soc Nephrol 10(5) (1999) 923-34.

[115] O. Soderberg, M. Gullberg, M. Jarvius, K. Ridderstrale, K.J. Leuchowius, J. Jarvius, K. Wester, P. Hydbring, F. Bahram, L.G. Larsson, U. Landegren, Direct observation of individual endogenous protein complexes in situ by proximity ligation, Nat Methods 3(12) (2006) 995-1000.

[116] C. Kiourtis, A. Wilczynska, C. Nixon, W. Clark, S. May, T.G. Bird, Specificity and off-target effects of AAV8-TBG viral vectors for the manipulation of hepatocellular gene expression in mice, Biol Open 10(9) (2021).

First authorships, co-authored publications and congress posters

The results of this work were published in following publications and congress posters:

First authorships:

- M. Worn, B.N. Bohnert, F. Alenazi, K. Boldt, F. Klose, K. Junger, M. Ueffing, A.L. Birkenfeld, H. Kalbacher, F. Artunc, Proteasuria in nephrotic syndrome-quantification and proteomic profiling, J Proteomics 230 (2021) 103981.
- M. Worn, H. Kalbacher, F. Artunc, Proteolytic Activity against the Distal Polybasic Tract of the Gamma Subunit of the Epithelial Sodium Channel ENaC in Nephrotic Urine, Curr Med Chem 29(42) (2022) 6433-6445.

Co-authored publications:

ENaC + Aprotinin treatment

- B.N. Bohnert, D. Essigke, A. Janessa, J.C. Schneider, M. Worn, M.Z. Kalo, M. Xiao, L. Kong, K. Omage, J. Hennenlotter, B. Amend, A.L. Birkenfeld, F. Artunc, Experimental nephrotic syndrome leads to proteolytic activation of the epithelial Na(+) channel in the mouse kidney, Am J Physiol Renal Physiol 321(4) (2021) F480-F493.
- B.N. Bohnert, M. Menacher, A. Janessa, M. Worn, A. Schork, S. Daiminger, H. Kalbacher, H.U. Haring, C. Daniel, K. Amann, F. Sure, M. Bertog, S. Haerteis, C. Korbmacher, F. Artunc, Aprotinin prevents proteolytic epithelial sodium channel (ENaC) activation and volume retention in nephrotic syndrome, Kidney Int 93(1) (2018) 159-172.
- S. Worner, B.N. Bohnert, M. Worn, M. Xiao, A. Janessa, A.L. Birkenfeld, K. Amann, C. Daniel, F. Artunc, Renal effects of the serine protease inhibitor aprotinin in healthy conscious mice, Acta Pharmacol Sin (2021).

Investigated KO mouse models:

- M. Xiao, B.N. Bohnert, H. Aypek, O. Kretz, F. Grahammer, U. Aukschun, M. Worn, A. Janessa, D. Essigke, C. Daniel, K. Amann, T.B. Huber, E.F. Plow, A.L. Birkenfeld, F. Artunc, Plasminogen deficiency does not prevent sodium retention

in a genetic mouse model of experimental nephrotic syndrome, Acta Physiol (Oxf) (2020) e13512.

- B.N. Bohnert, S. Daiminger, M. Worn, F. Sure, T. Staudner, A.V. Ilyaskin, F. Batbouta, A. Janessa, J.C. Schneider, D. Essigke, S. Kanse, S. Haerteis, C. Korbmacher, F. Artunc, Urokinase-type plasminogen activator (uPA) is not essential for epithelial sodium channel (ENaC)-mediated sodium retention in experimental nephrotic syndrome, Acta Physiol (Oxf) 227(4) (2019) e13286.
- D. Essigke, B.N. Bohnert, A. Janessa, M. Worn, K. Omage, H. Kalbacher, A.L. Birkenfeld, T.H. Bugge, R. Szabo, F. Artunc, Sodium retention in nephrotic syndrome is independent of the activation of the membrane-anchored serine protease prostasin (CAP1/PRSS8) and its enzymatic activity, Pflugers Arch 474(6) (2022) 613-624.
- F. Artunc, B.N. Bohnert, J.C. Schneider, T. Staudner, F. Sure, A.V. Ilyaskin, M. Wörn, D. Essigke, A. Janessa, N.V. Nielsen, A.L. Birkenfeld, M. Etscheid, S. Haerteis, C. Korbmacher, S.M. Kanse, Proteolytic activation of the epithelial sodium channel (ENaC) by factor VII activating protease (FSAP) and its relevance for sodium retention in nephrotic mice, Pflugers Arch (2021)
- S. Haerteis, A. Schork, T. Dörffel, B.N. Bohnert, R. Nacken, M. Wörn, M. Xiao, D. Essigke, A. Janessa, A.H. Schmaier, E.P. Feener, H.U. Haring, M. Bertog, C. Korbmacher, F. Artunc, Plasma kallikrein activates the epithelial sodium channel (ENaC) in vitro but is not essential for volume retention in nephrotic mice, Acta physiologica (Oxford, England) 224(1) (2018) e13060

Further co-authored publications:

- A. Schork, M. Woern, H. Kalbacher, W. Voelter, R. Nacken, M. Bertog, S. Haerteis, C. Korbmacher, N. Heyne, A. Peter, H.U. Haring, F. Artunc, Association of Plasminuria with Overhydration in Patients with CKD, Clin. J. Am. Soc. Nephrol. 11(5) (2016) 761-769.

Congress posters, as first author:

- Wörn M, Alenazi F, Kalbacher H, Heyne N, Artunc F. Charakterisierung und Quantifikation der Proteasurie beim nephrotischen Syndrom; Abstract, 9. Annual meeting of Dt. Ges. f. Nephrologie, Mannheim, 2017
- Wörn M, Boldt K, Ueffing M, Heyne N, Artunc F. Identifikation von Serinproteasen im Urin von Patienten mit nephrotischem Syndrom mittels proteomischem Ansatz; Abstract, 10. Annual meeting of Dt. Ges. f. Nephrologie, Berlin, 2018
- Wörn M, Kalbacher H, Xiao M, Artunc F. Nachweis einer spezifischen proteolytischen Aktivität gegen die γ-Untereinheit des epithelialen Natriumkanals ENaC in nephrotischen Urinproben mittels HPLC-MALDI-TOF-MS-Analyse; Abstract, 11. Annual meeting of Dt. Ges. f. Nephrologie, Rostock, 2019
- Wörn M, Boldt K, Ueffing M, Artunc F. Bioinformatische Betrachtung von aberrant filtrierten Proteinen beim nephrotischen Syndrom anhand der GO und KEGG Datenbanken 12. Annual meeting of Dt. Ges. f. Nephrologie, Berlin, 2020
- Wörn M, Boldt K, Ueffing M, Artunc F. Identifikation der im nephrotischen Syndrom relevanten Serinproteasen im Urin von Patienten und Mäusen mittels Aprotinin-Pulldown-Proteomics; Abstract, 13. Annual meeting of Dt. Ges. f. Nephrologie, Rostock, 2021
- Wörn M, Kalbacher H, Artunc F. Proteolytische Aktivität gegen den distalen polybasischen Trakt der Gamma-Untereinheit des epithelialen Natriumkanals ENaC im nephrotischem Urin; Abstract, 14. Annual meeting of Dt. Ges. f. Nephrologie, Berlin, 2022
- Wörn M, Schork A, Essigke D, Bohnert BN, Heyne N, Artunc F. Aktivierung des alternativen Komplementwegs im Urin von Patienten mit nephrotischem Syndrom in Abhängigkeit von der Grunderkrankung; Abstract, 17. Annual meeting of Dt. Ges. f. Nephrologie, Berlin, 2025

Explanation of the personal contribution to this dissertation

The study was designed in collaboration with my doctoral supervisor, Professor Ferruh Artunc. The experiments were carried out independently by me after initial training by Ferruh Artunc or members of his research group.

The sample preparation steps for the mass spectrometry experiments were performed by myself. The subsequent LC–MS/MS measurements were executed by the proteomics center as "Core Facility Medical Proteomics" in the eye clinic, Tübingen, with the staff around Prof. Marius Ueffing, Dr. Karsten Boldt, Franziska Klose and Katrin Junger, who are also co-authors of the publication about proteomic profiling. I received the resulting LFQ raw data from them and after instruction help from Karsten Boldt, I analyzed these data and their statistics by the proteomics software MaxQuant and Perseus by myself. The presented methods and results in these thesis sections 2.4, 2.5, 3.1 and 3.2 based on the first-author publication "Proteasuria in nephrotic syndrome-quantification and proteomic profiling", J Proteomics 230 (2021) 103981, except for 2.4.2.2 and 3.2.2.2 with aprotinin MS approach.

The western blot experiments with all steps from sample preparation to electrophoresis and blotting, antibody incubations until chemiluminescence/fluorescence recordings were carried out by myself

I performed the incubation experiments with the peptide substrates, both with the universal peptide substrate library as well as with the AMCA and AMC substrates of peptides representing the distal polybasic tract of γ-EnaC, and also the subsequent fluorescence measurements of the universal and AMC substrates on the microplate reader or the HPLC separation of the AMCA substrates with subsequent fluorescence recording of the chromatogram peaks and retention time and area-under-the-curve analyses. The universal peptide substrate with the trade name "P-Check" was purchased from Panatecs, Germany. The individual synthesis of the AMCA and AMC substrates were planned together with the strongly involved co-author Dr. Hubert Kalbacher from the IFIB institute, Tübingen. Then, he synthesized these substrates in his own laboratory by peptide solid-phase synthesis and coupling of the fluorophores. The presented methods and results in these thesis sections based for method section 2.3 with the universal peptide substrate on the first-author publication "Proteasuria in nephrotic syndrome-

quantification and proteomic profiling", J Proteomics 230 (2021) 103981, and for the sections 2.7 and 3.4 on the first-author publication "Proteolytic Activity against the Distal Polybasic Tract of the Gamma Subunit of the Epithelial Sodium Channel ENaC in Nephrotic Urine", Curr Med Chem 29(42) (2022) 6433-6445.

The statistical analysis of these experiments was performed independently by me, the proteomics data by the "MaxQuant" and "Perseus" programs and the other quantitative data with creating the diagrams and graphs by the statistic software "GraphPad Prism".

I declare that I have written this doctoral thesis independently. For translation of some words and sentences into English and for checking of spelling and grammar, I have used online translation websites "Google Translator" and "Linguee". For some variations and synonyms of sentence structures, the paraphrasing function at the "ChatGPT 5" website was used, with text modification tool "Canvas", and a further paraphrasing tool at the "QuillBot" website, but no generation of longer text sections. I carefully checked and adjusted the synonymous words and changed sentences of the tools before including them in the manuscript.

I further declare that I have not used any sources other than those listed in the references.

Acknowledgment

I would like to express my sincere gratitude to Professor Ferruh Artunc for his great supervision, continuous encouragement, and for entrusting me with such a fascinating and challenging topic. His scientific vision with many great ideas for new experiments and projects, and his guidance in preparing publications and conference presentations have been invaluable to my development as a researcher. Dear Ferruh, I sincerely thank you for your patience, trust, and the many discussions that have shaped both this thesis and my way of thinking as a researcher.

My warm thanks also go to the Senior Scientist Dr. Hubert Kalbacher, whose exceptional biochemical expertise greatly enriched this work. I am especially grateful for his ideas and help by synthesis of the peptide substrates in his laboratory, including the universal penta-peptide library and the γ-ENaC peptide sequences with AMCA and AMC fluorophores, which were essential to several key experiments in this thesis. From our scientific and biochemical discussions, I was able to learn a great deal and gain valuable insights.

Furthermore, I would like to thank my colleagues Zaher Kalo, Andrea Janessa, Dr. Daniel Essigke, and Dr. Bernhard Bohnert for their collegial spirit, helpful discussions, and great support in the daily laboratory work and in our collaborative projects. Working together with you made even the long experimental days both productive and enjoyable.

Finally, I would like to express my sincere appreciation to my parents, whose constant encouragement, understanding and support provided the foundation for all my efforts. Their belief in me has been a continuous source of motivation throughout my studies and beyond.